LA STAZIONE GEOFISICA IPOGEA
DELLA GROTTA GIGANTE (CARSO TRIESTINO)

Responsabile Scientifico: Dr. Carla Braitenberg
Hanno collaborato:

DiGeo: INGV:
Dr. Ing. Ildikò Nagy   Dott. Gianni Romeo
Dott. Barbara Grillo   Dott. Quintilio Taccetti
Dott. Daniele Tenze   Ing. Giuseppe Spinelli
Dott. Patrizia Mariani   Sig. Paolo Benedetti.
Dipl. Tecn. Sergio Zidarich

Japan 11/03/2011 05:46 UTC M=9.0

Istituto Nazionale di Geofisica e Vulcanologia

Indice

1 - Introduzione

L'anno 2011 e' stato segnato dall'evento sismico del Giappone (11 Marzo 2011, M=9.0), che si colloca al quarto posto nella scala degli maggiori eventi sismici mai registrati. L'evento del Cile del 1960 (22 Maggio 1960, M=9.5), é l'evento di magnitudo massima in assoluto mai registrato, seguito dall'evento dell'Alaska del 1964 (28 Marzo 1964, Prince William Sound, M=9.2), e da quello delle Isole Sumatra-Andamane del 2004 (26 dicembre 2004, M=9.1). La stazione della Grotta Gigante, a nostra saputa, e' l'unico strumento al mondo, ancora esistente ed attivo nella medesima collocazione, che vanta di aver registrato il 75 % dei quattro eventi maggiori. Infatti, solo a causa di un periodo di manutenzione non e' stato registrato l'evento del 1964, mentre le registrazioni degli altri eventi sono tutte disponibili. I pendoli della Grotta Gigante hanno un periodo di oscillazione particolarmente elevato, pari a 6 minuti, per cui registrano bene la parte bassa dello spettro in frequenze, dominato dalle frequenze delle oscillazioni libere, che sono importanti nella valutazione completa dell'energia generata da un mega-sisma. La registrazione dell'evento del Cile 1960, ci permette di comparare i mega-eventi piu' recenti, come quello del Giappone, in termini delle ampiezze delle oscillazioni libere e conseguentemente delle sorgenti. Qui presentiamo il confronto delle ampiezze spettrali per i tre eventi Cile 1960, Isole Sumatra-Andamane 2004, e Giappone 2011.

Altro argomento di interesse generale risale nel segnale dei pendoli generato da flussi idrici carsici. Nel presente fascicolo illustriamo come il tilting dei pendoli e' proporzionale all'integrale nel tempo del flusso di acqua immesso nel sistema carsico durante una piena. L'utilizzo dei pendoli come strumento d'indagine di idrogeologia sta prendendo piede attualmente, con applicazioni diverse.

Si segnala che l'anno 2011 vede la pubblicazione dell'Enciclopedia della Geofisica (Encyclopedia of Geophysics, Ed. Harsh Gupta), editore Springer. Con soddisfazione vediamo che la nuova edizione comprende una voce dedicata ai pendoli orizzontali a banda larga, ed in particolare sulle osservazioni dei pendoli della Grotta Gigante, considerati di rilevanza internazionale. E' auspicabile che anche in futuro potremmo mantenere la stazione attiva e cosi' seguire l'evoluzione temporale della serie continua ed ininterrotta del tilting locale, disponibile dal 1966.

3 - Osservazioni delle inclinazioni della verticale e di parametri ambientali per il periodo 2009 – giugno 2011.

Qui di seguito vengono riportate le registrazioni effettuate con i pendoli e con i clinometri della Grotta Gigante per il periodo 2009-2011. I pendoli si riferiscono ai pendoli orizzontali che hanno dimensione di 95 m in altezza, mentre con i clinometri si intende la coppia di strumenti di dimensioni piu' piccole (altezza di 0.5 m). (Braitenberg, 1999; Braitenberg e Zadro, 1999). Inoltre si riportano i grafici delle registrazioni orarie della temperatura, della pressione atmosferica e della piovosità. Infine viene dato un quadro d'insieme della disponibilità delle registrazioni estensimetriche e clinometriche della intera rete strumentale clino-estensimetrica del Friuli gestita dal Dipartimento di Geoscienze.

Ambedue strumenti geodetici (pendoli orizzontali = Long Peirod Horiozntal Pendulum = LPHP; Clinometro = Medium Period Tiltmeter = MPT) sono collocati nella stazione geodetica della Grotta Gigante, ma causa la loro diversa costruzione hanno risposte diverse a seconda delle deformazioni in atto. I pendoli orizzontali hanno l'attacco superiore fissato nella volta della grotta, mentre quello inferiore e' fissato nella base. I clinometri invece sono accoppiati al movimento della grotta tramite un treppiede che appoggia sul fondo della grotta. La diversa costruzione implica una differente risposta ai movimenti della grotta che comprendono una deformazione di taglio, come viene illustrato nella Figura 3.1. Una rotazione della grotta invece viene rilevata da ambedue strumenti allo stesso modo.
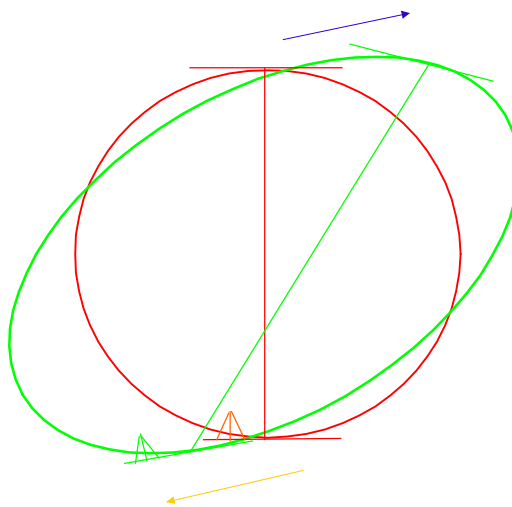

Fig. 3.1 Illustrazione della diversa inclinazione indotta per un clinometro che poggia sul fondo della grotta ed uno che e' fissato sulla volta e sul fondo della grotta. Il primo tipo di clinometro è rappresentato dal clinometro MPT ed il secondo dal pendolo della Grotta Gigante LPHP. Quando la deformazione contiene una deformazione di taglio come nel disegno, i due strumenti si inclinano in direzione opposta. Nella pratica questo avviene nella Grotta Gigante per deformazioni indotte dal fiume sotterraneo Timavo.
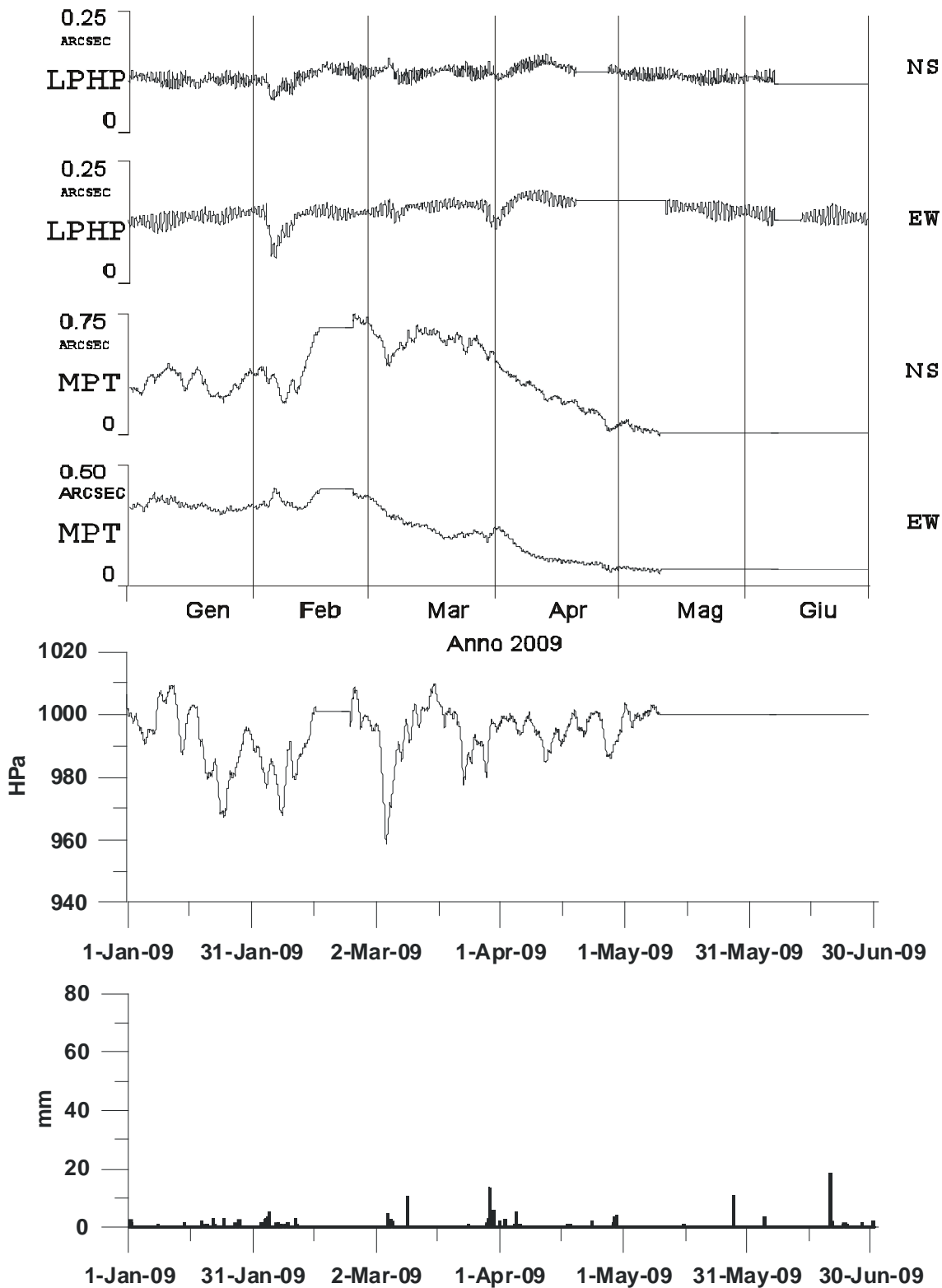
**Fig. 3.2-** *Grafico delle registrazioni effettuate con i pendoli LPHP (Long Period Horizontal Pendulum) e con i clinometri MPT (Medium Period Tiltmeter) della Grotta Gigante per il periodo 2009-2011. Nella parte inferiore del grafico è riportata la registrazione pluviometrica giornaliera (stazione di Trieste. Stravisi, comunicazione personale) e la pressione barometrica. A) Periodo gennaio-giugno 2009*
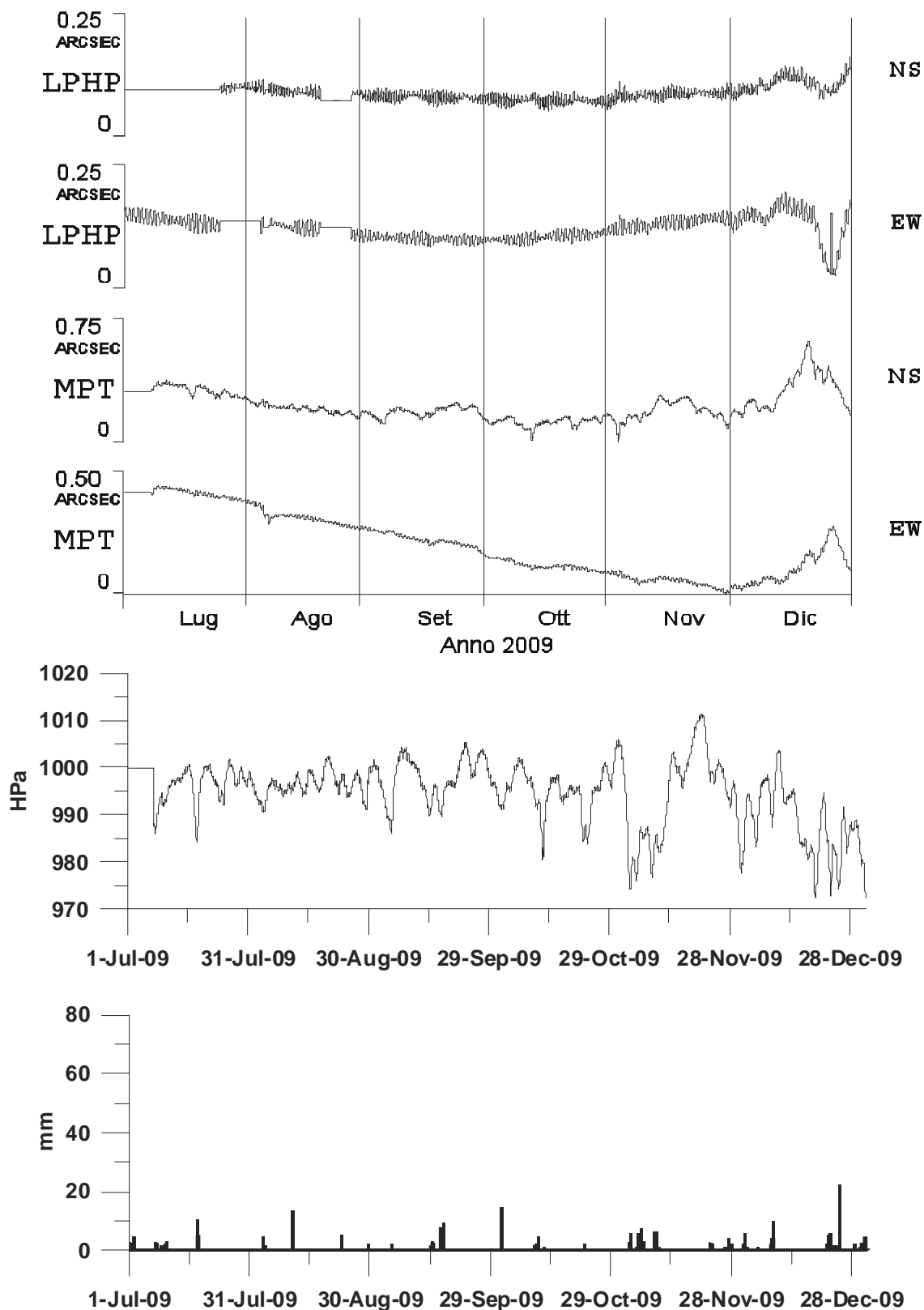
Fig. 3.2b - *Grafico delle registrazioni effettuate con i pendoli LPHP e con i clinometri MPT della Grotta Gigante per il periodo 2009-2011. Nella parte inferiore del grafico è riportata la registrazione pluviometrica giornaliera (stazione di Trieste. Stravisi, comunicazione personale) e la pressione barometrica. B) periodo luglio-dicembre 2009*
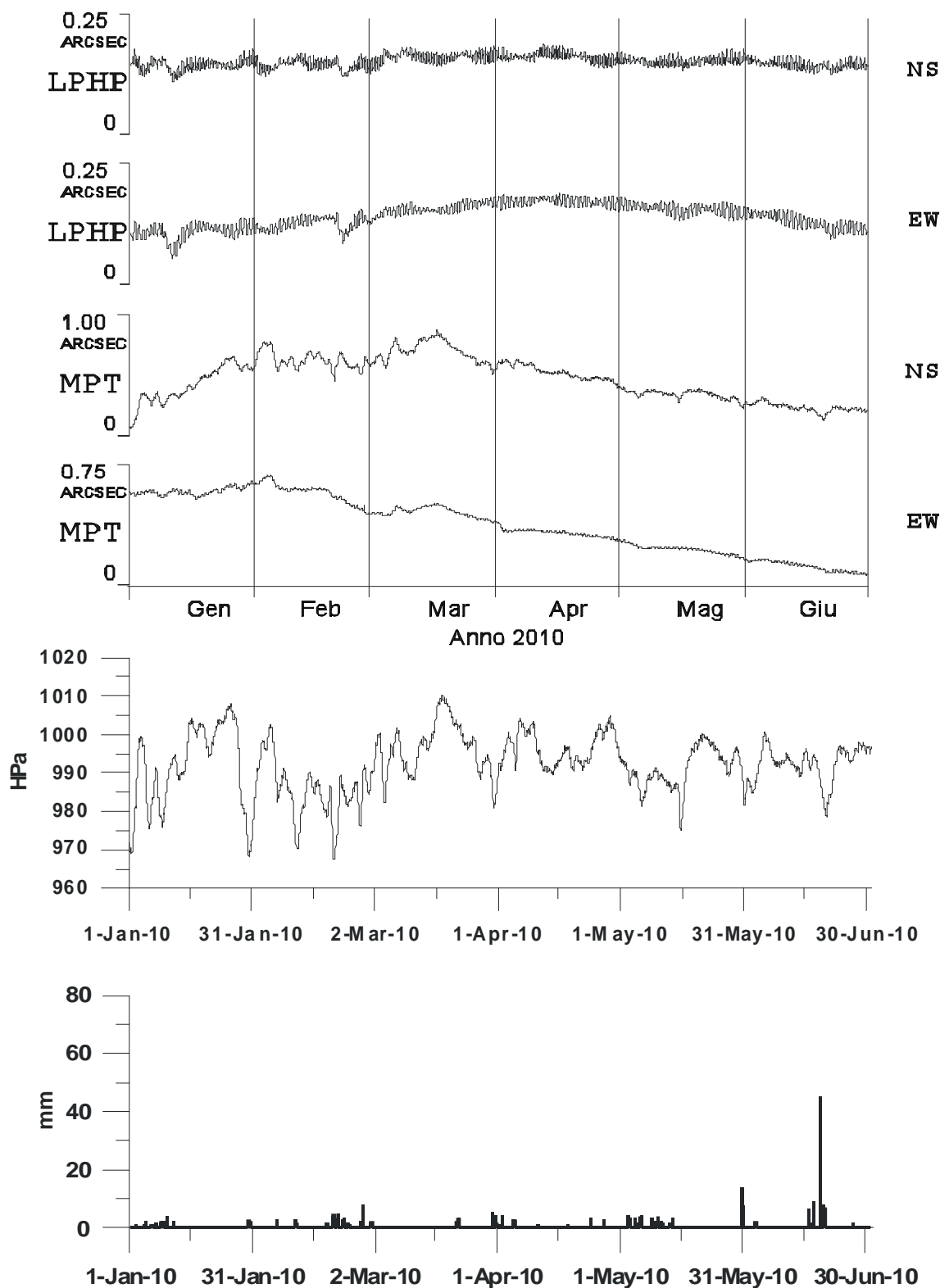
Fig. 3.2c - *Grafico delle registrazioni effettuate con i pendoli LPHP e con i clinometri MPT della Grotta Gigante per il periodo 2009-2011. Nella parte inferiore del grafico è riportata la registrazione pluviometrica giornaliera (stazione di Trieste. Stravisi, comunicazione personale) e la pressione barometrica. C)Periodo gennaio-giugno 2010*
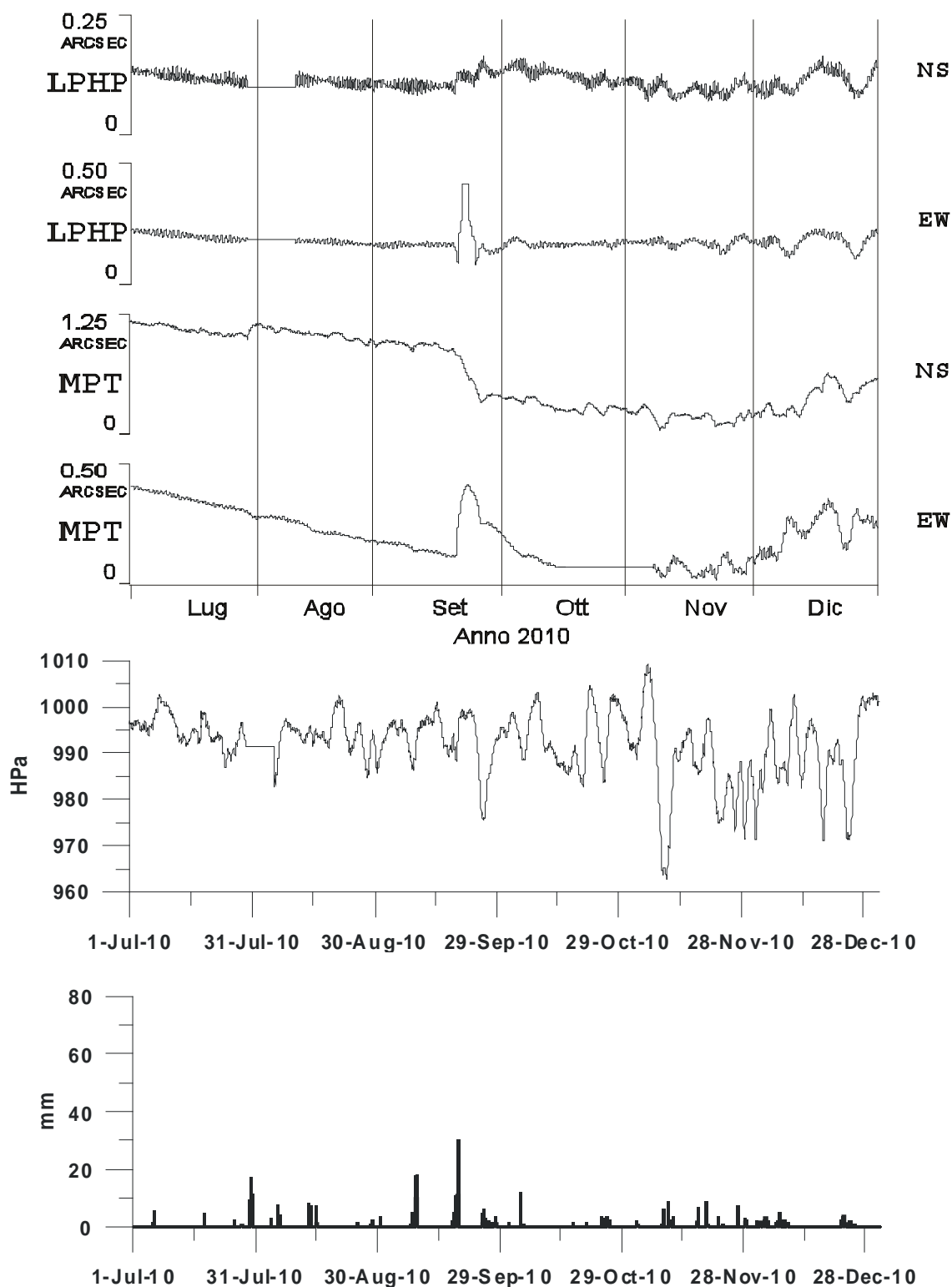
Fig. 3.2d - *Grafico delle registrazioni effettuate con i pendoli LPHP e con i clinometri MPT della Grotta Gigante per il periodo 2009-2011. Nella parte inferiore del grafico è riportata la registrazione pluviometrica giornaliera (stazione di Trieste. Stravisi, comunicazione personale) e la pressione barometrica. D) Periodo luglio-dicembre 2010.*
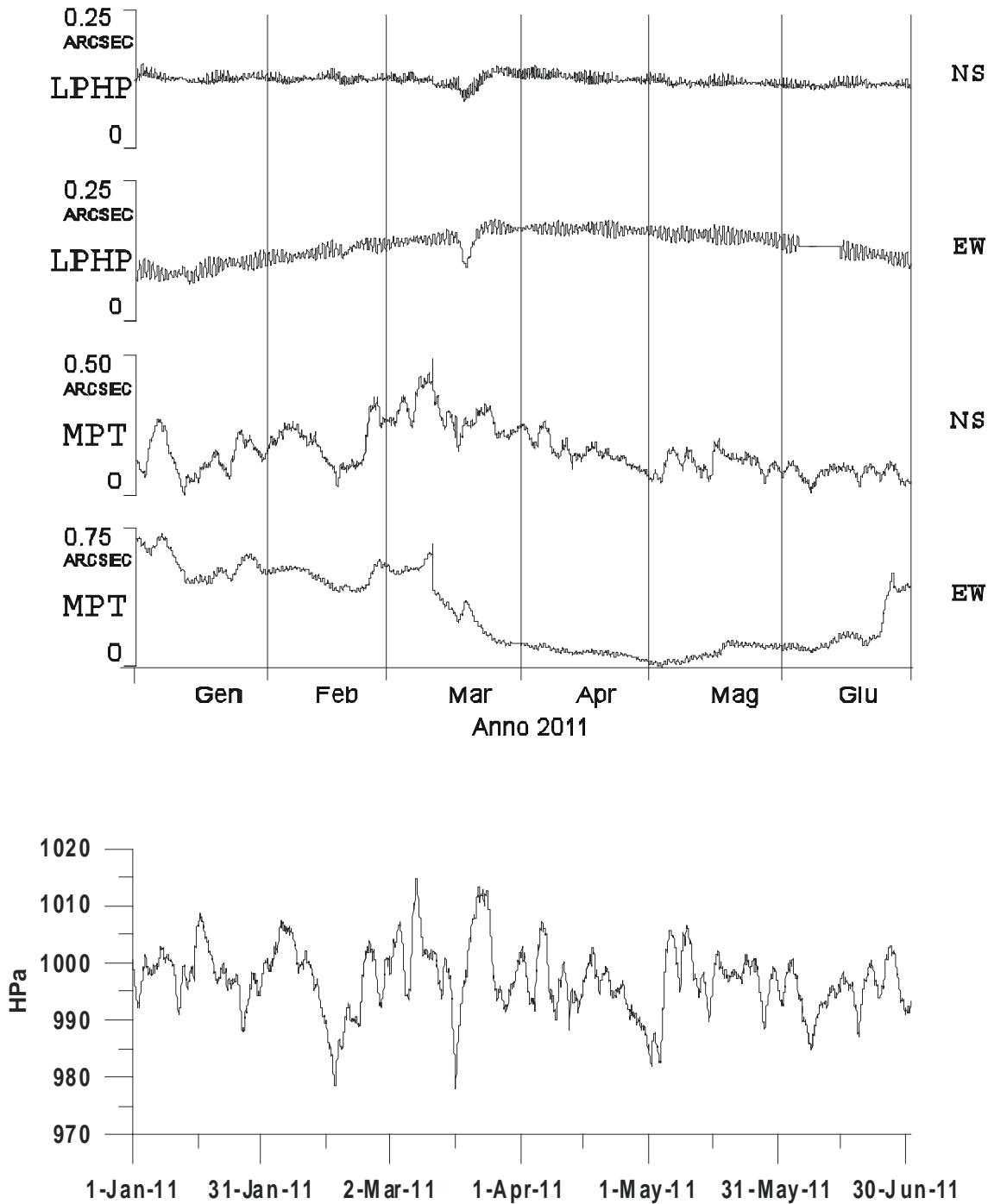
Fig. 3.2e - *Grafico delle registrazioni effettuate con i pendoli LPHP e con i clinometri MPT della Grotta Gigante per il periodo 2009-2011. E) Periodo gennaio-giugno 2011. Per questo intervallo temporale attendiamo i dati della precipitazione.*
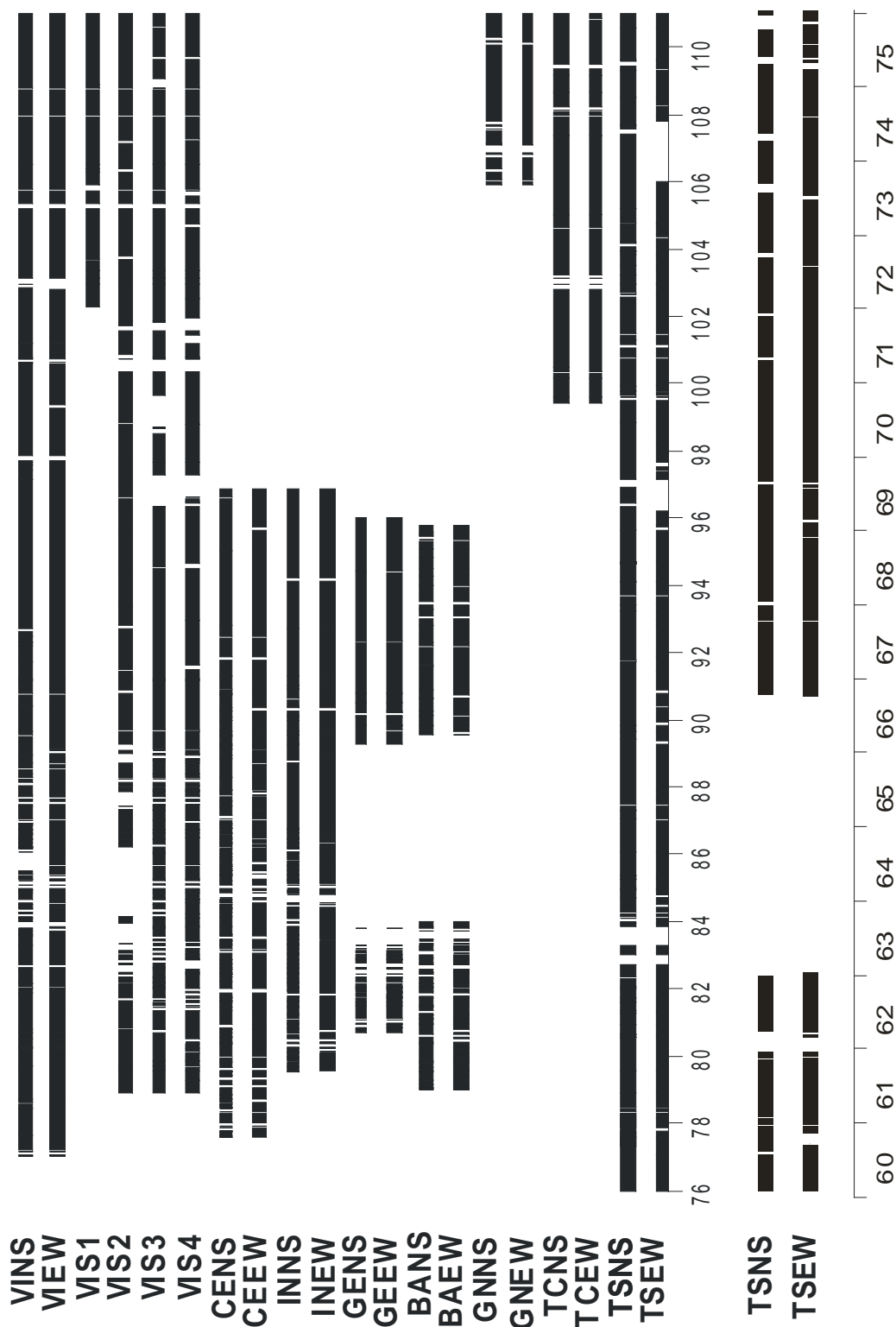
Fig. 3.3 - *Quadro d'insieme della disponibilità delle registrazioni della rete strumentale clino-estensimetrica del Friuli e della Grotta Gigante gestita dal Dipartimento di Geoscienze. Le sigle si riferiscono a: VI:Villanova, CE: Cesclans, IN: Invillino, GE: Gemona, BA: Barcis, GN: Genziana. I clinometri (pendoli orizzontali) sono identificati con NS ed EW, mentre i quattro strainmeter(3 orizzontali, uno verticale) con S1,S2,S3,S4. Le sigle TSNS e TSEW si riferiscono ai pendoli LPHP della Grotta Gigante. Il database comprende inoltre l'osservazione di temperatura e pressione, e dei clinometri tradizionali MPT (sigle TCNS e TCEW; dal 1999) della Grotta Gigante.*

Riportiamo qui di seguito anche l'insieme delle osservazioni della coppia di pendoli per il periodo dal 1 gennaio 2010 al 30 giugno 2011. Si osserva bene le diverse componenti del segnale, come la variazione annuale, i segnali indotti dalle piene del fiume sotterraneo Timavo, la marea terrestre e la variazione a lungo termine (Zadro e Braitenberg, 1999; Braitenberg, 1999b; Pagot, 2002).
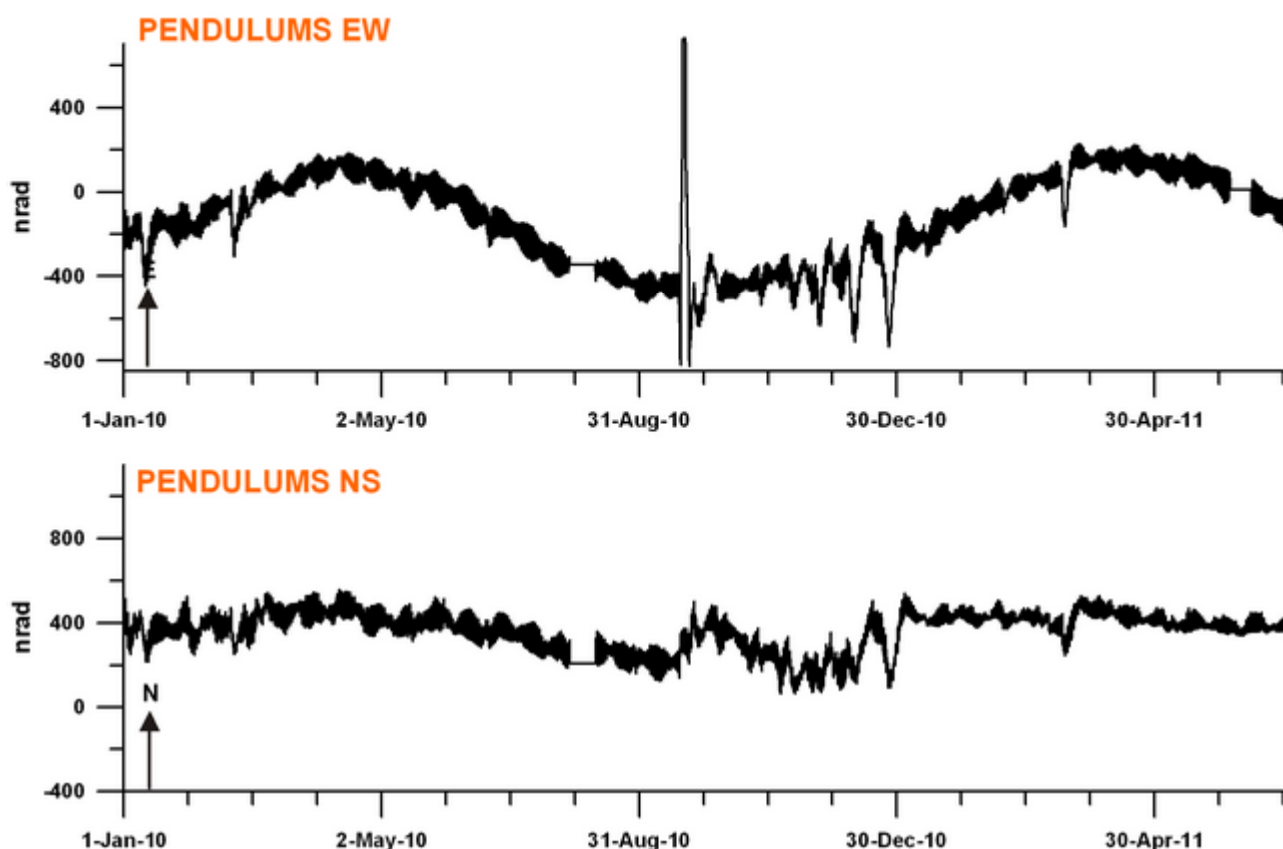
Fig. 3.4 – Registrazioni della coppia di pendoli LPHP ottenute dall'acquisizione digitale per il periodo 01/01/2010 – 30/06/2011, campionamento 1 ora.

Chiudiamo questo capitolo con la rappresentazione dell'andamento secolare del tilting in Grotta Gigante per tutta la serie temporale a disposizione, in un grafico che unisce le due componenti NS ed EW e mostra l'odogramma del vettore tilting nello spazio bi-dimensionale NS ed EW. Troviamo un tilting a lungo periodo orientato verso Nord-Ovest, un basculamento annuale ortogonale ad esso, in direzione NE-SW. Vedremo nel capitolo 6, che la direzione NE-SW corrisponde anche al tilting indotto dalle piene del reticolo sotterraneo carsico.
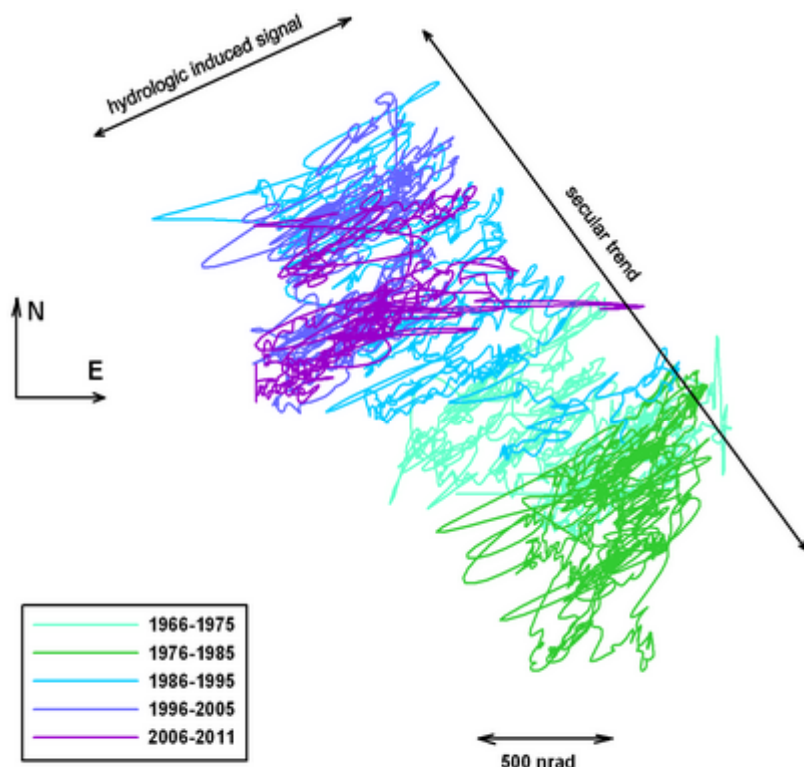
Fig. 3.5 – Movimento nel piano del vettore di inclinazione per l'intervallo dal 13/10/66 fino al 30/06/2011

4 -Osservazioni dei pendoli LPHP con acquisizione digitale nell'ambito di frequenze delle onde sismiche

Come accennato nel paragrafo 2, il sistema di acquisizione digitale dei pendoli LPHP preleva i dati ad una frequenza elevata: il sistema digitale di prima generazione (CCD) acquisiva i dati ad una frequenza di approssimativamente 15 campioni al secondo, mentre quello di seconda generazione (PSD) li preleva alla frequenza doppia di approssimativamente 30 campioni al secondo. Il sistema di acquisizione digitale fornisce quindi registrazioni nell'ambito delle onde sismiche. A partire da dicembre 2003 si è iniziata l'archiviazione sistematica di tutti gli eventi sismici di magnitudo elevata (M ≥ 6). La soglia e' stata abbassata al valore di M ≥ 4 per gli eventi piu' vicini, come per esempio quelli generati nell'area del Mediterraneo, dell'Adriatico e nello spazio Alpino. L'elenco di questi eventi e' riportato nella **Tab. 4.1**, e le rispettive registrazioni sono disponibili a richiesta. Gli eventi sono stati selezionati basandosi sul database del NEIC (2010-2011).

Tab.4.1 Maggiori eventi sismici rilevati dai pendoli della Grotta Gigante durante il periodo 01/01/10-30/06/11 (NEIC, 2010-2011). Selezione: Telesismi: M ≥ 6, eventi Mediterraneo, Adriatico, Alpi: M ≥ 4. I dati sono stati archiviati e sono disponibili a richiesta.

Selezione: Telesismi: M ≥ 6, eventi Mediterraneo: M ≥ 4
TABELLA GRAFICI TERREMOTI DATI DIGITALI INGV

No.	Località	Data	Ora	Mag	File grf, dat
460	Sandwich Isl.	05/01/10	04:56	6.7	10005-0507f.dat 050110Sandwich.grf
461	Solomon Isl.	05/01/10	12:16	6.8	10005-1214f.dat 050110Solomon.grf
			13:12	6.0	
462	Solomon Isl.	09/01/10	05:52	6.3	10009-0608f.dat 090110Solomom.grf
462	California	10/01/10	00:28	6.5	10010-0002f.dat 100110California.grf
463	Haiti	12/01/10	21:53	7.0	10012-2201f.dat 120110Haiti.grf
464	Greece	18/01/10	15:56	5.4	10018-1516f.dat 180110Greece.grf
465	Greece	22/01/10	00:47	5.4	10022-0001f.dat 220110Greece.grf
			00:51	5.2	
466	S.Indian Rid.	05/02/10	06:59	6.2	10036-0709fi.dat 050210SIndR.grf
467	Kuril Island	06/02/10	04:45	6.1	10037-0406f.dat 060210Kuril.grf
468	Japan	07/02/10	06:10	6.4	10038-0608f.dat 070210Japan.grf
469	Crete	11/02/10	21:57	5.3	10042-2122f.dat 110210Crete.grf
470	China-Russia	18/02/10	01:13	6.9	10049-0103f.dat 180210CRKNB.grf
471	Japan	26/02/10	20:31	7.0	10057-2023f.dat 260210Japan.grf
472	Chile	27/02/10	06:34	8.8	10058-0609f.dat 270210Chile.grf
			06:53	6.2	
			07:12	6.0	
			07:37	6.0	
			08:01	6.9	
			08:25	6.1	
473	Chile	28/02/10	11:26	6.1	10059-1113f.dat 280210Chile.grf
474	Chile	03/03/10	17:44	6.0	10062-1719f.dat 030310Chile.grf
475	Taiwan	04/03/10	00:19	6.4	10063-0002f.dat 040310TaiChi.grf
	Chile		02:00	6.1	
476	Chile	04/03/10	22:39	6.3	10063-2200f.dat 040310Chile.grf
477	Chile	05/03/10	11:47	6.6	10064-1113f.dat 050310Chile.grf
478	Indonesia	05/03/10	16:07	6.5	10064.1618f.dat 050310Indonesia.grf
479	Turkey	08/03/10	02:33	6.0	10067-0203f.dat 080310Turkey.grf
480	Chile	11/03/10	14:40	6.9	10070-1416f.dat 110310Chile.grf
			14:55	6.7	
			15:06	6.0	

481	Indonesia	14/03/10	00:58	6.4	10073-0103f.dat 140310Indonesia.grf
482	Japan	14/03/10	08:08	6.5	10073-0810f.dat 140310Japan.grf
483	Chile	15/03/10	11:08	6.1	10074-1113f.dat 150310Chile.grf
484	Chile	16/03/10	02:22	6.7	10075-0204f.dat 160310Chile.grf
485	Papua	20/03/10	14:01	6.2	10079-1416f.dat 200310Papua.grf
486	Andaman Is.	30/03/10	16:55	6.6	10089-1719f.dat 300310Andaman.grf
487	Mexico	04/04/10	22:41	7.2	10094-2201f.dat 040410Mexico.grf
488	Indonesia	06/04/10	22:15	7.7	10096-2201f.dat 060410Indonesia.grf
489	Solomon Isl.	11/04/10	09:41	6.8	10101-0911f.dat 110410Solomon.grf
490	Spain	11/04/10	22:08	6.3	10101-2200f.dat 110410Spain.grf
491	China	13/04/10	23:50	6.9	10103-2301f.dat 130410China.grf
492	Papua	17/04/10	23.15	6.2	10107-2301f.dat 170410Papua.grf
493	Crete	24/04/10	15:01	5.2	10114-1516f.dat 240410Crete.grf
494	Taiwan	26/04/10	03:00	6.5	10116-0305f.dat 260410Taiwan.grf
495	Bering Sea	30/04/10	23:12	6.4	10120-2301f.dat 300410Bering.grf
			23:16	6.0	
496	Chile	03/05/10	23:10	6.3	10123-2301f.dat 030510Chile.grf
497	Sumatra	05/05/10	16:29	6.5	10125-1618f.dat 050510Sumatra.grf
498	Peru	06/05/10	02:43	6.2	10126-0204f.dat 060510Peru.grf
499	Sumatra	09/05/10	06:00	7.2	10129-0609f.dat 090510Sumatra.grf
500	Brazil	24/05/10	16:18	6.5	10144-1618f.dat 240510Brazil.grf
501	N.M-Atl. R.	25/05/10	10:09	6.3	10145-1012f.dat 250510NMAR.grf
502	Ryukyu Isl.	26/05/10	08:53	6.4	10146-0911f.dat 260510Ryukyu.grf
503	India	31/05/10	19:52	6.4	10151-1921f.dat 310510India.grf
504	Vanuatu	09/06/10	23:23	6.0	10160-2301f.dat 090610Vanuatu.grf
505	Nicobar Isl.	12/06/10	19:27	7.5	10163-1922f.dat 120610Nicobar.grf
506	Japan	13/06/10	03:33	6.1	10164-0305f.dat 130610Japan.grf
507	Papua	16/06/10	03:06	6.2	10167-0306f.dat 160610Papua.grf
			03:16	7.0	
			03:58	6.6	
508	Mexico	30/06/10	07:22	6.3	10181-0709f.dat 300610Mexico.grf
509	Vanuatu	02/07/10	06:04	6.3	10183-0608f.dat 020710Vanuati.grf
510	Japan	04/07/10	21:56	6.3	10185-2200f.dat 040710Japan.grf
511	Mariana Isl.	10/07/10	11:44	6.2	10191-1113f.dat 100710Mariana.grf
512	Chile	14/07/10	08:32	6.5	10195-0810f.dat 140710Chile.grf
513	Alaska	18/07/10	05:57	6.7	10199-0608f.dat 180710Alaska.grf
514	Papua New G	18/07/10	13:04	6.9	10199-1316f.dat 180710Papua.grf
			13:53	7.3	
515	Alaska	18/07/10	19:48	6.0	10199-1921f.dat 180710Alaska_2.grf
516	Papua	20/07/10	19:18	6.3	10201-1921f.dat 200710Papua.grf

517	Philippines	23/07/10	22:08 22:51 23:15	7.3 7.6 7.4	10204-2201f.dat 230710Philippines. grf
518	Philippines	24/07/10	05:35	6.5	10205-0507f.dat 240710Philippines.g
519	Philippines	29/07/10	07:32	6.6	10210-0709f.dat 290710Philippines.g
520	Ecuador	12/08/10	11:54	7.1	10224-1215f.dat 120810Ecuador.grf
521	Mariana Isl.	13/08/10	21:20	6.9	10225-2123f.dat 130810Mariana.grf
522	Mariana Isl.	14/08/10	07:30	6.2	10226-0709f.dat 140810Mariana.grf
523	Mariana Isl.	14/08/10	23:01	6.6	10226-2301f.dat 140810Mariana_2.gr
524	Mauritius	16/08/10	03:31	6.3	10228-0305f.dat 160810Mauritus.grf
525	Mariana Isl.	18/08/10	16:28	6.3	10230-1618f.dat 180810Mariana.grf
526	Papua New G	20/08/10	17:56	6.1	10232-1820f.dat 200810Papua.grf
527	Ionian See	22/08/10	10:23	5.3	10234-1011f.dat 220810Ionian.grf
528	Mexico	24/08/10	02:12	6.1	10236-0204f.dat 240810Mexico.grf
529	Alaska	03/09/10	11:16	6.3	10246-1113f.dat 030910Alaska.grf
530	New Zealand	03/09/10	16:36	7.0	10246-1720f.dat 030910NewZ.grf
531	Fiji	07/09/10	16:14	6.3	10250-1618f.dat 070910Fiji.grf
532	Vanuatu	08/09/10	11:38	6.2	10251-1113f.dat 080910Vanuatu.grf
534	Chile	09/09/10	07:28	6.1	10252-0709f.dat 090910Chile.grf
535	Hindu Kush	17/09/10	19:21	6.2	10260-1921f.dat 170910HinduK.grf
536	Indonesia	29/09/10	17:10 17:11	6.2 7.2	10272-1720f.dat 290910Indonesia.grf
537	Japan	04/10/10	13:29	6.3	10277-1315f.dat 041010Japan.grf
538	Alaska	08/10/10	03:26 03:49	6.4 6.1	10281-0305f.dat 081010Alaska.grf
549	Gulf of Calif.	21/10/10	17:53	6.7	10294-1820f.dat 211010GCalif.grf
550	Indonesia	25/10/10	14:42	7.7	10298-1417f.dat 251010Indonesia.grf
551	Indonesia	25/10/10	19:38	6.1	10298-1921f.dat 251010Ind_2.grf
552	Pac.Ant.Rid.	30/10/10	15:19	6.4	10303-1517f.dat 301010PARidge.grf
553	S. Indian Rid.	10/11/10	04:05	6.3	10314-0406f.dat 101110SIRidge.grf
554	Bonin Islands	30/11/10	03:25	6.8	10334-0305f.dat 301110Bonin.grf
555	Papua New G	02/12/10	03:12	6.7	10336-0305f.dat 021210Papua.grf
556	S. Sandwich	08/12/10	05:25	6.5	10342-0507f.dat 081210Ssandwich.gr
557	Iran	20/12/10	18:42	6.5	10354-1820f.dat 201210Iran,grf
558	Bonin Island	21/12/10	17:20	7.4	10355-1720f.dat 211210Bonin.grf
559	Bonin Island	22/12/10	21:50	6.3	10356-2123f.dat 221210Bonin.grf
560	Alaska	23/12/10	14:01	6.2	10357-1416f.dat 231210Alaska.grf
561	Vanuatu	25/12/10	13:17	7.3	10359-1316f.dat 251210Vanuatu.grf
562	Vanuatu	29/12/10	06:54	6.4	10363-0709f.dat 291210Vanuatu.grf
563	Argentina	01/01711	09:57	7.0	11001-1013f.dat 010111Argentina.grf

564	Chile	02/01/11	20:20	7.1	11002-2023f.dat 020111Chile.grf
565	Vanuatu	09/01/11	10:04	6.6	11009-1012f.dat 090111Vanuatu.grf
566	Loyality Isl.	13/01/11	16:17	7.0	11013-1619f.dat 130111Loyality.grf
567	Pakistan	18/01/11	20:23	7.2	11018-2023f.dat 180111Pakistan.grf
568	Tajikistan	24/01/11	02:46	6.1	11024-0204f.dat 240111Tajikistan.grf
569	Iran	27/01/11	08:38	6.0	11027-0810f.dat 270111Iran.grf
570	Celebes Sea	10/02/11	14:39	6.5	11041-1416f.dat 100211Celebes.grf
			14:42	6.7	
571	Chile	11/02/11	20:06	6.8	11042-2022f.dat 110211Chile.grf
572	Chile	12/02/11	01:17	6.1	11043-0103f.dat 120211Chile.grf
573	Chile	14/02/11	03:40	6.6	11045-0305f.dat 140211Chile.grf
574	Indonesia	15/02/11	13:34	6.1	11046-1315f.dat 150211Indonesia.grf
575	Fiji	21/02/11	10:58	6.4	11052-1113f.dat 210211Fiji.grf
576	Crete	28/02/11	07:49	5.2	11059-0708f.dat 280211Crete.grf
577	Easter Island	01/03/11	00:54	6.0	11060-0103f.dat 010311EasterI.grf
578	S. Sandwich	06/03/11	14:33	6.5	11065-1416f.dat 060311Sandwich.grf
579	Solomon Isl.	07/03/11	00:10	6.6	11066-0002f.dat 070311Solomon.grf
580	Japan	09/03/11	02:45	7.2	11068-0306f.dat 090311Japan.grf
581	Japan	09/03/11	18:16	6.1	11068-1820f.dat 090311Japan_2.grf
			18:45	6.0	
582	Japan	09/03/11	21:22	6.1	11068-2123f.dat 090311Japan_3.grf
	Papua		21:25	6.5	
583	Bali Sea	10/03/11	17:09	6.5	11069-1719f.dat 100311Bali.grf
584	Japan	11/03/11	05:46	9.0	11070-0609f.dat 110311Japan.grf
			06:06	6.4	
			06:07	6.4	
			06:16	6.8	
			06:26	7.1	
			06:49	6.3	
			06:57	6.3	
			07:15	6.3	
			07:26	6.1	
			07:28	6.1	
			08:12	6.2	
			08:16	6.2	
			08:19	6.5	
			08:31	6.1	
585	Japan	11/03/11	10:11	6.0	11070-1012f.dat 110311Japan_2.grf
			11:37	6.5	
586	Japan	11/03/11	15:13	6.2	11070-1517f.dat 110311Japan_3.grf

587	Japan	11/03/11	18:59	6.2	11070-1820f.dat 110311Japan_4.grf
			19:03	6.1	
			19:47	6.6	
			20:11	6.3	
588	Tonga	12/03/11	01:19	6.1	11071-0103f.dat 120311To_Ja.grf
	Japan		01:34	6.0	
			01:46	6.2	
			01:47	6.8	
589	Japan	12/03/11	13:16	6.4	11071-1315f.dat 120311Japan.grf
590	Japan	12/03/11	17:29	6.0	11071-1719f.dat 120311Japan_2.grf
591	Japan	12/03/11	22:13	6.3	11071-2200f.dat 120311japan_3.grf
			23:25	6.1	
592	Japan	13/03/11	01:26	6.2	11072-0103f.dat 130311Japan.grf
			02:24	6.2	
593	Japan	13/03/11	11:38	6.0	11072-1113f.dat 130311Japan_2.grf
594	Japan	14/03/11	06:13	6.1	11073-0608f.dat 140311Japan.grf
595	Japan	15/03/11	09:50	6.0	11074-0911f.dat 150311Japan.grf
596	Japan	15/03/11	13:32	6.2	11074-1315f.dat 150311Japan_2.grf
597	Japan	15/03/11	15:24	6.1	11074-1517f.dat 150311Japan_3.grf
598	Japan	16/03/11	03:52	6.0	11075-0406f.dat 160311Japan.grf
599	Japan	17/03/11	04:14	6.1	11076-0406f.dat 170311Japan.grf
600	Japan	19/03/11	09:57	6.1	11078-1012f.dat 190311Japan.grf
601	Japan	22/03/11	07:19	6.6	11081-0709f.dat 220311Japan.grf
602	Japan	22/03/11	09:19	6.4	11081-0911f.dat 220311Japan_2.grf
			09:44	6.6	
603	S. Mid-Atl. R	22/03/11	13:31	6.1	11081-1416f.dat 220311Japan_3.grf
	Japan		15:04	6.1	
604	Japan	24/03/11	08:21	6.1	11083-0810f.dat 240311Japan.grf
605	Myanmar	24/03/11	13:55	6.8	11083-1416f.dat 240311Myanmar.grf
606	Japan	25/03/11	11:36	6.4	11084-1113f.dat 250311Japan.grf
607	Japan	27/03/11	22:24	6.1	11086-2200f.dat 270311Japan.grf
608	Japan	29/03/11	10:55	6.1	11088-1113f.dat 290311Japan.grf
609	Japan	30/03/11	05:30	6.0	11089-0507f.dat 300311Japan.grf
610	Fiji	31/03/11	00:12	6.4	11090-0002f.dat 310311Fiji.grf
611	Japan	31/03/11	07:16	6.2	11090-0709f.dat 310311Japan.grf
612	Indonesia	03/04/11	20:07	6.7	11093-2022f.dat 030411Indonesia.grf
613	Indonesia	05/04/11	11:14	6.0	11095-1113f.dat 050411Indonesia.grf
614	Mexico	07/04/11	13:11	6.5	11097-1315f.dat 070411Mexico.grf
615	Japan	07/04/11	14:33	7.1	11097-1417f.dat 070411Japan.grf
616	Japan	09/04/11	12:58	6.1	11099-1315f.dat 09041Japan.grf

617	Japan	11/04/11	08:16	6.6	11101-0810f.dat 110411Japan.grf
618	Japan	11/04/11	23:08	6.2	11101-2301f.dat 110411Japan_2.grf
619	Japan	12/04/11	05:08	6.0	11102-0507f.dat 120411Japan.grf
620	Japan	13/04/11	19:57	6.1	11103-2022f.dat 130411Japan.grf
621	Kermadec I.	18/04/11	13:03	6.6	11108-1315f.dat 180411Kermades.grf
622	Japan	21/04/11	01:55	6.0	11111-0204f.dat 210411Japan.grf
623	Solomon I.	23/04/11	04:17	6.9	11113-0406f.dat 230411Solomon.grf
624	Japan	23/04/11	10:13	6.0	11113-1012f.dat 230411Japan.grf
625	Japan	05/05/11	14:58	6.1	11125-1517f.dat 050511Japan.grf
626	Greece	08/05/11	06:50	5.1	11128-0607f.dat 080511Greece.grf
627	Loyality Isl.	10/05/11	08:55	6.8	11130-0911f.dat 100511Loyalty.grf
628	Japan	13/05/11	23:36	6.2	11133-2301f.dat 130511Japan.grf
629	CMAtl. Ridg.	15/05/11	13:08	6.0	11135-1315f.dat 150511CMARidge.g
630	Papua	15/05/11	18:37	6.5	11135-1820f.dat 150511Papua.grf
631	W. Turkey	29/05/11	20:15	5.8	11139-2021f.dat 190511Turkey.grf
632	Chile	01/06/11	12:55	6.2	11152-1315f.dat 010611Chile.grf
634	Japan	03/06/11	00:05	6.3	11154-0002f.dat 030611Japan.grf
635	Macquari Isl.	05/06/11	11:51	6.3	11156-1214f.dat 050611Macquary.grf
636	Molucca Sea	13/06/11	14:31	6.4	11164-1416f.dat 130611Molucca.grf
637	Papua	16/06/11	00:04	6.6	11167-0002f.dat 160611Papua.grf
638	Chile	20/06/11	16:36	6.5	11171-1618f.dat 200611Chile.grf
639	Japan	22/06/11	21:51	6.7	11173-2200f.dat 220611Japan.grf
640	Alaska	24/06/11	03:10	7.2	11175-0306f.dat 240611Alaska.grf
641	Indonesia	26/06/11	12:17	6.3	11177-1214f.dat 260611Indonesia.grf

Allo scopo di isolare le osservazioni sismologiche dal restante segnale osservato, è stato applicato un filtro al coseno di passa banda, con periodi di taglio di 120 sec e 4 sec, rispettivamente. La limitazione nella frequenza superiore e' dettata dalla soglia di rumore della registrazione. E' stato calcolato lo spettro di ampiezza medio per le sequenze di cui sopra, ed e' stata stimata la frequenza superiore, alla quale lo spettro devia dalla relazione lineare nella rappresentazione bi-logaritmica. Tale frequenza è stata stimata a 0.25 Hz. La frequenza inferiore e' stata scelta in modo da eliminare le periodicità lunghe, ed e' stata scelta pari a 0.0167 Hz, che corrisponde al periodo di 120 sec. I dati filtrati passa banda sono rappresentati nelle **Fig. 4.1 A-Z**, per una selezione degli eventi disponibili.

A)
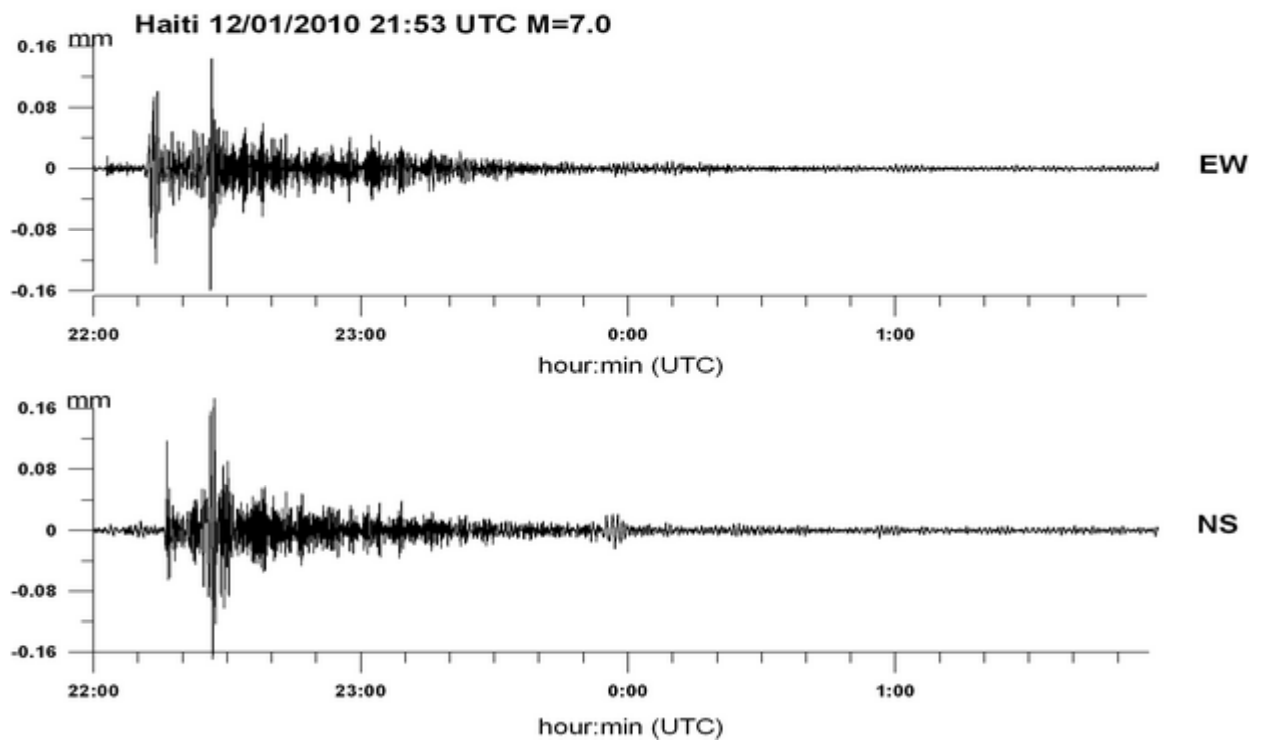
Fig. 4.1 (A-Z) – Registrazione di alcuni eventi sismici di magnitudo rilevante avvenuti durante il periodo dal 01 gennaio 2010 a 30 giugno 2011 (vedi Tab. 4.1). I dati originali sono stati filtrati con un filtro passa banda con banda passante per le frequenze comprese fra 0.0167 Hz e .25 Hz.

B)

Japan 26/02/2010 20:31 UTC M=7.0

EW

NS

C)

Chile 27/02/2010 06:34 UTC M=8.8
06:53 UTC M=6.2
07:12 UTC M=6.0
07:37 UTC M=6.0
08:01 UTC M=6.9
08:25 UTC M=6.1

EW

NS
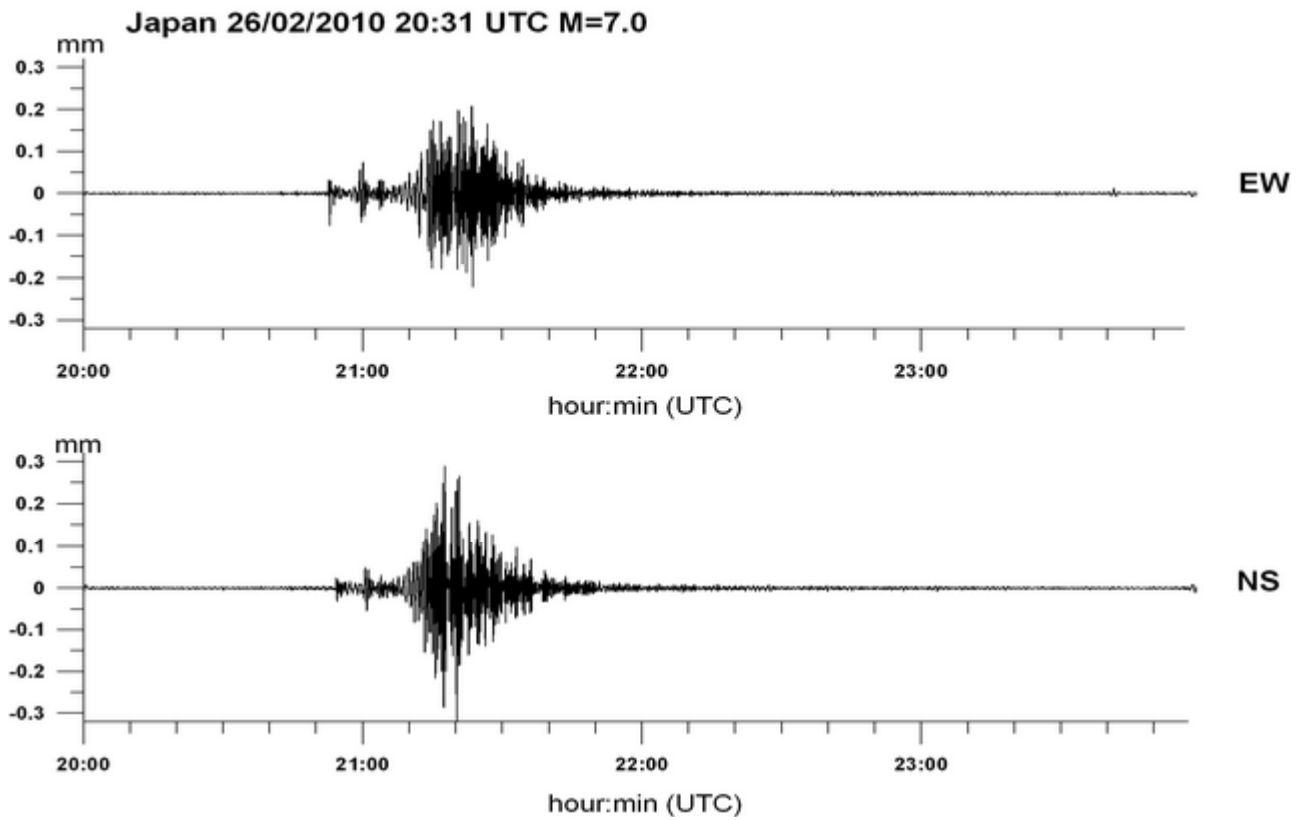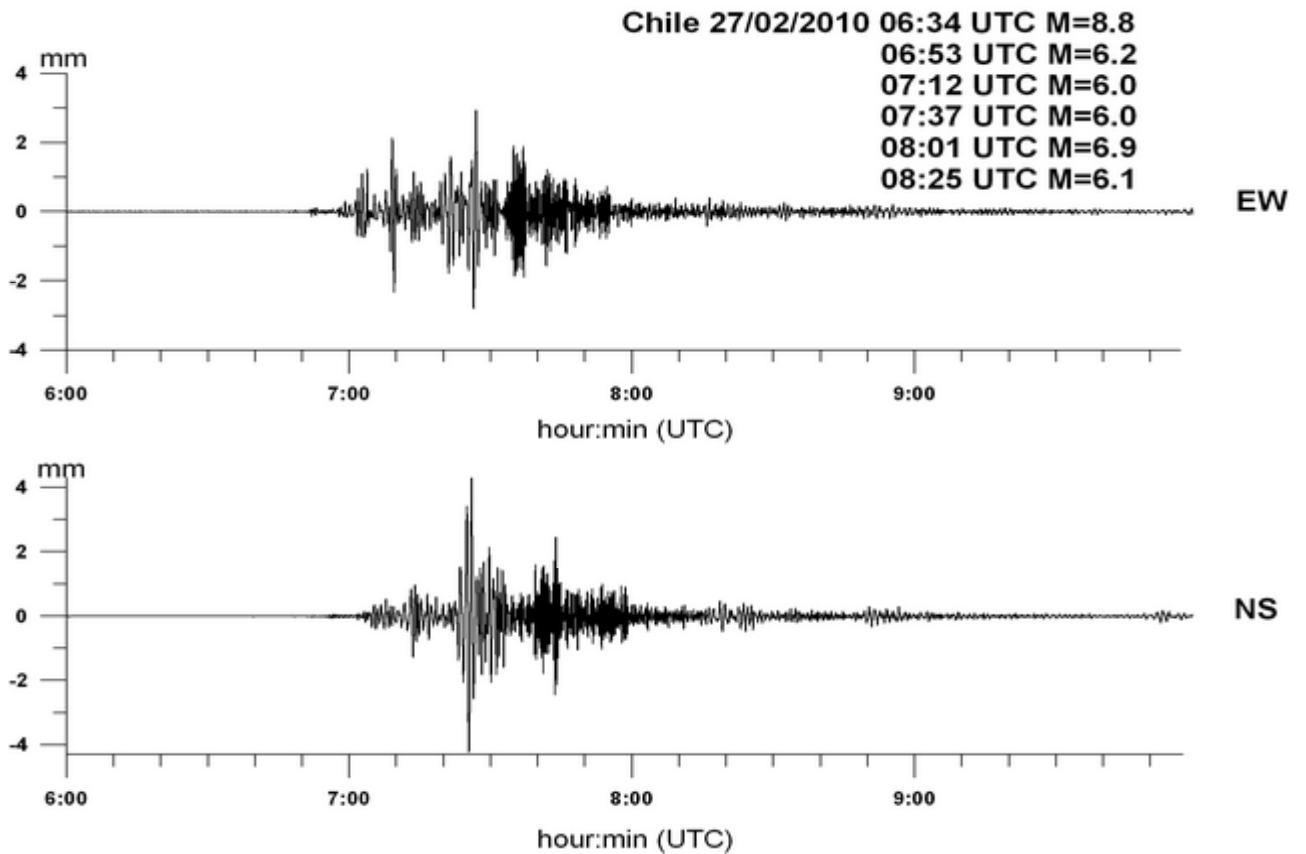
D) Japan 14/03/2010 08:08 UTC M=6.5

EW

NS
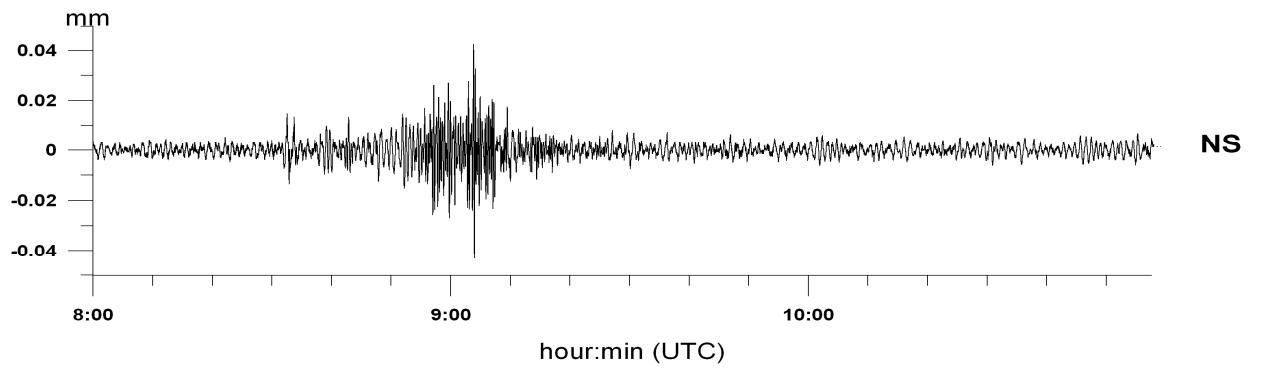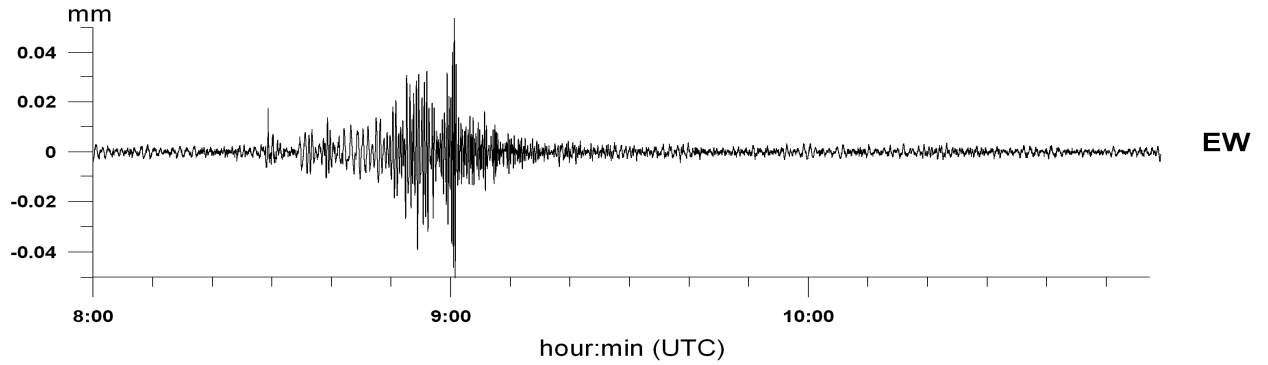
E) Mexico 04/04/2010 22:41 UTC M=7.2

EW

NS
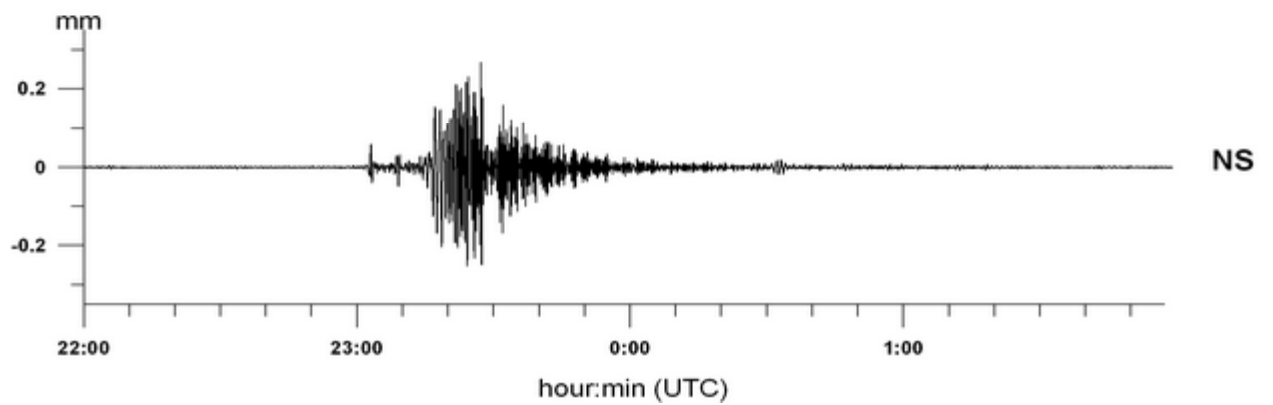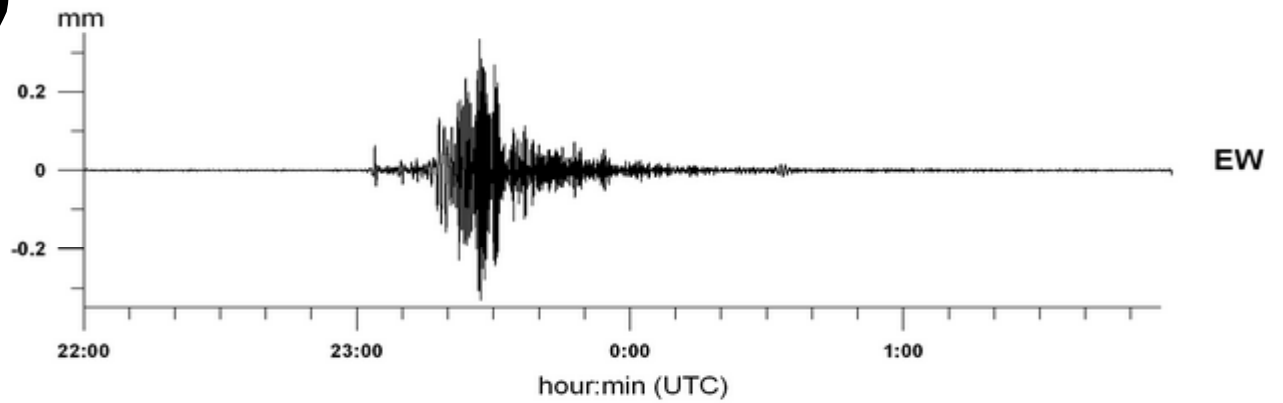
F)

Indonesia 06/04/2010 22:15 UTC M=7.7

EW

NS
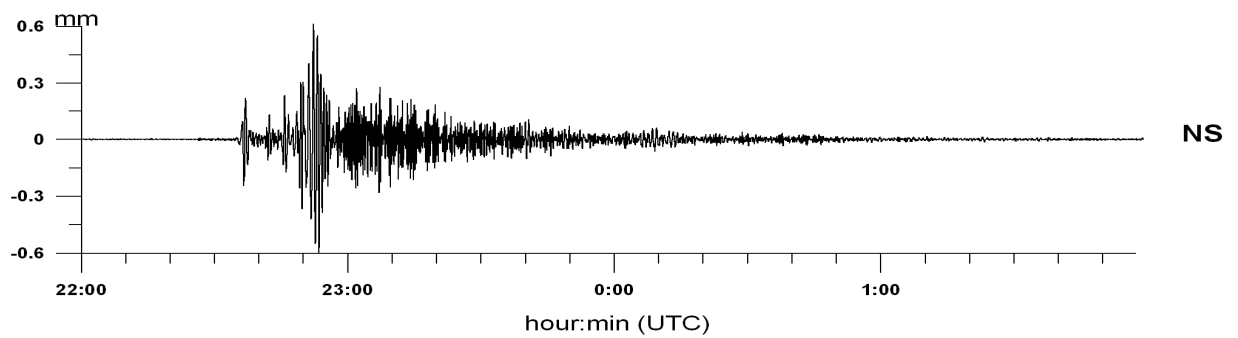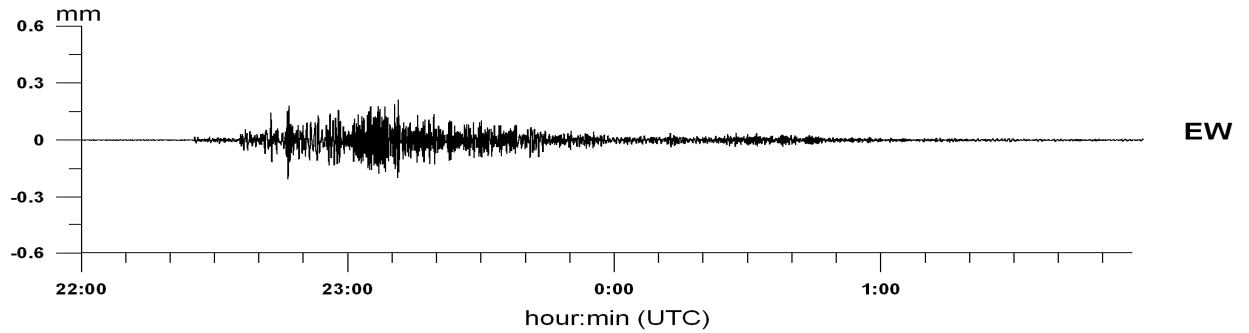
G)

Sumatra 09/05/2010 06:00 UTC M=7.2

EW

NS
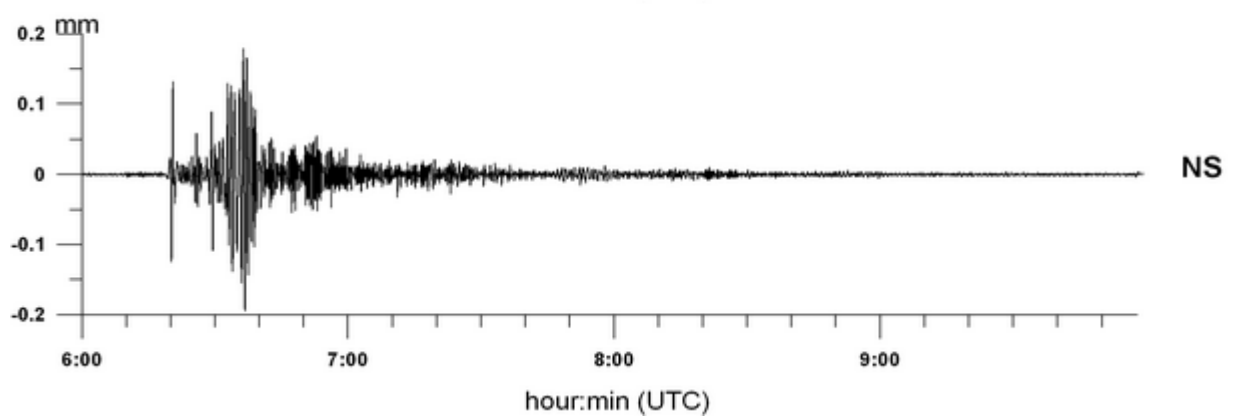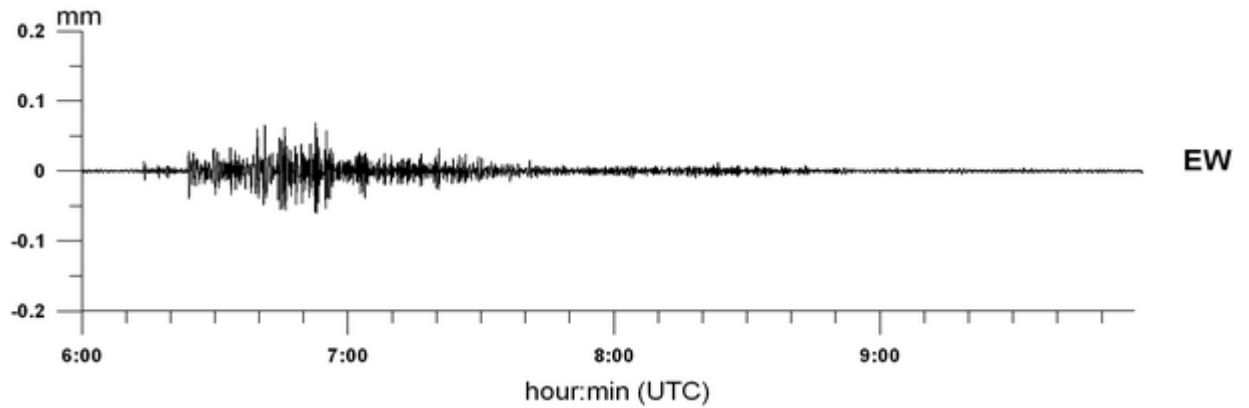
H)

Nicobar Islands, India Region 12/06/2010 19:27 UTC M=7.5

EW

NS
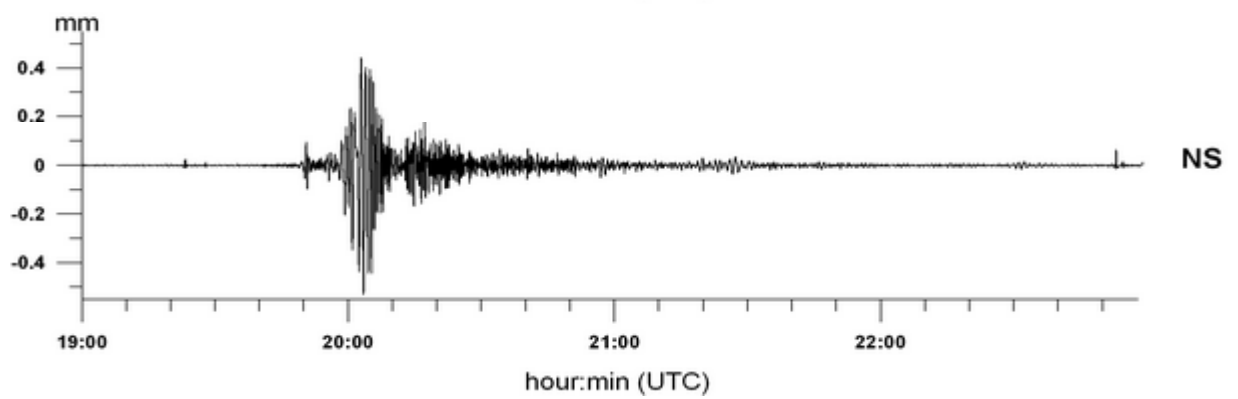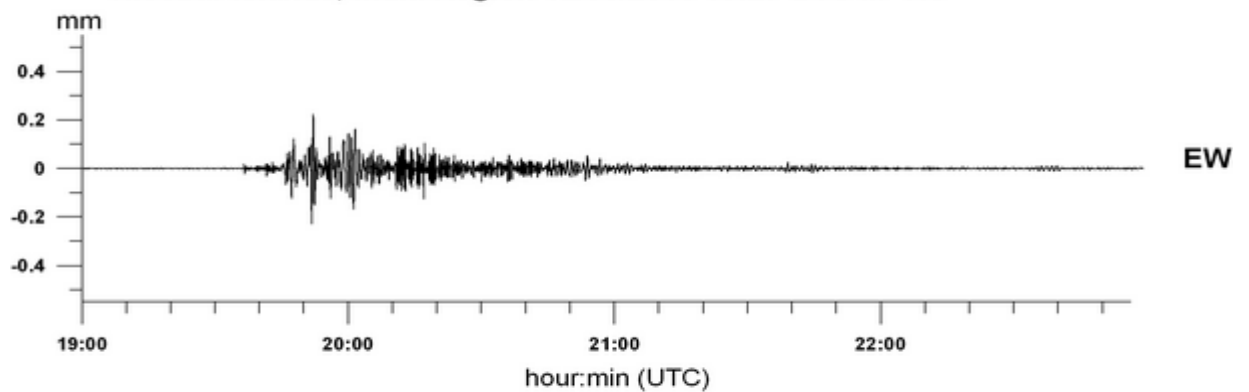
I)

Papua 16/06/2010 03:06 UTC M=6.2
03:16 UTC M=7.0
03:58 UTC M=6.6

EW

NS
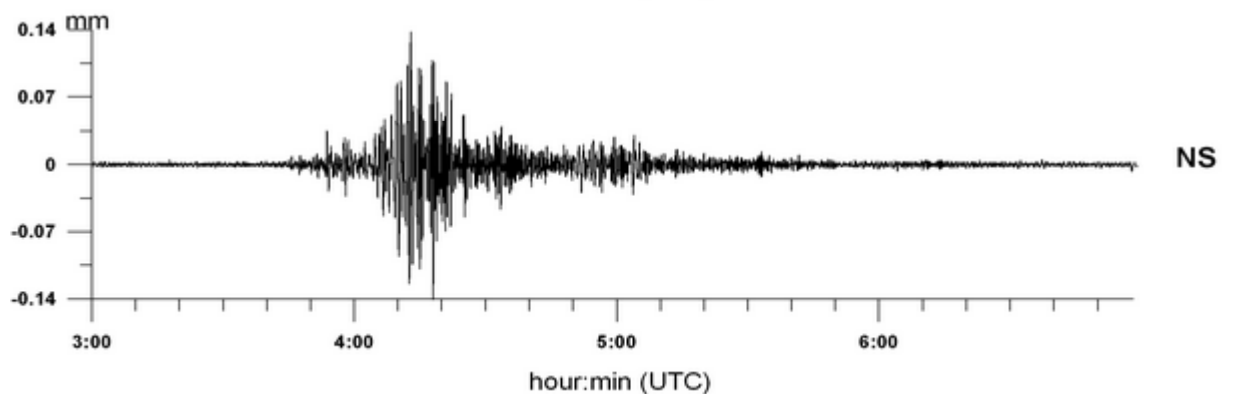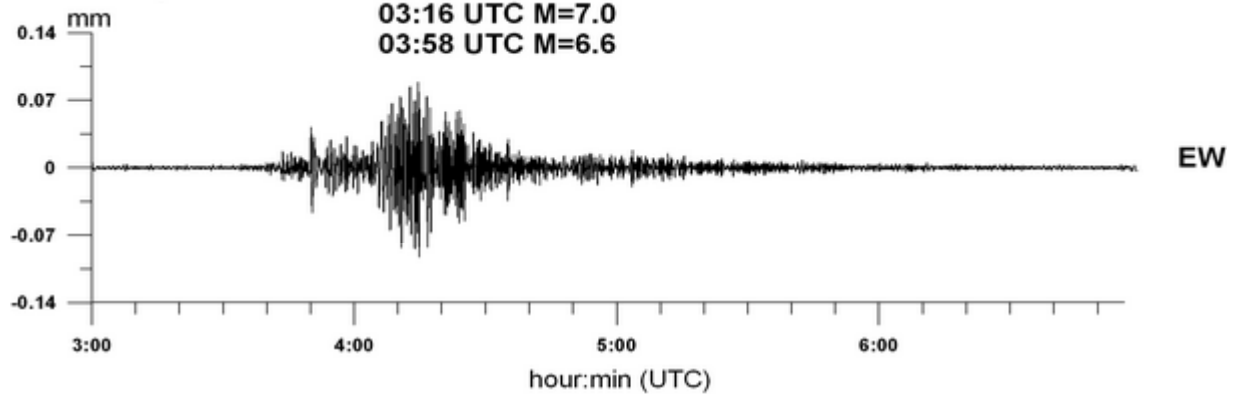
J) Papua New Guinea 18/07/2010 13:04 UTC M=6.9
13:53 UTC M=7.3
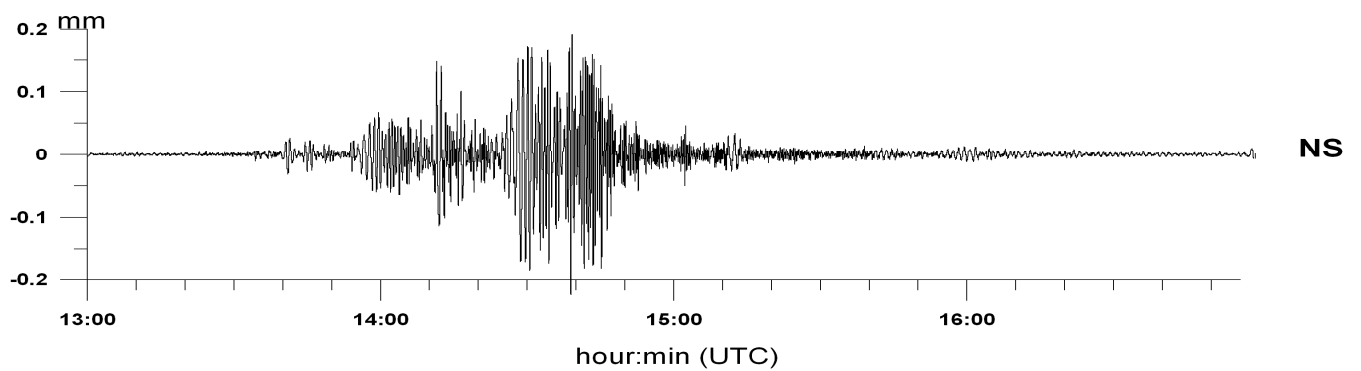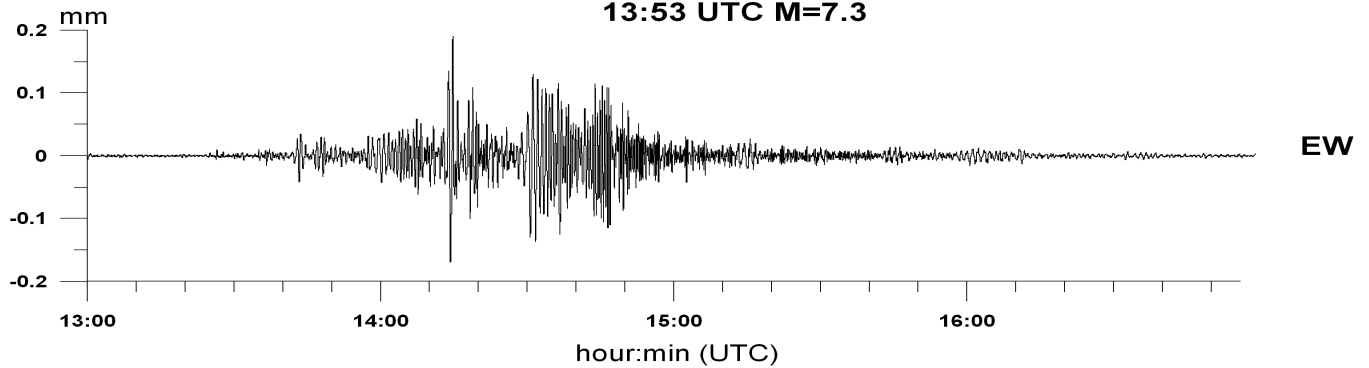
K) Philippines 23/07/2010 22:08 UTC M=7.3
22:51 UTC M=7.6
23:15 UTC M=7.4
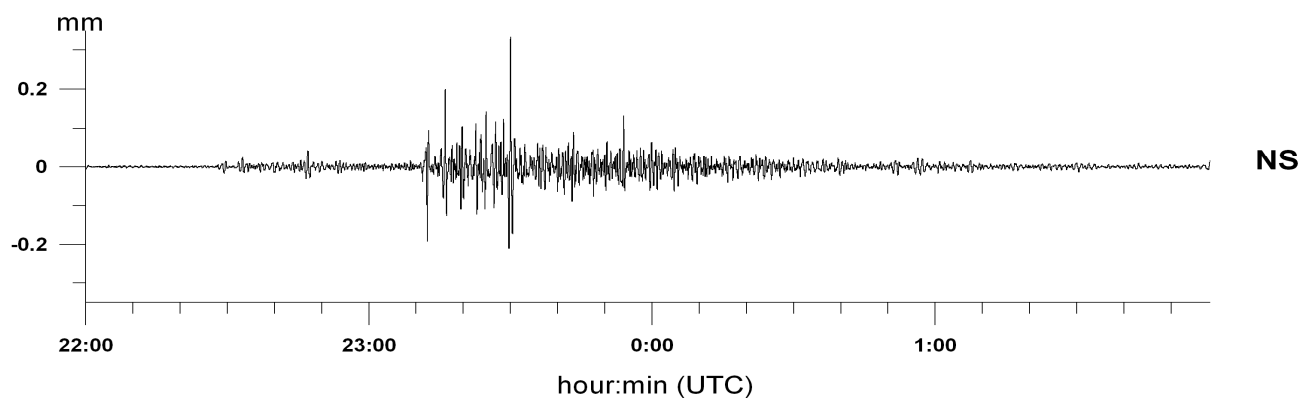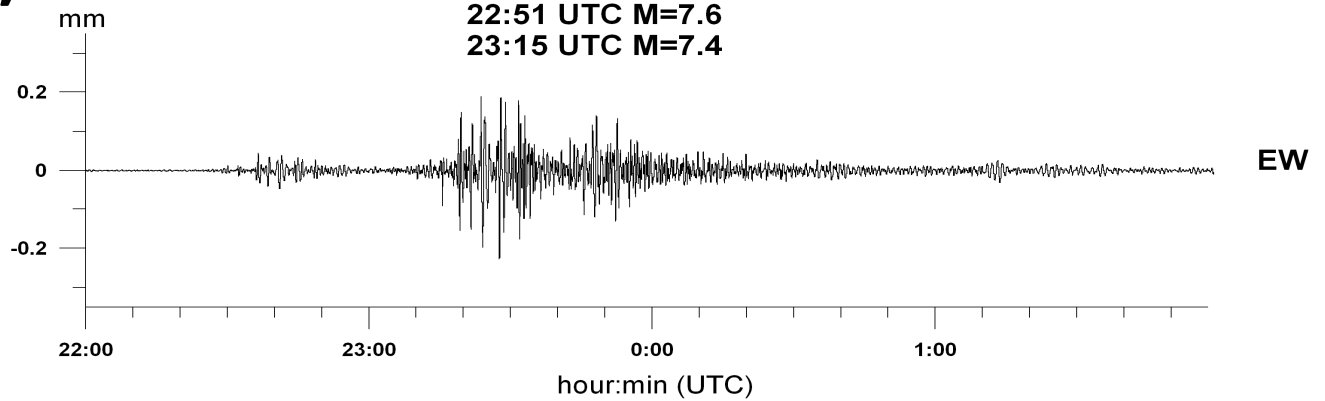
L)

Ecuador 12/08/2010 11:54 UTC M=7.1
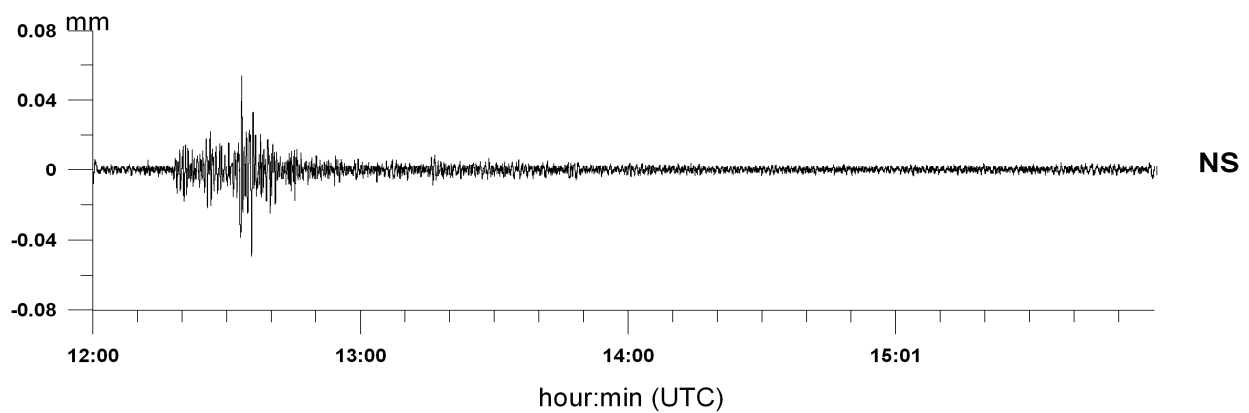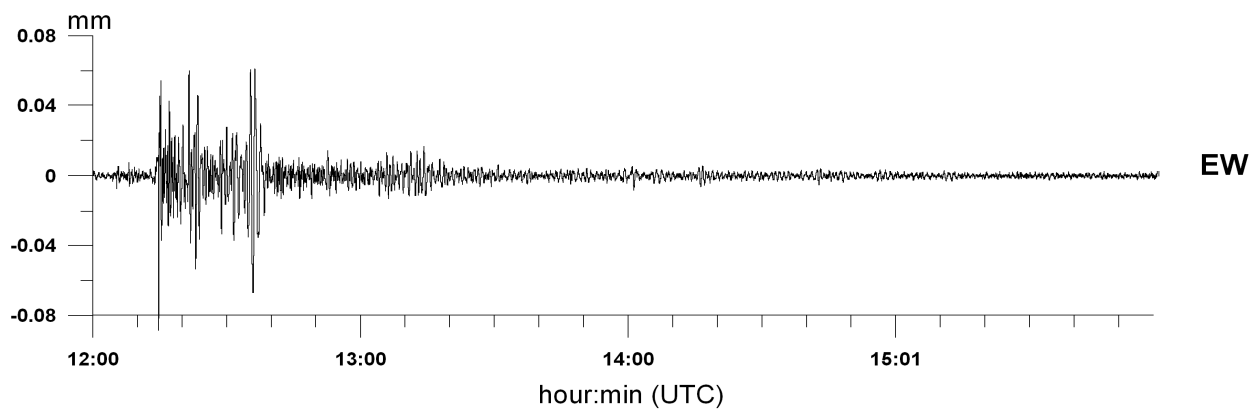
M)

Mariana Islands 13/08/2010 21:20 UTC M=6.9
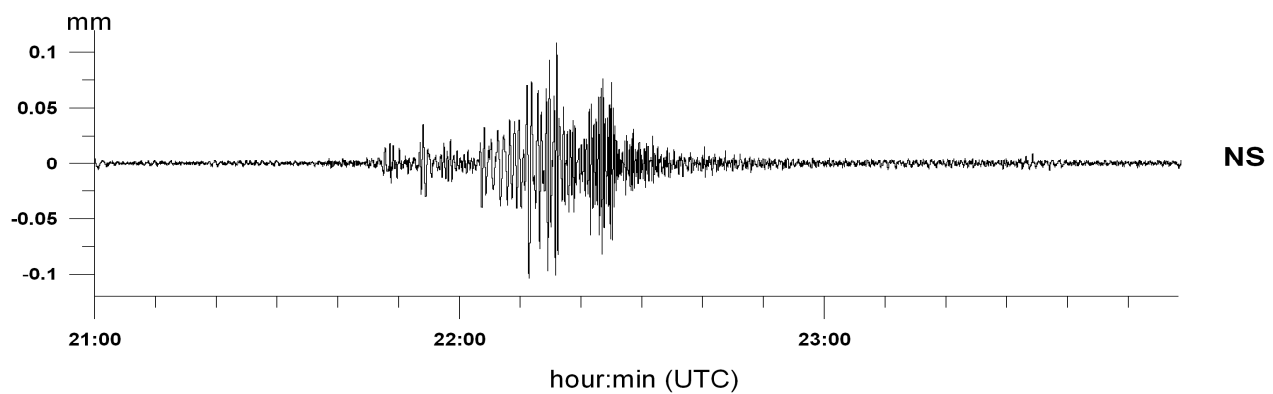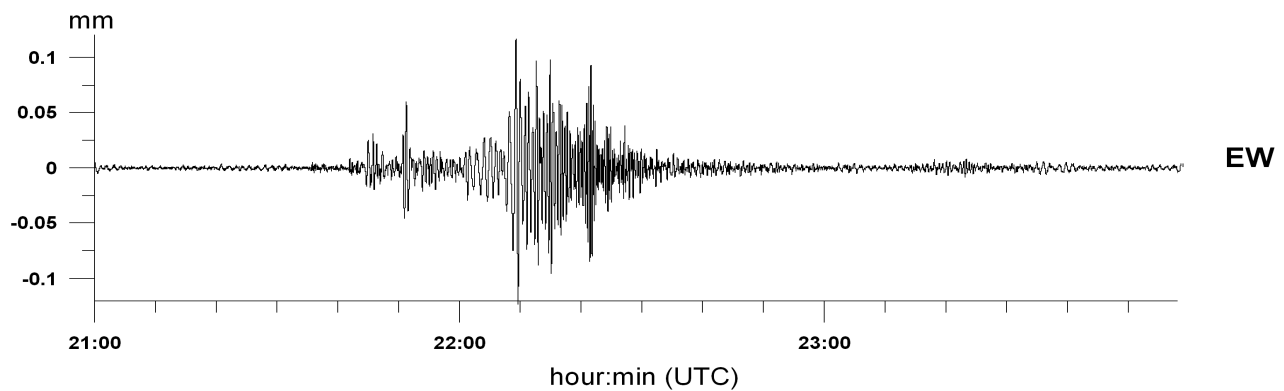
N)

## South Island of New Zealand 03/09/2010 16:36 UTC M=7.0
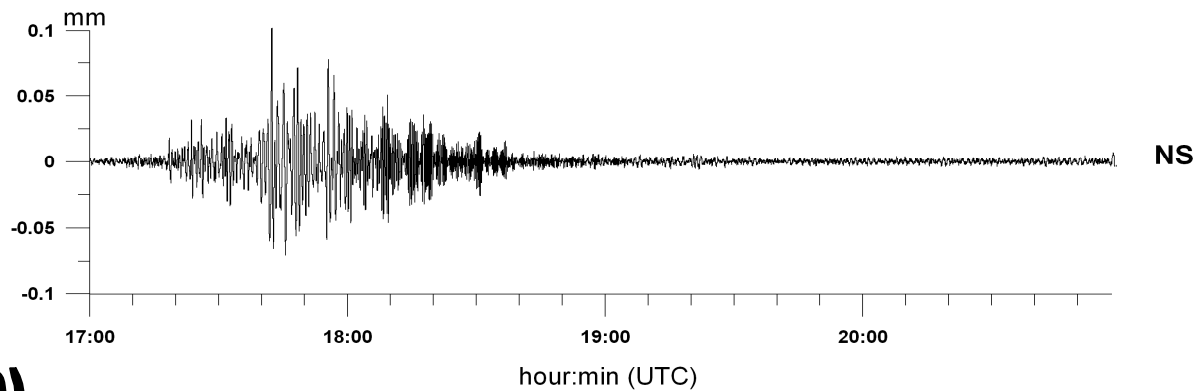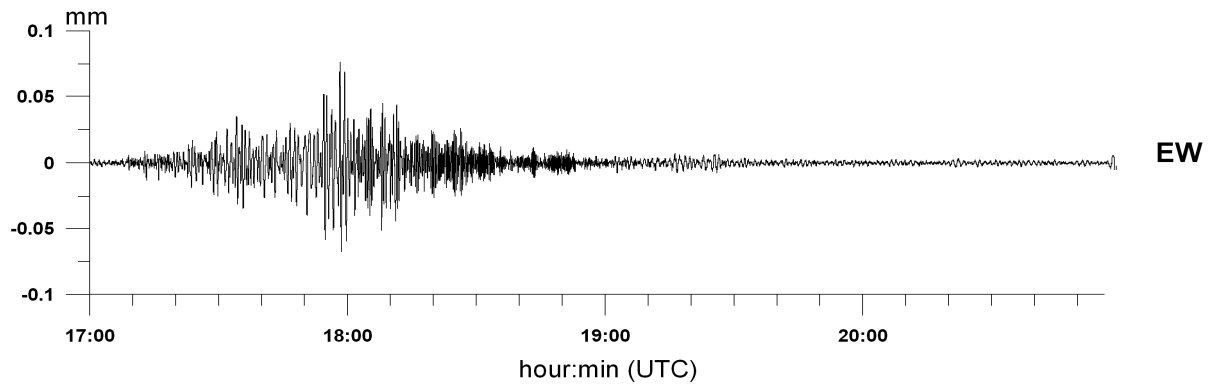
O)

## Gulf of California 21/10/2010 17:53 UTC M=6.7
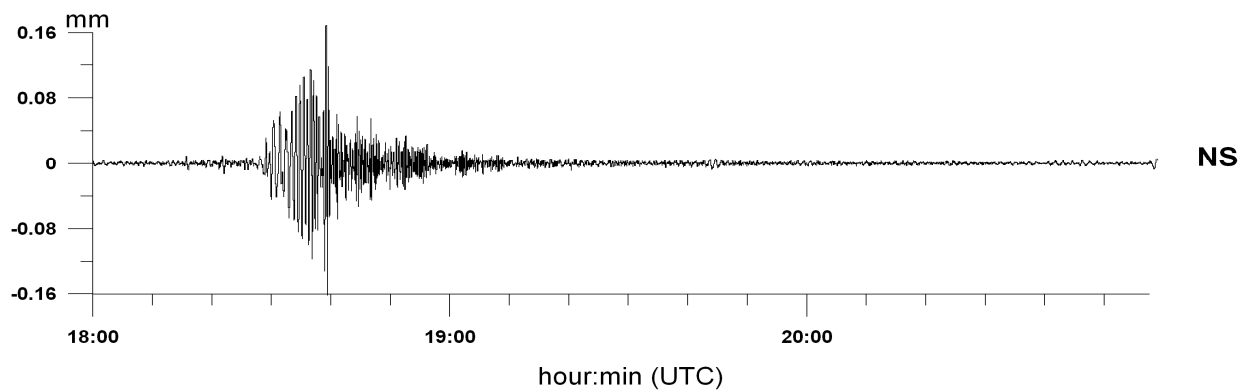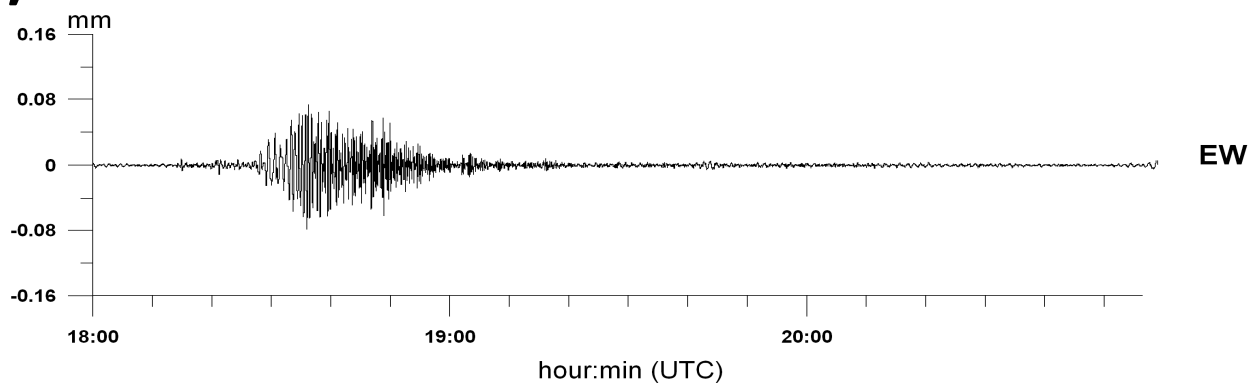
P) Indonesia 25/10/2010 14:42 UTC M=7.7

EW

NS
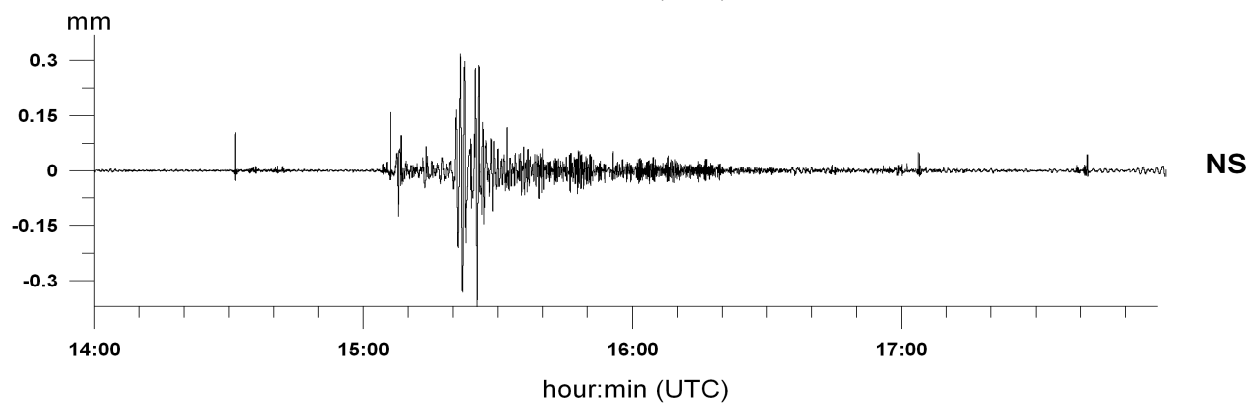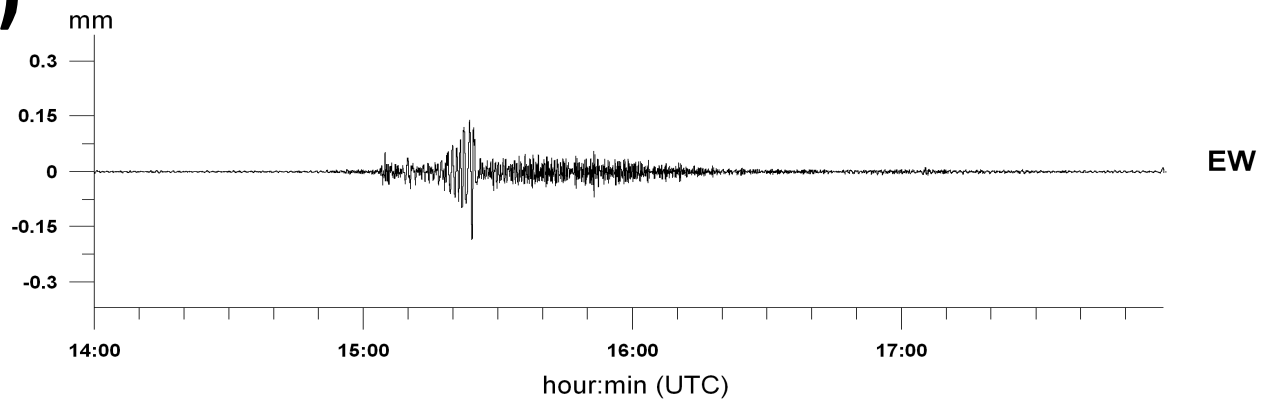
Q) Vanuatu 25/12/2010 13:17 UTC M=7.3

EW

NS
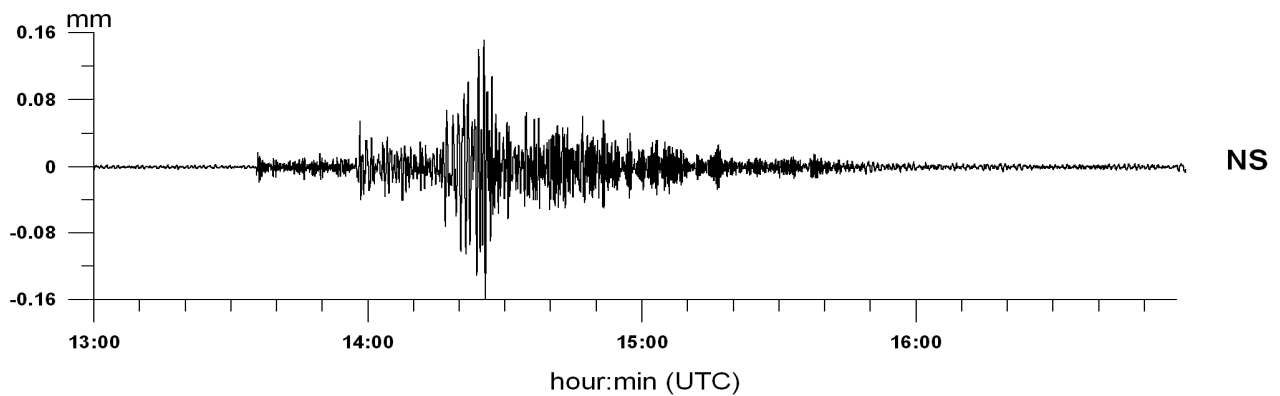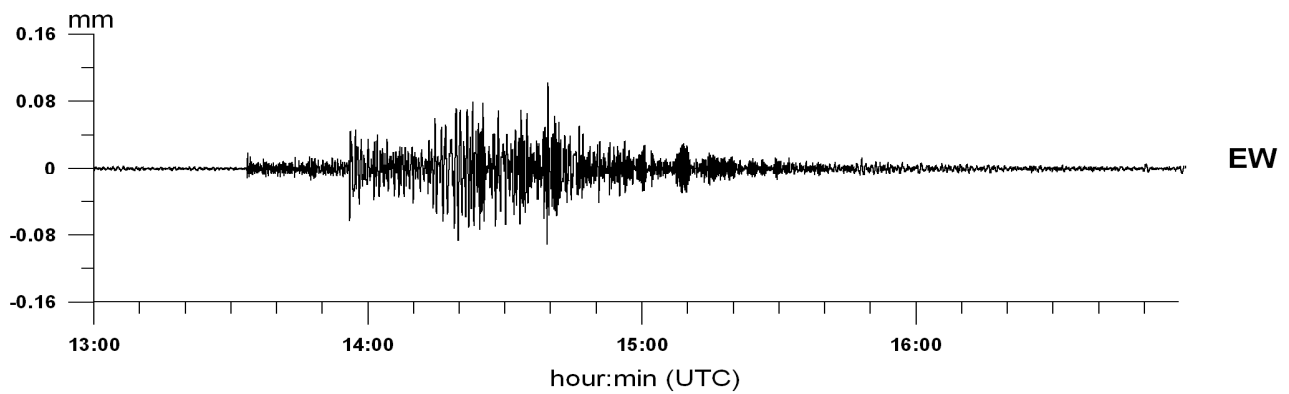
R) Chile 02/01/2011 20:20 UTC M=7.1
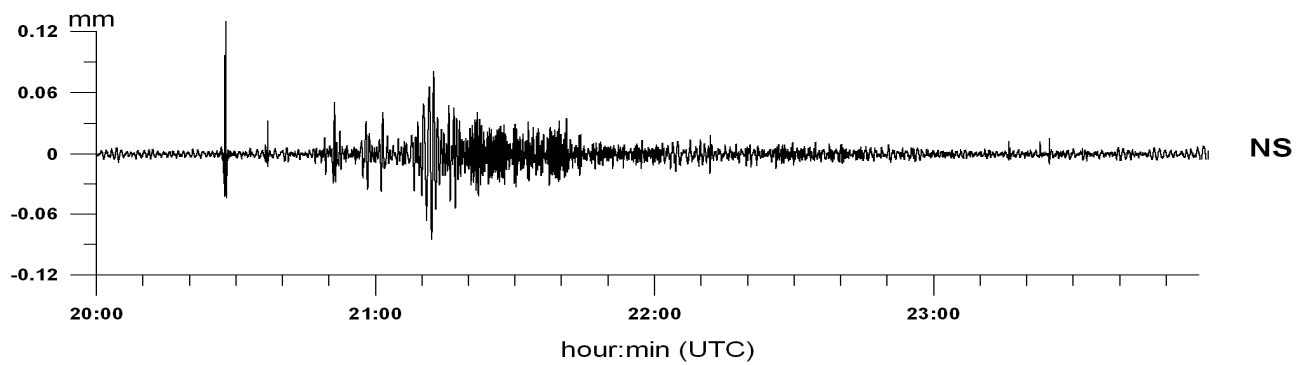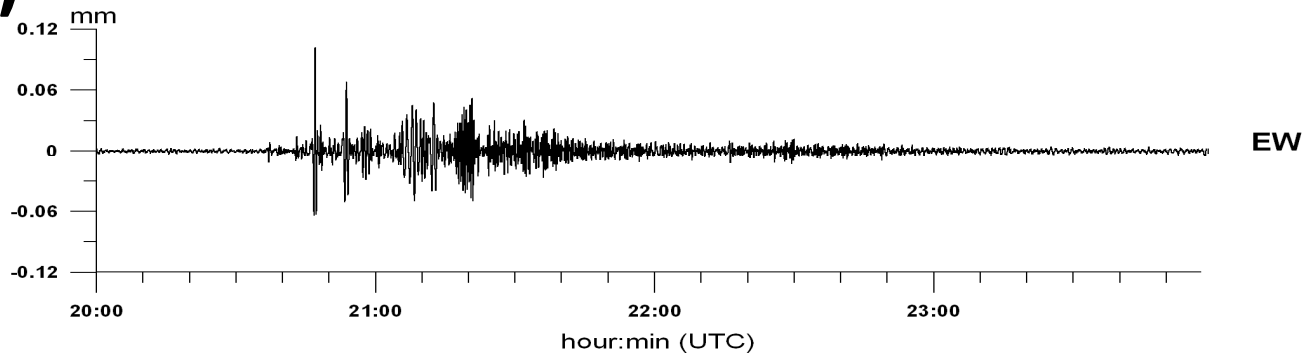
S) Loyality Islands 13/01/2011 16:17 UTC M=7.0
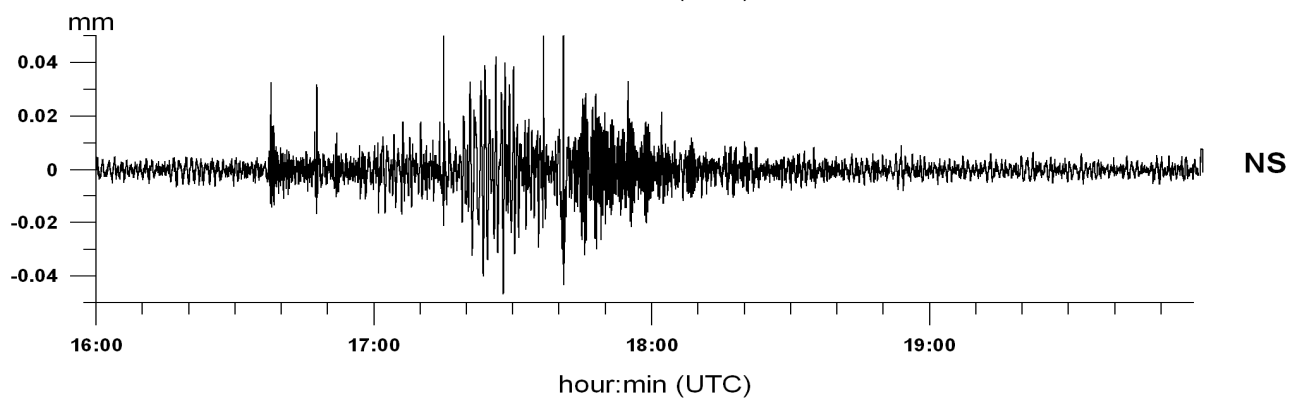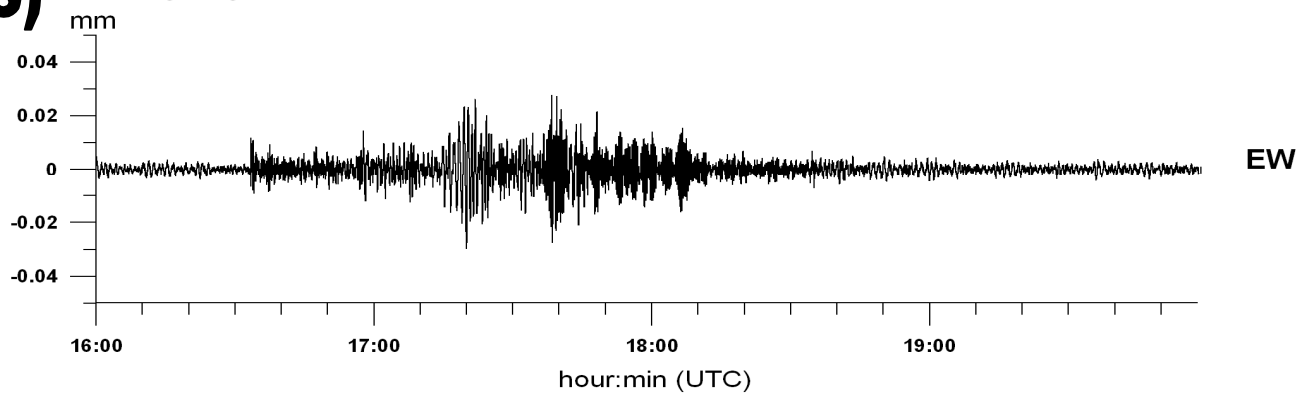
T)

Pakistan 18/01/2011 20:23 UTC M=7.2

EW

NS
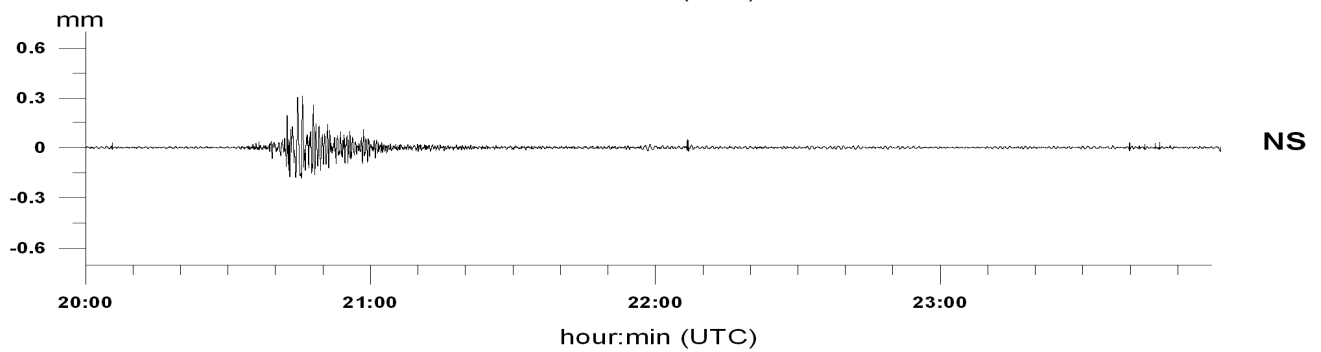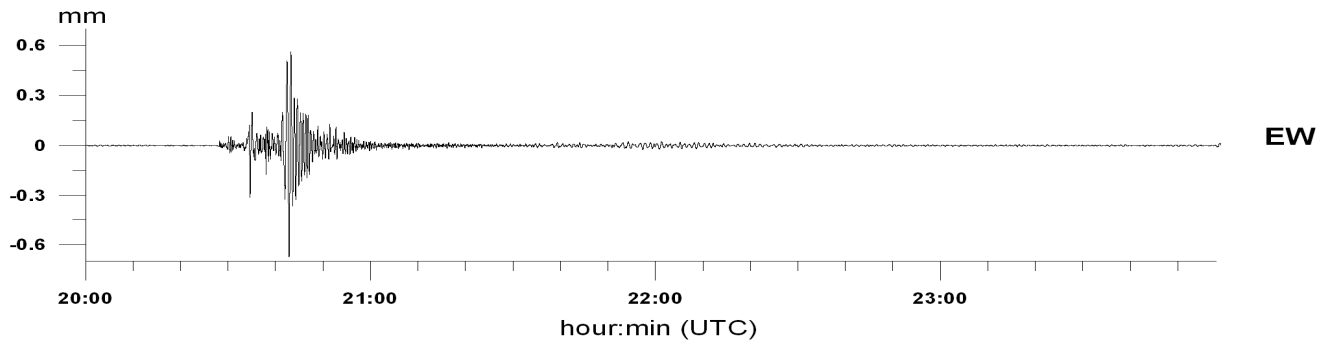
U)

Japan 09/03/2011 02:45 UTC M=7.2

EW

NS
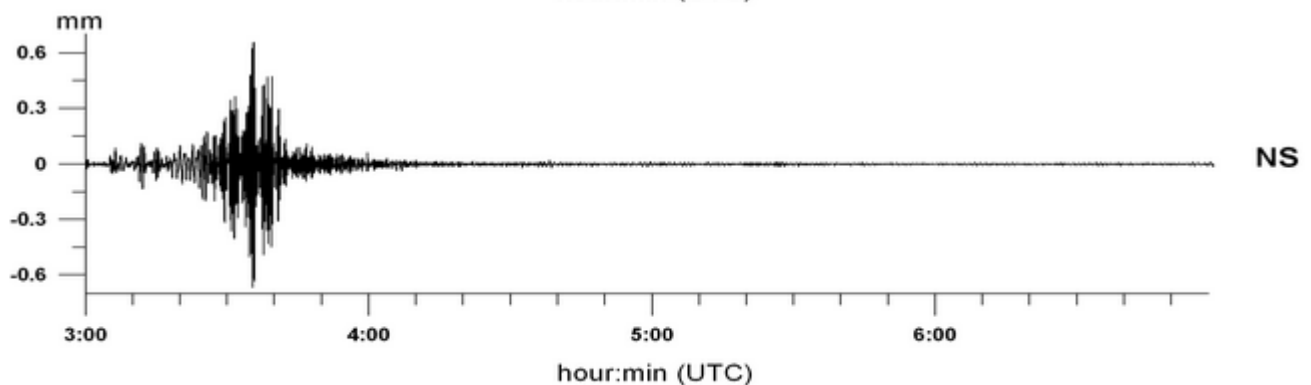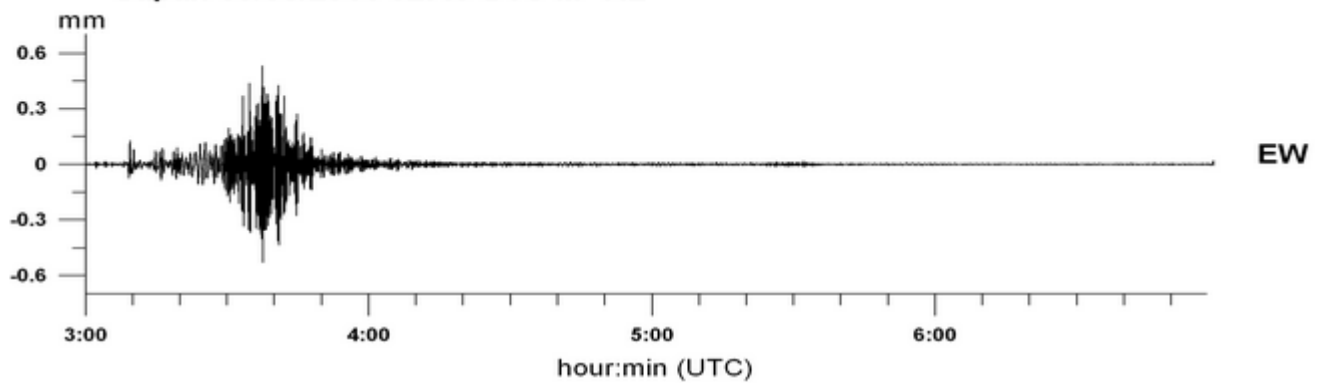
V)

Japan 11/03/2011 05:46 UTC M=9.0 11/03/11 06:06 UTC M=6.4
06:07 UTC M=6.4   06:16 UTC M=6.8
06:26 UTC M=7.1   06:49 UTC M=6.3
06:57 UTC M=6.3   07:15 UTC M=6.3
07:26 UTC M=6.1   07:28 UTC M=6.1
08:12 UTC M=6.2   08:16 UTC M=6.2
08:19 UTC M=6.5   08:31 UTC M=6.1

EW

hour:min (UTC)

NS

hour:min (UTC)
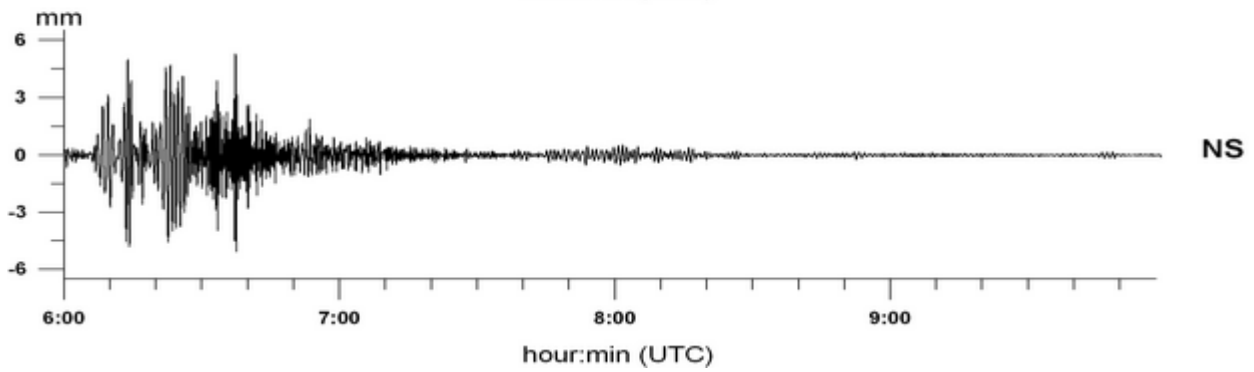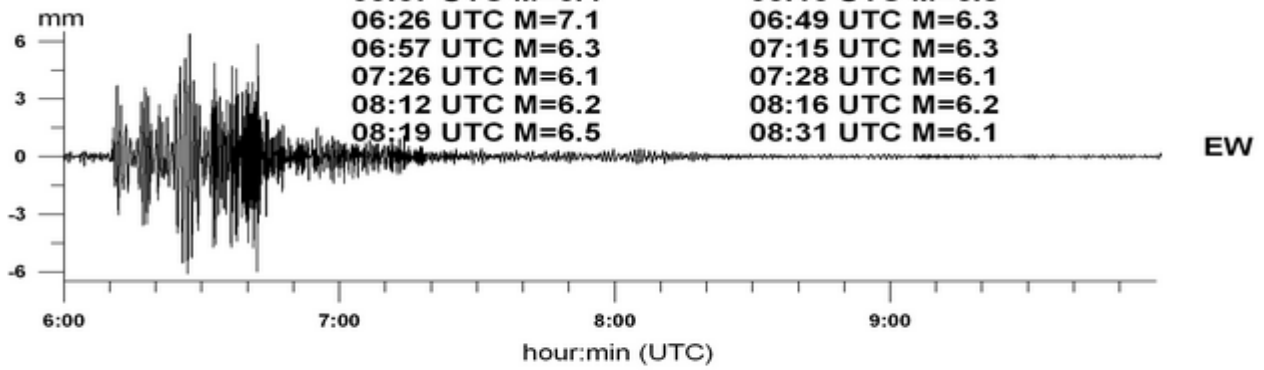
W)

Myanmar 24/03/2011 13:55 UTC M=6.8

EW

hour:min (UTC)

NS

hour:min (UTC)
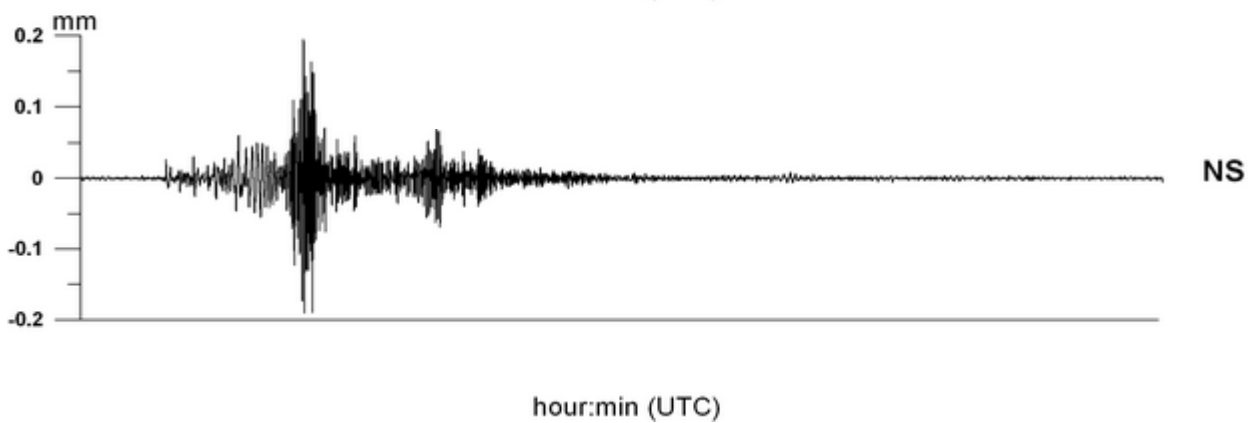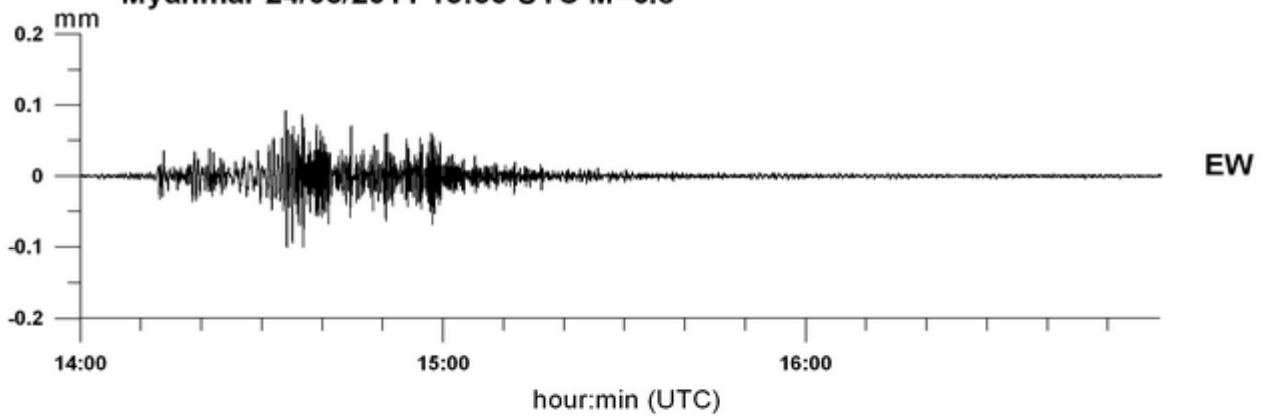
X)

Japan 07/04/2011 14:33 UTC M=7.1
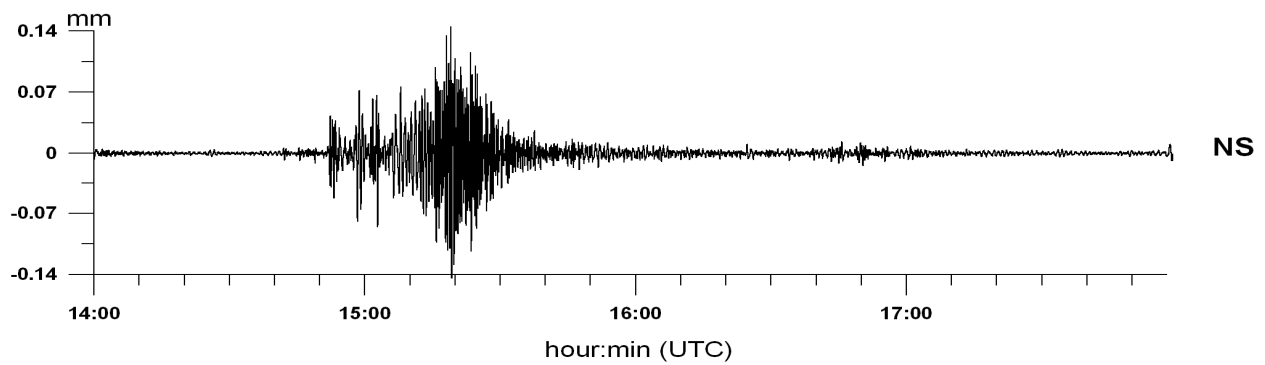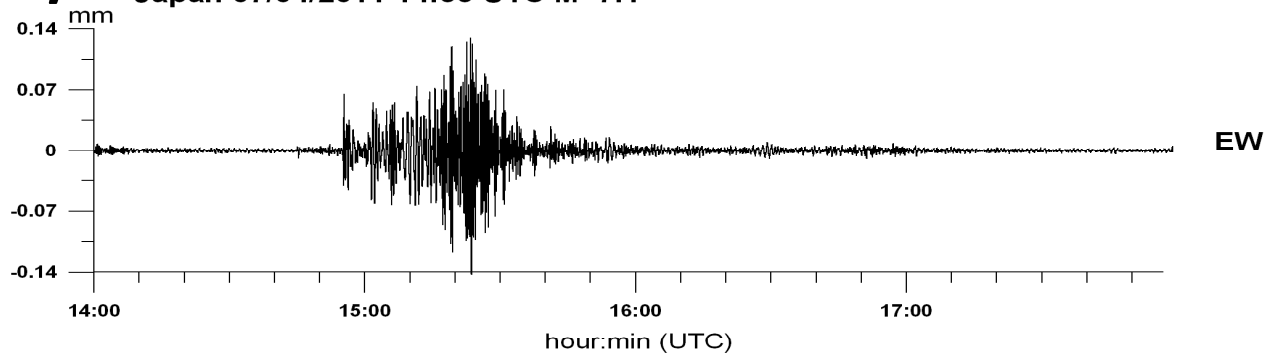
Y)

Western Turkey 19/05/2011 20:15 UTC M=5.8
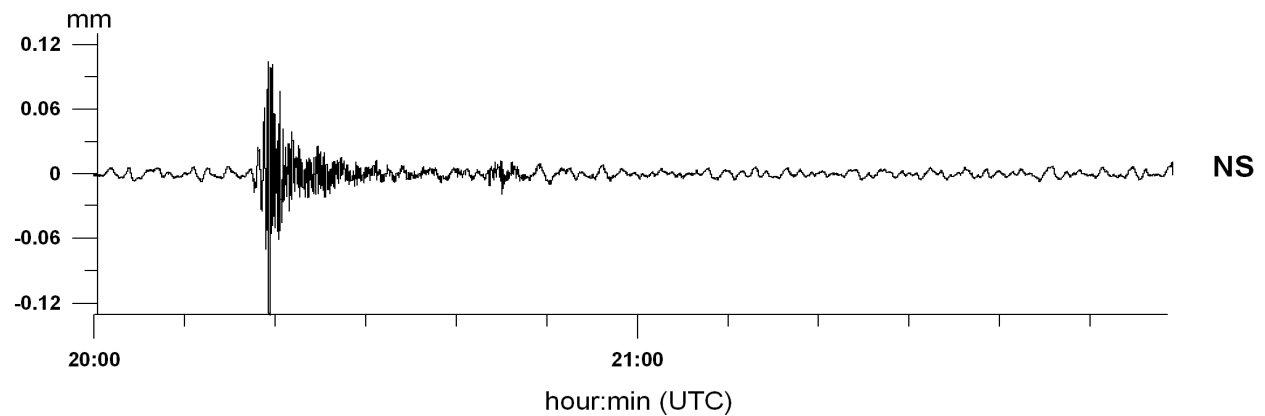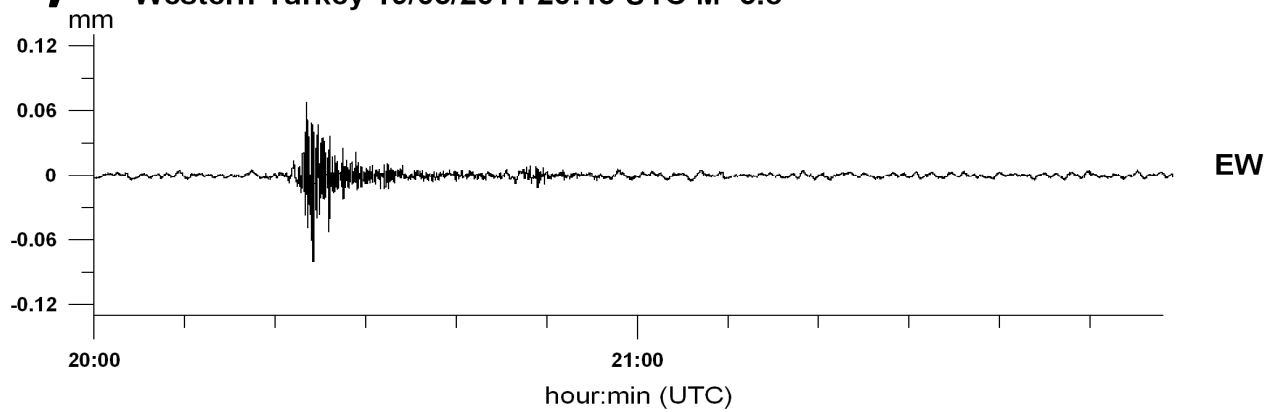
Z)

Alaska 24/06/2011 03:10 UTC M=7.2

EW

NS
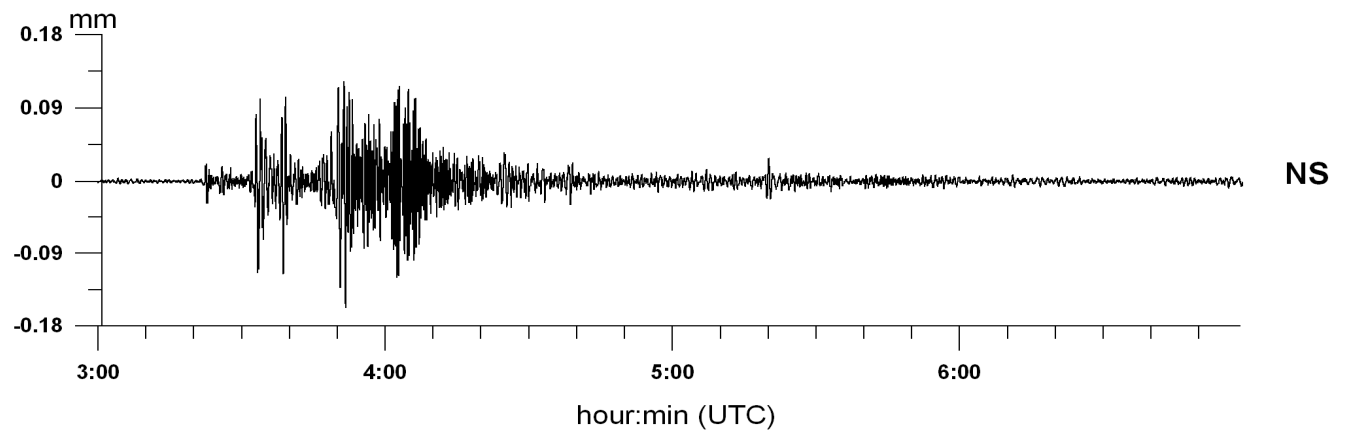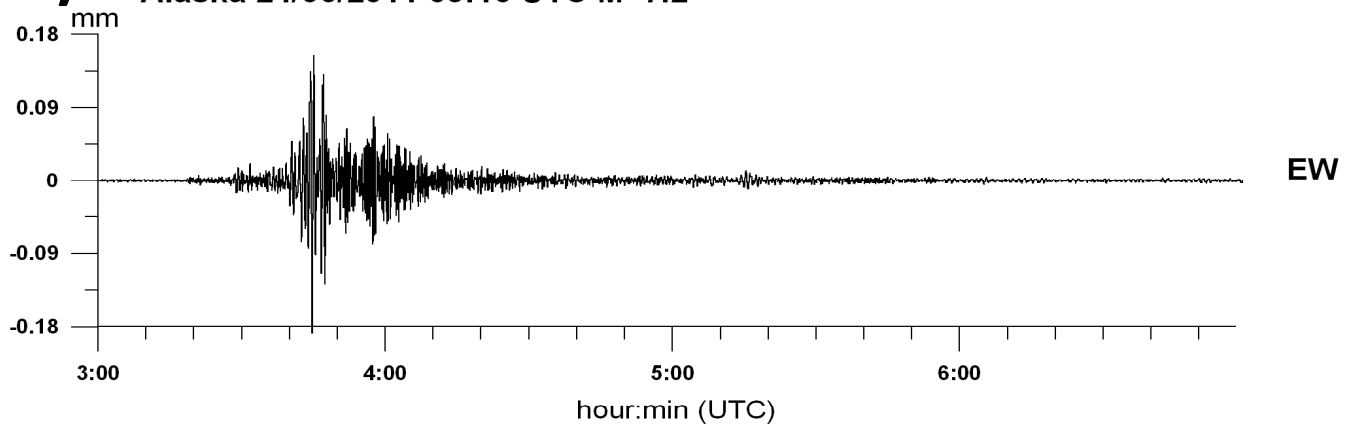
5) Analisi comparata delle registrazioni degli eventi Cile 1960, Sumatra 2004, Giappone 2011

I pendoli della Grotta Gigante hanno registrato con ottima qualita' tre dei quattri eventi maggiori storici che erano l'evento di Cile 1960 (M=9.5), l'evento delle Isole Sumatra-Andaman 2004 (M=9.0) e l'evento del Giappone 2011 (M=9.0), dove le magnitudo si riferiscono a quelle pubblicate da NEIC. Pur avendo subito degli aggiornamenti dal 1960, le proprietà meccaniche dei pendoli sono rimaste invariate, come anche il luogo di misura. Infatti i pendoli dal 1960 sono stati sempre nella stessa stazione, ed il fattore di ampiezza è perfettamente controllabile grazie al rilevamento delle maree terrestri, stabili nel tempo.

La Figura 5.1 riporta le osservazioni dell'evento del Giappone 11/03/2011.
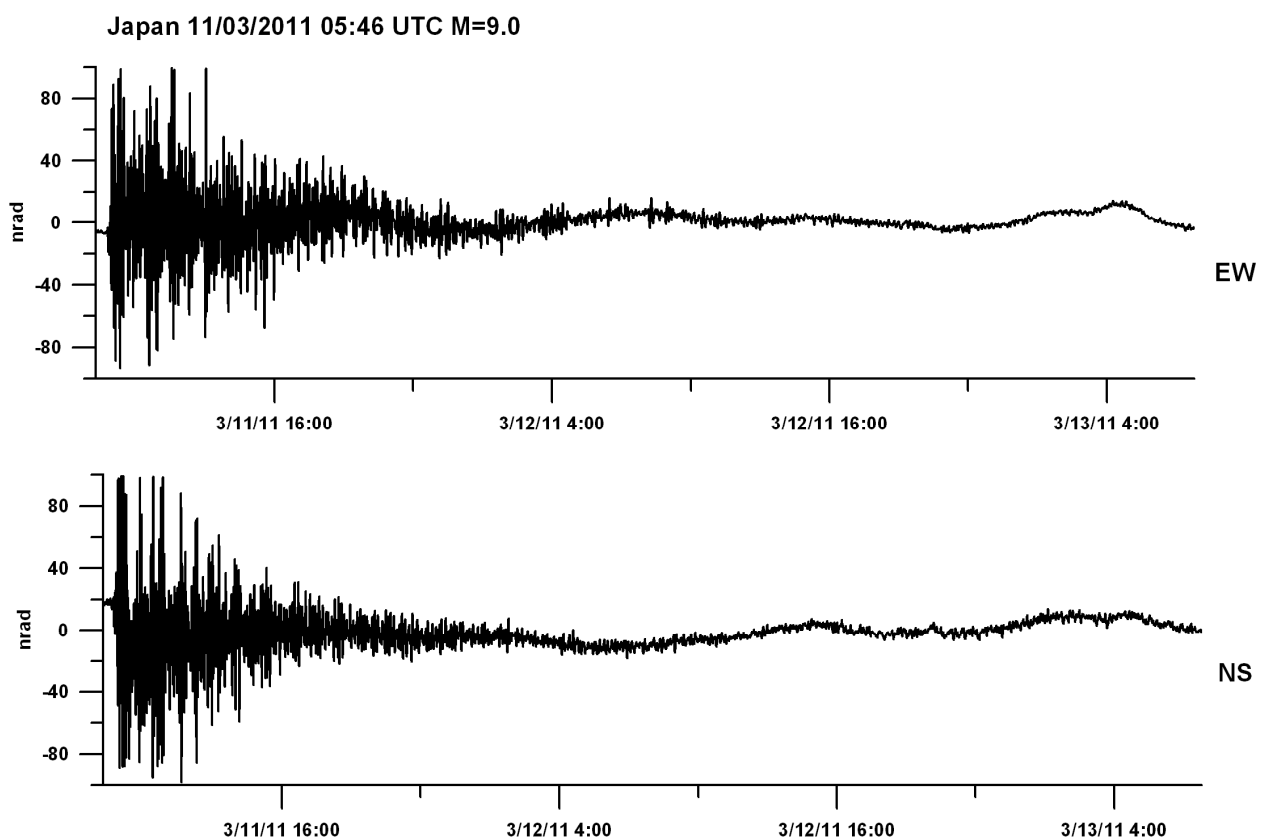
Fig. 5.1 Evento Giappone 11/03/2011 - 48 ore di oscillazione continua

Allo scopo dell'analisi comparata degli eventi, analizziamo le ampiezze dei modi delle oscillazioni libere attivate. Eseguiamo l'analisi spettrale delle diverse osservazioni seguendo la procedura illustrata in Braitenberg e Zadro (2007). Il metodo consiste nel calcolare K spettri della serie temporale di N campioni equidistanti. Ogni spettro viene calcolato con una diversa lunghezza della serie temporale, variabile dalla lunghezza massima di $T_{max}=(N-1)dt$ fino alla lunghezza minima $T_K=(N-1)dt-(K-1)dt_K$, con dt_K un intervallo temporale opportunamente scelto. I K spettri risolvono allora diverse frequenze $fnK=(n-1)/T_K$, con n=1,2,..., N/2. I K spettri diversi vengono uniti in uno spettro composito unico. Il vantaggio di questo metodo e', che i picchi spettrali che possibilmente ricadono fra due frequenze risolte dello spettro unico, vengono risolte senza condizioni di ambiguita'. In Fig. 5.2a si mostra l'esempio di una serie emporale sintetica, consistente di quattro oscillazioni smorzate. Nella Fig. 5.2b Si mostrano i diversi spettri: lo spettro di Fourier (linea

33

pesante), lo spettro composito usando una funzione di finestra al coseno con M=N/2 (linea tratteggiata) e M=N/3 (linea coninua leggera). Il parametro M indica il numero di campioni affetti dallo smussamento della finestra con la funzione cosinusoidale (vedi dettagli in Braitenberg e Zadro, 2007). Si osserva come lo spettro composito risolve meglio le oscillazioni della serie temporale.
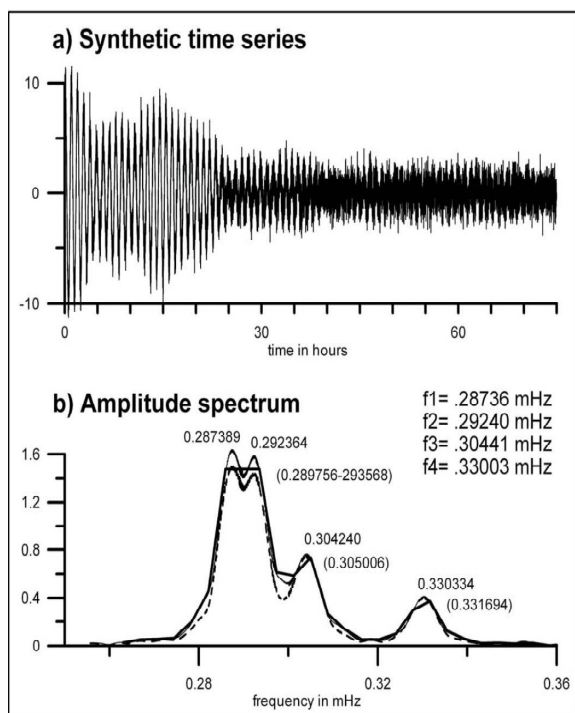
Fig. 5.2 Spettro di Fourier (linea pesante) e spettro composito (linea tratteggiata e linea fine) di una sequenza sintetica (da Braitenberg e Zadro, 2007).

L'analisi spettrale delle sequenze temporali degli eventi sismici viene eseguita su una serie temporale della lunghezza pari a 75 ore. Questo corrisponde ad un numero di campioni pari a N=9000 per l'evento del Cile 1960 (campionamento 30 sec) ed un numero pari a N=18000 per tutti gli altri eventi (campionamento 15 sec). Nella Figura 5.3 presentiamo gli spettri per l'evento Cile 1960, di Sumatra-Andamane 2004, e Giappone 2011. Nella figura si osserva come i modi delle oscillazioni libere sono bene individuati. L'evento del Cile 1960 presenta ampiezze relativamente maggiori nei modi piu' bassi. Analizzando in dettaglio i modi piu' bassi 0S2, 0T2 e 2S1, possiamo osservare lo splitting delle frequenze, causato dall'influenza della rotazione terrestre. L'evento di Sumatra si distingue dall'evento del Giappone nelle frequenze basse della componente NS, dove le ampiezze spettrali fino alla 0T8 sono visibilmente piu' ampie. Si modi piu' alti e sulla componente EW invece le ampiezze dei due eventi sono comparabili. L'evento del Cile si distingue con ampiezze maggiori sulla componente NS, e soprattutto nei modi d'oscillazioni piu' bassi fino alla 0T17.

Spectrum EW component
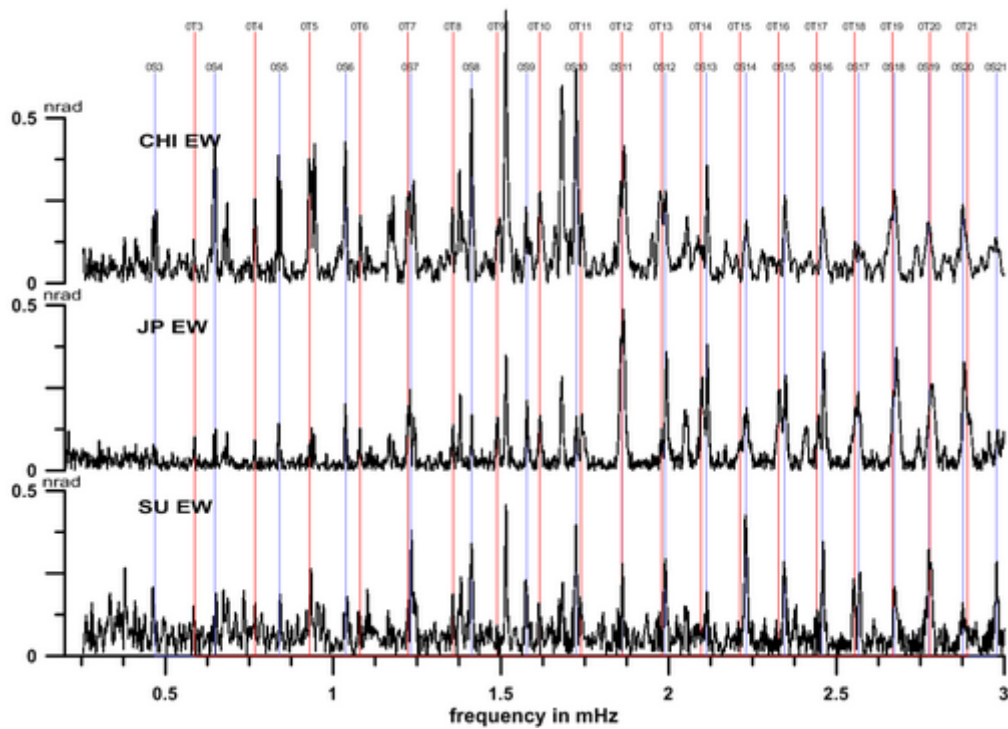
Spectrum NS component
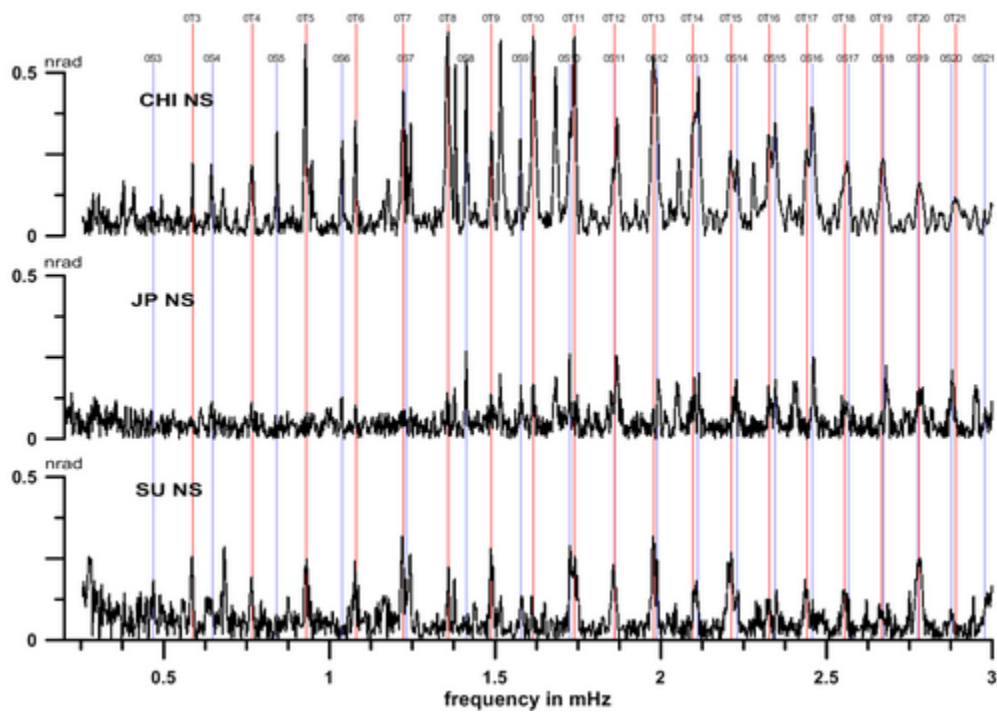
Fig.5.3 Spettro di ampiezza delle osservazioni dei pendoli della Grotta Gigante nell'intervallo delle oscillazioni libere. Linee verticali indicano dei modi torsionali (rosso) e sferiodali (blu).Spettri per gli eventi sismici di Cile 1960, Sumatra-Andamane 2004, Giappone 2011.

6) Relazione lineare fra segnale tilt in Grotta Gigante e quantita' di acqua immesso nel sistema Carsico durante una piena (in inglese).

In questo capitolo riportiamo le analisi che hanno dimostrato che il tilting dei pendoli durante una fase di grande piovosita' e' proporzionale al volume integrato della piena immesso nel sistema idrico del Carso. Questa analisi completa il lavoro eseguito nel 2008-2009 (vedi rapporto Grotta Gigante 2009) nel quale avevamo analizzato il tilting in relazione alle piene registrate in una altra Grotta della Carso, l'abbisso di Trebiciano. Troviamo che il volume totale immesso nel sistema sotterraneo idrico e' un parametro migliore alla comprensione del tilting osservato nei pendoli, rispetto al livello di acqua nella grotta vicina. Questo significa che il tilting non e' dovuto ad un effetto locale, ma che esso registra piuttosto il movimento di tutta la rete idrica che si muove all'interno del Carso, dal suo cammino dalla sorgente posta in Slovenia, alla sua foce a Duino, in mare. Il lavoro e' attualmente in fase di pubblicazione sul Bollettino di Geofisica Teorica ed Applicata - riportiamo qui il testo redatto in inglese.

KARST DEFORMATIONS DUE TO ENVIRONMENTAL FACTORS: EVIDENCES FROM THE HORIZONTAL PENDULUMS OF GROTTA GIGANTE, ITALY

D. Tenze, C. Braitenberg, I. Nagy

Abstract
The aim of this work is to characterize the deformation of a natural cave induced by temperature variations and by the underground water flow. We consider the tilt recorded by two horizontal pendulums installed in the largest cave of the Italian Karst, the Grotta Gigante. The environmental factors we consider are temperature, rainfall and level and flow rate of the river Reka that feeds the underground Karstic waters. The tilt and temperature have a regular annual cycle, with period of 365 days, which is caused primarily by the thermo-elastic deformation. Semiannual periods are present but more than 10 times smaller. For rainfall and river level the semi-annual and annual oscillation have comparable amplitudes. The effect induced by the underground water flow consists in a tilting towards SW, that has a linear relation between maximum tilting and the integrated amount of water entering the Karst during the flood, with tilting coefficient $a = 10.7 \; 10^{-6}$ nrad/m^3. The minimum amount of water giving a tilt signal is $V_0 = 5.2 \; 10^6$ m^3.
.

Introduction
The aim of this work is to quantify the tilting of the Grotta Gigante cave situated in the Trieste Karst (NE-Italy) due to environmental factors and the underground water discharge. The deformation of the cave is monitored by a couple of long-baseline horizontal pendulums, the first edition of which was installed in 1959 in occasion of the International Geophysical year (Marussi, 1960). The station belongs to the network of subsurface geodetic stations of the University of Trieste that includes two more stations, the Bus de la Genziana (Fregona, Treviso) and the Grotta Nuova of Villanova, Udine (Braitenberg and Zadro, 1999; Braitenberg, 1999). The locations of all stations can be examined on the homepage of the network (http://www2.units.it/geodin/).
The horizontal pendulums of the Grotta Gigante measure tilting, being sensitive to differential horizontal movements of the bottom and the vault of the cave. These differential movements are caused either by a rotation or by a shear-deformation of the cave. There are several known causes that make the cave deform, and the recorded tilt signal is the superposition of the different aspects, which are the long period tectonic deformations due to plate tectonic convergence of the Adria plate and the Eurasian plate, Earth's free oscillations, Earth's tides and the loading effects of the Adriatic Sea's tides, seismic waves, co-seismic effects but also presumably the atmospheric agents and

hydrologic effects.

Studies conducted on more than 40 years of recordings, have allowed to identify most of these deformations and to estimate the entity of their influence (e.g Zadro and Chiaruttini, 1975; Rossi and Zadro; 1996; Zadro and Braitenberg, 1999; Braitenberg and Zadro, 1999; 2007; Braitenberg, 1999; Braitenberg et al., 2001; 2006). In this work we want to identify the effects of the underground water and of the environmental parameters of temperature and pressure. Recent publications on the study of hydrologic effects on gravity and tilt include the works of Boy et al., (2009), Longuevergne et al., (2009) and Florsch et al., (2009). There has been recently a revival in the interest to the study of tilting induced by subsurface run-off in Karstic areas, as documented in the recent works of Tenze et al., (2010) and Grillo et al., (2011) for the Italian Karst and Gilli et al., (2009) for the Plateau of Calern (Alpes Maritimes, France). The time variation of water storage in a Karst system was investigated by Jacob et al. (2010) with repeated relative and absolute gravity measurements. The tilt induced by the hydrologic flow is due to a combination of deformation caused by the load of the water mass, poroelasticity (Kümpel, 1986; Weise et al., 1991; Jahr et al., 2008; 2009) and the deformation of crevices and cracks typical for a Karstic rock due to the temporary saturation with water (Gilli et al., 2009). First results from finite element modeling (Gilli et al., 2009) show that the loading alone is insufficient to generate the large observed tilt signals, and that the other two mechanisms are necessary to explain the observations, at least for what concerns the observation in the Maritime Alps (France). A side-product of the research relating geodetic observations as tilt and gravity to the underground water flow, is that the results can be used as an observational parameter to study the Karst hydrology. For the Trieste Karst one important question regards the ramification and depth of the underground river flow, which is still unknown to date.

Here we study the relation of the tilt observations to the amount of water entering the Karst system and that is observed flowing in the river Reka, which is the river that disappears in correspondence of the Skocjan caves (Slovenia) near the border between Italy and Slovenia and continues underground in the Italian Karst, until it emerges as the Timavo river at the base of the Karst close to the sea (**Figure 1**). We use the observations of the level and flow rate of the river Reka accomplished by the Environment Agency of the Republic of Slovenia. The atmospheric factors we have considered are the data series of temperature and rainfall recorded by the meteorological station installed outside the Grotta Gigante of the Commissione Grotte "Eugenio Boegan".

2. Geographic, geomorphologic and geologic context

The classical Karst is an area of about 900 km², that extends across the border between Italy and Slovenia from the Trieste bay area to Postojna and Skocjan (**Figure 1**). The Classical Karst is a vast area of a mature Karst system that has a well developed hydrostructure, characterized by a diffuse karstification that protrudes also below the sea level. The area is characterized by a large number of natural cavities and by a complex underground water flow. From a structural point of view, the Karst belongs to the Karst-Friulian carbonatic platform, the northern extension of the Adria plate. The whole platform is formed by three layers: Triassic limestone at the base, Eocenic limestone at the top (with a section up to 2000 m) and a third cover layer, Eocenic, formed by layers of flysch. The last two layers are placed in an anticlinal, slightly asymmetric position on a Dinaric NE-SW axis (Carulli and Cucchi, 1991, Bensi et. al., 2009). The south-western face of the anticline overlooks the Trieste Gulf delimiting the Karst highlands.

The river Reka, or Timavo in Italian, originates between Croatia and Slovenia, on the slope of Mount Dletvo. After 40 km, still on Slovenian territory, the river disappears in the big complex cave of Skocjan. The underground path is supposed to be 70-80 km long, with direction NW, and is composed by a very complex network of primary and secondary flows, with many changes of

direction. For example, inside the Trebiciano Abyss the water flows from South to North, while on the bottom of the Lazzaro Jerko cave it flows from East to West (Cucchi et al., 2001). At San Giovanni di Duino the river emerges from the foot of the Karst with the name of Timavo. **Figure 1** shows the locations of places and stations cited in the text.
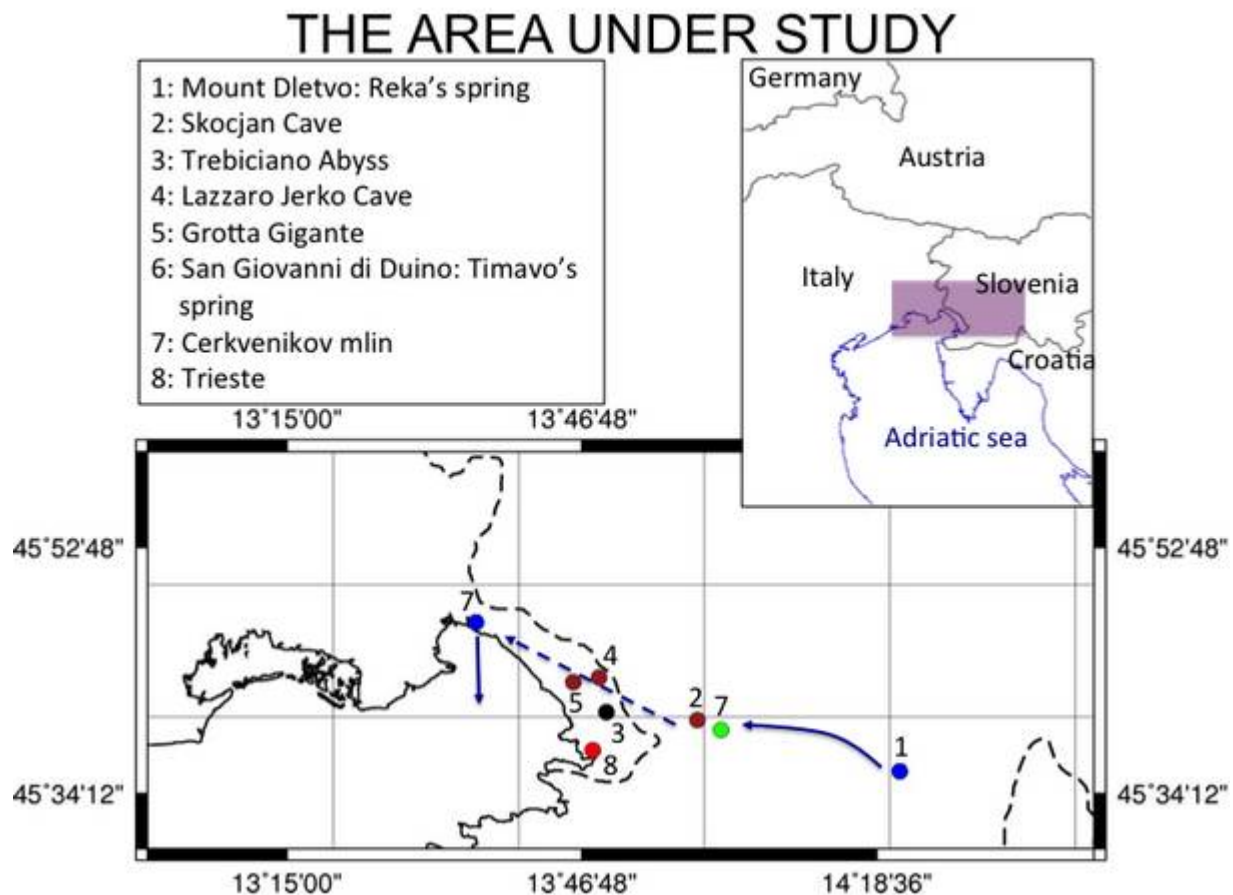
Fig.1- Schematic map with the sites mentioned in the paper. The blue arrows represent the general trend of the water flows. The Timavo's spring (1), Skocjan Cave (2), Trebiciano Abyss (3), Lazzaro Jerko Cave (4), Grotta Gigante (5), the Timavo's spring in San Giovanni di Duino (6), Cerkvenikov mlin station (7) and Trieste (8). The blue arrows represent the general trend of the water flows. The dotted line represents the state boundaries.

3. The Grotta Gigante underground geodetic station, the surface meteorological station and the river Reka station.

The Grotta Gigante cave, situated on the Trieste Karst, bears the Guinness Award for the greatest tourist cave in the world; the main room of the cave has an overall volume of 600000 m³, the bottom of the cave is at 151 m above sea level, it has a length of 160 m, a width of 65 m and a height of 107 m. In 1959 Antonio Marussi exploited the height of the cave to build a couple of long-base tiltmeters of the horizontal pendulum type with Zöllner suspension (Marussi, 1960; Zöllner, 1872). The horizontal pendulums consist of a sub-horizontal pendulum arm suspended by an upper wire fixed at the vault of the cave and a lower wire fixed to the ground of the cave (**Figure 2**). The distance between upper and lower mountings is 95 m and the period of oscillation of the pendulum in the horizontal plane is presently kept at 6 min (Marussi, 1960; Braitenberg, 1999; Braitenberg and Zadro, 1999; Zadro and Braitenberg, 1999). Horizontal shifts of the upper mounting in respect to the lower mounting of the pendulum (shear) and a tilt of the cave are recorded as a rotation of the

beam in the horizontal plane around the rotation axis, which lies on the line connecting the upper and lower mounting points of the pendulum. The two pendulums record respectively the NS and the EW movements of the vault in respect to the bottom of the cave. The beam's movements are recorded by the reflection of a solid-state laser beam pointing on a mirror fixed to the pendulum arm. This reflection is recorded with a photosensitive device with a sampling of 30 values/sec. Thanks to their dimension (95 m) and to the amount of the data series collected (from 1966 to today) these pendulums are worldwide unique instruments. Their length gives them a great stability reducing the noise level in respect to smaller scale tiltmeters installed at the same site. The meteorological station outside the Grotta Gigante cave is managed by the Commissione Grotte "E. Boegan" and has been active since Janaury 1st, 1967, giving us continuous daily records of temperature and rain records. The measurement of the water level and flow rate of the river Reka is made by the Environment Agency of the Republic of Slovenia. The Agency holds two stations on the river Reka, Cerkvenikov mlin, with a continuous data series from 1952 to present, and the station Skocjan, for the years 1957-1966. For our purpose the station Cerkvenikov mlin is ideal, as it covers an extensive time-series that coincides with the one of the horizontal pendulums. Up to 1956 water level data were based on regular daily observations (staff-gauge, 1 observation per day, additional observations during high levels). From 1957 to 2006 the gauging station was equipped with a water level recorder (1957 – 1976 water level recorder "METRA"; 1976 – 1981 SEBA DELTA; 1981 – 2006 SEBA –OMEGA with pressure probe) and from 2004 with a data logger. Discharge data are derived from water level data with height-volume transformation according to a rating curve. The rating curve is based on discharge measurements with a current meter and lately (from 2005) with an acoustic Doppler current profiler (ADCP) or flow tracker ultrasonic velocimeter (321 discharge measurements between 1952 - 2011; precision ± 5%; 23 validated rating curves in 37 intervals). The daily water level data were then transformed to daily discharge data (personal communication Marjan Bat, Environment Agency of the Republic of Slovenia).
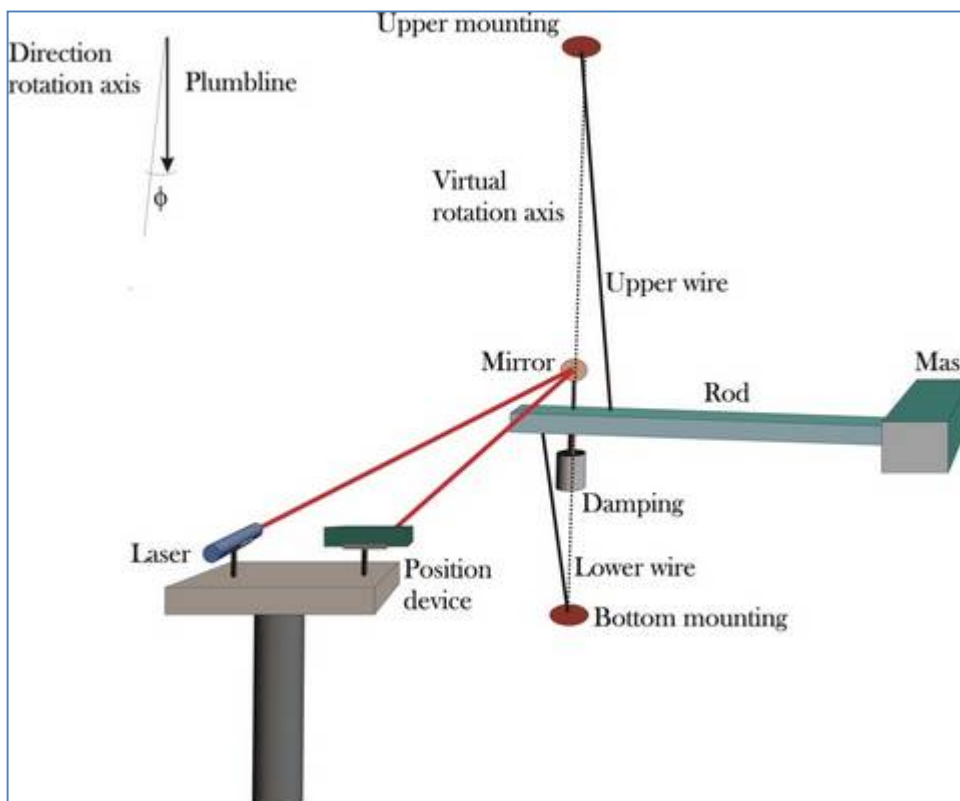
Fig. 2 - Schematic graph of the Grotta Gigante horizontal pendulums (Braitenberg, 2011).

4. Presentation of geodetic, meteorological and hydrological observations

In this paragraph we present the observations we use for our study. **Figure 3** shows the data series of the two pendulum components recorded from October 13th 1966 to March 22 2011. The original hourly data were resampled at one value a day after applying an anti-aliasing low pass filter. The long period trend is formed by an oscillatory function with a period of 33 years and a linear drift, which have been determined by a least squares approach. The linear variation corresponds to an inclination with direction N57W with a rate of 27 nrad/a (for more details see Braitenberg et al., 2006). It is also possible to see a regular annual variation that will be analyzed in greater detail in the next chapter. Beyond the annual signal and the 33-year-period oscillation there are other short-period or impulsive signals. These last signals will be shown to be generated by the underground water discharge.
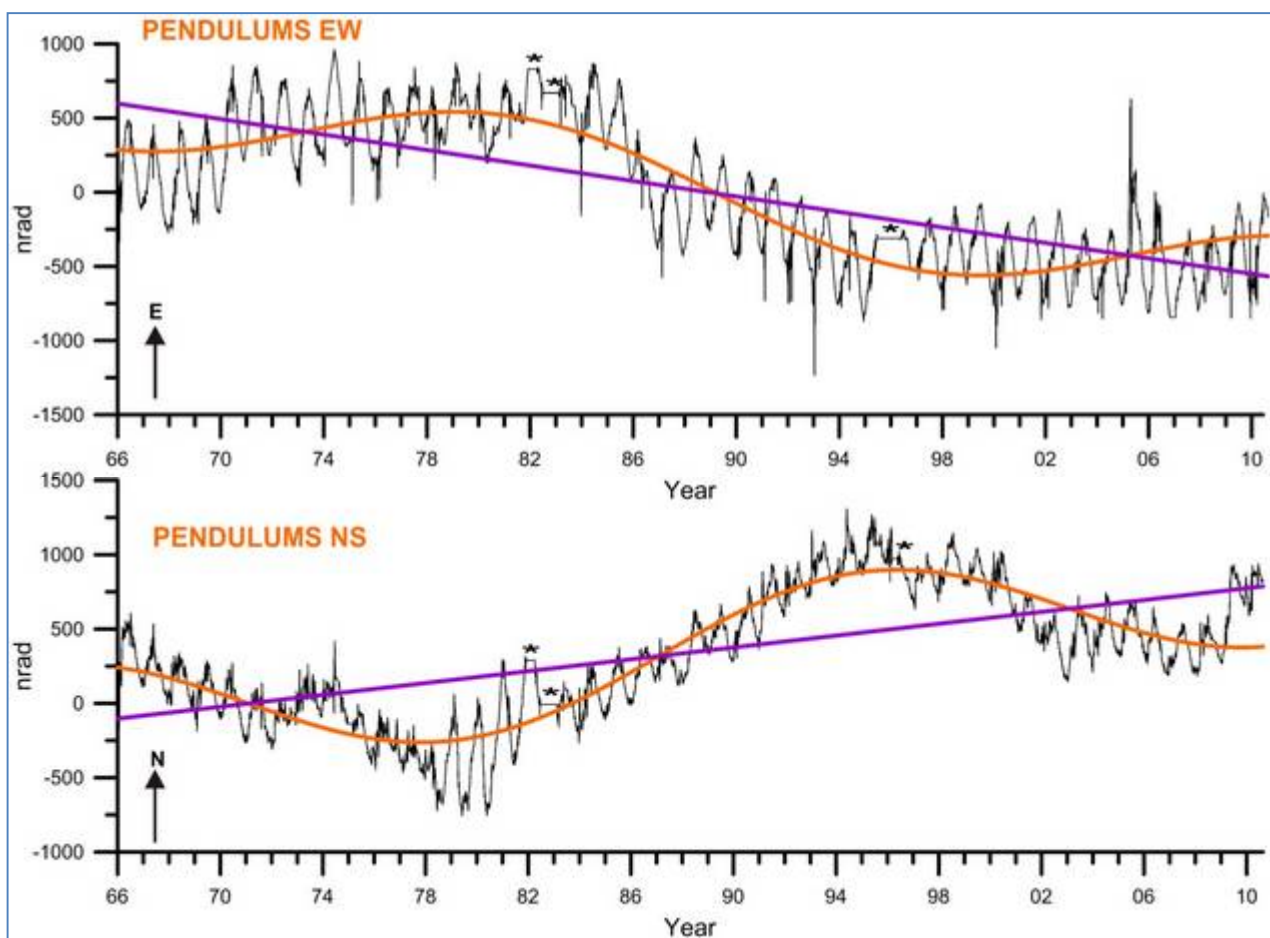
Fig. 3-The data series of the two pendulum components of the Grotta Gigante station recorded from October 13th 1966 to March 22nd 2011. Stars mark interruptions in the data acquisition.

In **Figure 4** the records of the daily temperature and the monthly rainfall observed at the surface above the Grotta Gigante cave, and the level and flow rate of the river Reka are shown. The continuous curve above the rainfall is the time integral of rainfall, to which the average rainfall-rate has been subtracted (111 mm/month). The rainfall function (Latynina et. al., 1993; Zadro and Braitenberg 1999) is an alternative way to present the precipitation variation, and has the advantage to be a continuous curve, same as the other quantities we analyze. The pressure and temperature show an evident yearly variation, which is not evident in the rainfall. The temperature and river

level variations are stationary, and do not show an evident long-term variation. The rainfall shows some pluri-annual variation, which is emphasized in the integrated rainfall, with two reductions in precipitation during the years 1973-1976 and 1989-1994.

In **Figure 4** we also present the time series of water level and flow rate of Reka river at station Cerkvenikov mlin used for our study. The characteristic variation is a fast level increase followed by an exponential decrease. The flood-events usually are contained in a time-interval of 20 days. The flow rate has a similar variation, covering 2 orders of magnitude, with a basic level of 2 m^3/sec increasing to maximal values of 280 m^3/sec during floods. One characteristic parameter which defines the flood is the total water that enters the Karst system and is defined by the time-integral of the river flow over the time interval of the flood. We will see further that this integrated quantity is proportional to the hydrologic tilting signal. Our goal being to quantify the inclination of the cave in correspondence of the floods, we select some major floods, during which the pendulums also are functioning. These events are marked with green color in **Figure 4**.
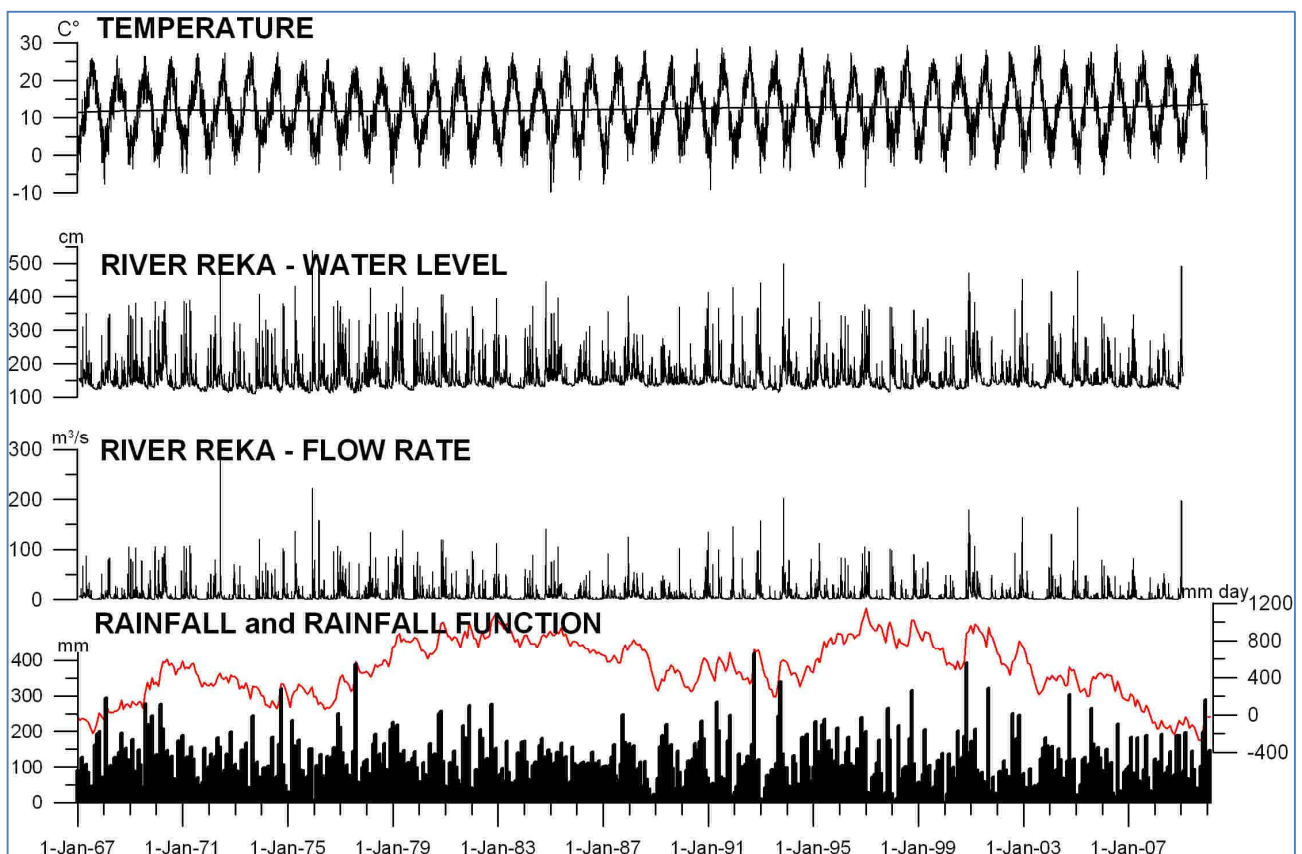
Fig. 4- Graph of environmental parameters: rainfall and temperature recorded at the Borgo Grotta meteorologic station (Commisione Grotta "Eugenio Boegan" Soc. Alpina delle Giule). Rainfall function (see text); level and flow rate for the river Reka at station Cerkvenikov mlin (Environment Agency of the Republic of Slovenia).

5. Data analysis

Here we present the data analysis used in studying the environmental effects on the tilt. Our first analysis is concerned with finding the exact spectral components in the yearly variation of temperature, rainfall, water-flow and tilting. The subsequent analysis aims at quantifying the tilt-signal induced by the floods of the river Reka.

5.1 Spectral content of environmental parameters and tilt

In order to obtain a comparative analysis between meteorological and geodetic data, we have calculated the power spectrum of tilting, temperature, rainfall and water level of river Reka. We analyze the data over the time-interval from January 1, 1968 to December 31, 2008 and present the spectra in the **Figure 5** for horizontal pendulums, temperature, rainfall, and the river Reka. The temperature data are available only until 2002, however the longer temperature time series will hardly change on the results. Visual inspection of the spectra shows that the temperature variations are dominated by the annual variation that is over 10 times greater than the remainder of the spectrum. The horizontal pendulums have a pronounced annual spectral component as well, more than 10 times the spectrum at smaller periods, although in this case the maximum centered on the annual frequency is broader. The rainfall and river Reka have a very different characteristic, the entire spectrum being flatter, and allowing a linear amplitude scale. For rain the semi-annual periods have greater amplitude than the annual period.
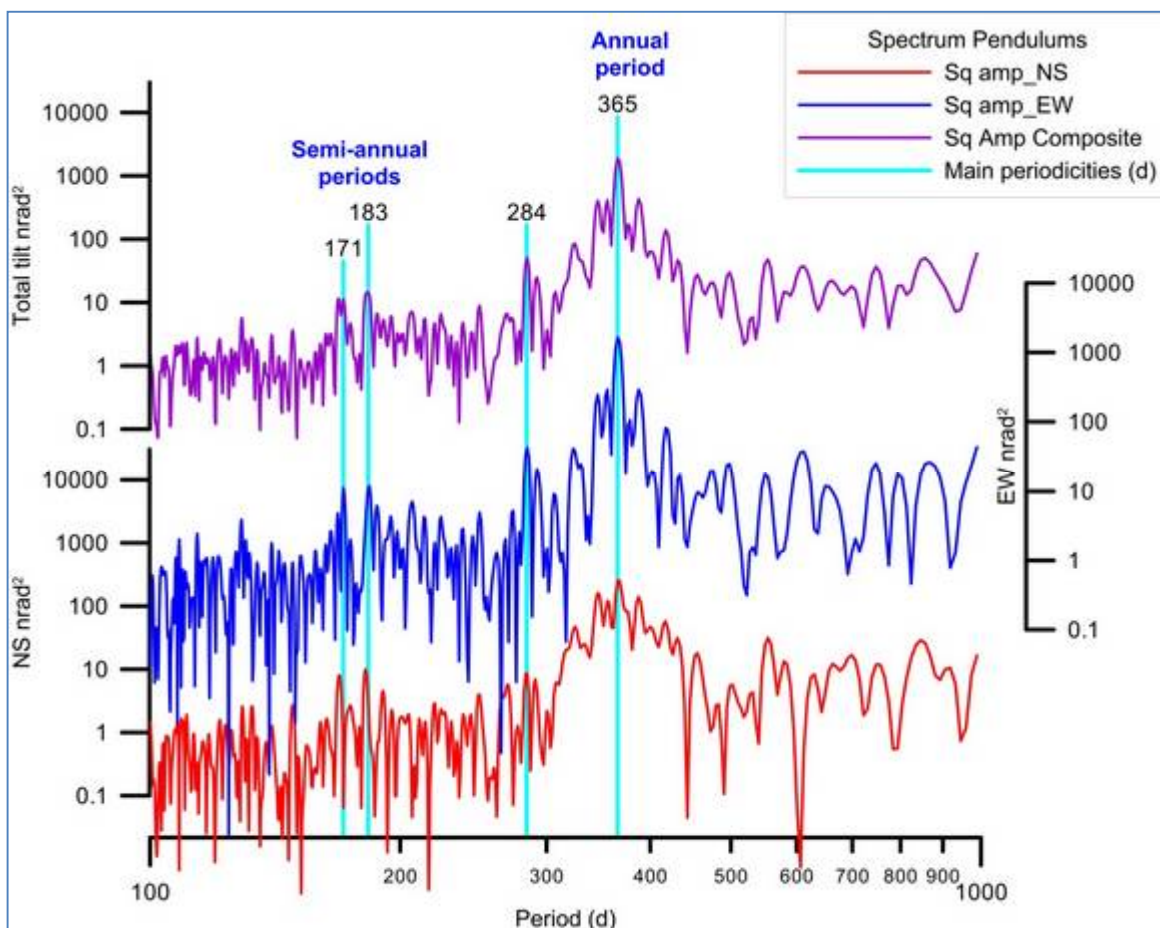
Fig. 5 Squared amplitude spectrum of the Tilt observations and the environmental parameters. a) Spectrum of the two tilt components and total squared amplitude of tilt. The main spectral peaks that emerge on both components are marked with vertical lines and their respective periodicity (in days)

We summarize the amplitude, phase and period of the principal annual and semi-annual periods in **Table 1**. The phase is illustrated by adding the corresponding date of the year of the maximum of the oscillation. We find that the temperature presents an annual variation with an amplitude of 9.2°C, with maximum value on July 22nd and minimum value on January 21st. For the semi-annual period we obtain two maximal values during the year. The temperature has a single spectral peak at
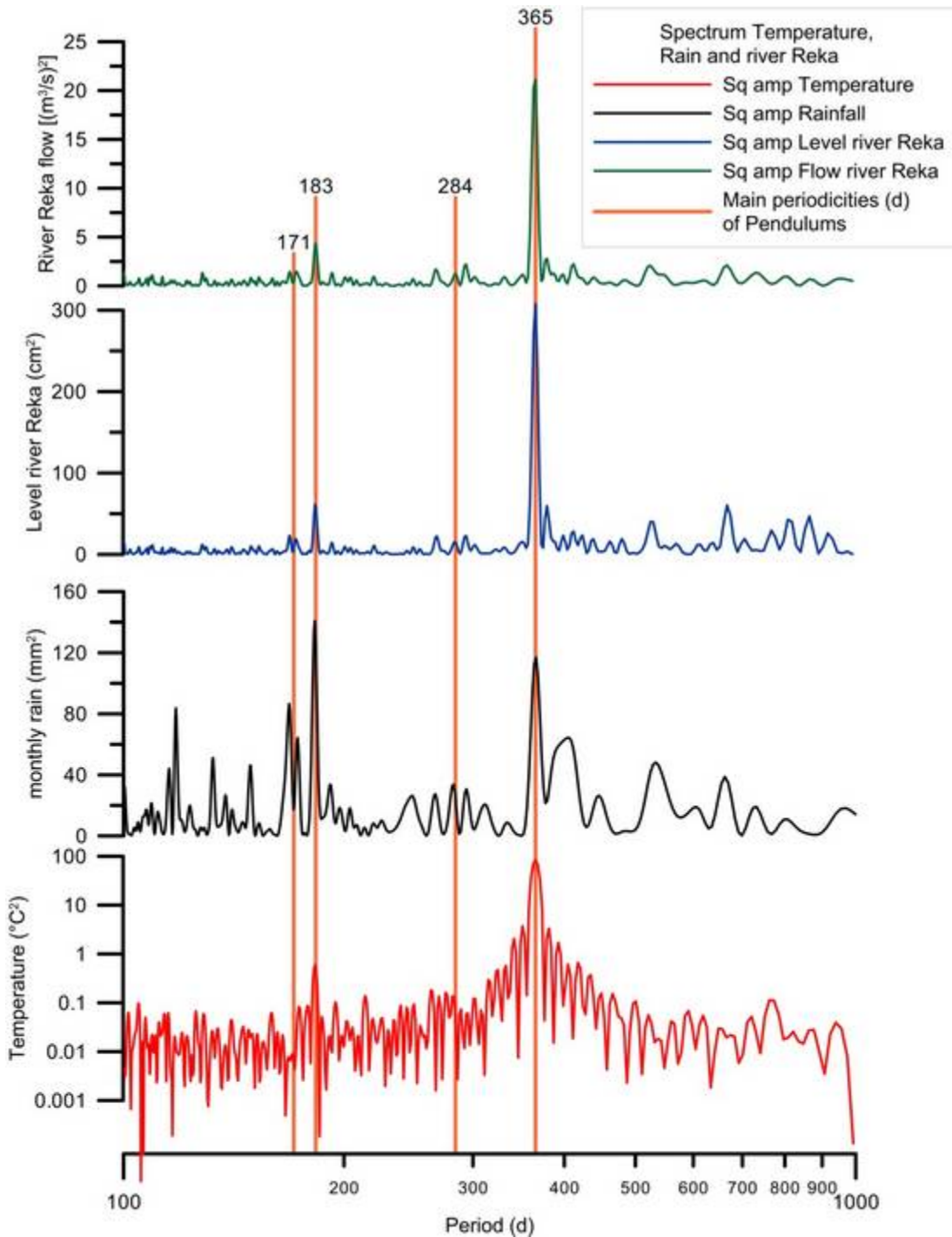
Fig. 5b) Squared amplitude spectrum of temperature, rainfall and river Reka. Notice that the scale for the spectrum of rainfall and river is linear. The main spectral peaks of the horizontal pendulums are marked with vertical lines and their respective periodicity (in days)

a period of 183 days. The tilt, rain and river level have three spectral peaks, near to 183, 172, and 168 days. The three periods have good agreement in the hydrologic and geodetic observations.

Of particular interest is the phase of the spectral components.

We find that the pendulums' yearly maximum tilting towards SW happens on the 266th day of the year, which is 63 days after the temperature maximum annual variation. When considering the

semi-annual periodicity of 183 days, though, tilt components have maxima near the months of January and July (towards SW), which lags about two months the hydrologic variations at the same periods.

	Period(d)	Phase	Amplitude	Day of maximum	Date of maximum
Temperature	183	257.7	0.77°C	52, 235	21 feb., 23 aug.
Temperature	365	158.8	9.1 °C	204	23 lug.
Rain	168	60.6	9.3 mm	140, 308	20 may, 4 nov.
Rain	173	70.1	8.0 mm	139, 312	19 may, 8 nov.
Rain	182	129.9	11.9 mm	117, 301	27 apr., 20 oct.
Rain	366	128.3	10.8 mm	236	24 aug.
Reka River level	169	80.0	5.1 cm	131, 300	11 may, 27 oct.
Reka River level	172	137.8	4.5 cm	106, 278	16 apr., 5 oct.
Reka River level	183	108.4	8.2 cm	128, 311	8 may, 7 nov.
Reka River level	365	-23.8	17.3 cm	24	24 jan.
Reka River flow rate	169	83.3	1.3 m3/sec	129, 297	9 may, 24 oct..
Reka River flow rate	172	133.0	1.2 m3/sec	108, 280	18 apr., 07.oct.
Reka River flow rate	183	108.7	2.2 m3/sec	128, 311	08 may, 07 nov.
Reka River flow rate	365	-16.6	4.6 m3/sec	17	17 gen.
Tilt composite	168	-	3.5 nrad	43, 211 EW 80, 248 NS	12 feb., 30 jul. tilt E 10 apr. 05 sept. N
Tilt composite	171	-	3.1 nrad	168, 339	17 apr., 05 dec. tilt SW
Tilt composite	183	-	4.0 nrad	20 , 203	20 jan., 22 jul. tilt SW
Tilt composite	365	-	42.2 nrad	85 266	26 mar. tilt NE 19 sept. tilt SW

Table 1- Results of the spectral analysis of temperature, rainfall, level of river Reka and tilting at Grotta Gigante station: periods of principal spectral components with amplitudes, phases, day in the year and dates corresponding to the maximum excursion.

5.2 The tilting of the cave during floods

In this section we analyze the tilt records and the level and water flow rate of the river Reka during a selection of floods. We consider the timeframe in which both data-types were available, which goes from January 1, 1968 to December 31, 2008. In order to isolate the deformations induced by the floods of the river on the pendulums' registrations, we had to clean the tilt-record from all the other components (induced for instance by tectonic plate movement, earthquakes, temperature, etc.)

through a specific process. In **Figure 6A** the EW pendulum component is shown for the time-interval from October 13, 1966 to March 22, 2011. The annual component and a slower variation (the sinusoid of 33 years and a linear variation described above) are evident. To neutralize these two components, and isolate the rapid hydrologic signal, we first removed the linear variation and the long period sinusoid, which removes the trend and shifted all the values around zero. Then, to remove the annual periodicity, we used a low pass filter to cut all the frequencies with periodicities higher than 300 days. **Figure 6B** shows the signal, without the disturbing components, used to find the correlation of tilt with water level, subject of this chapter.
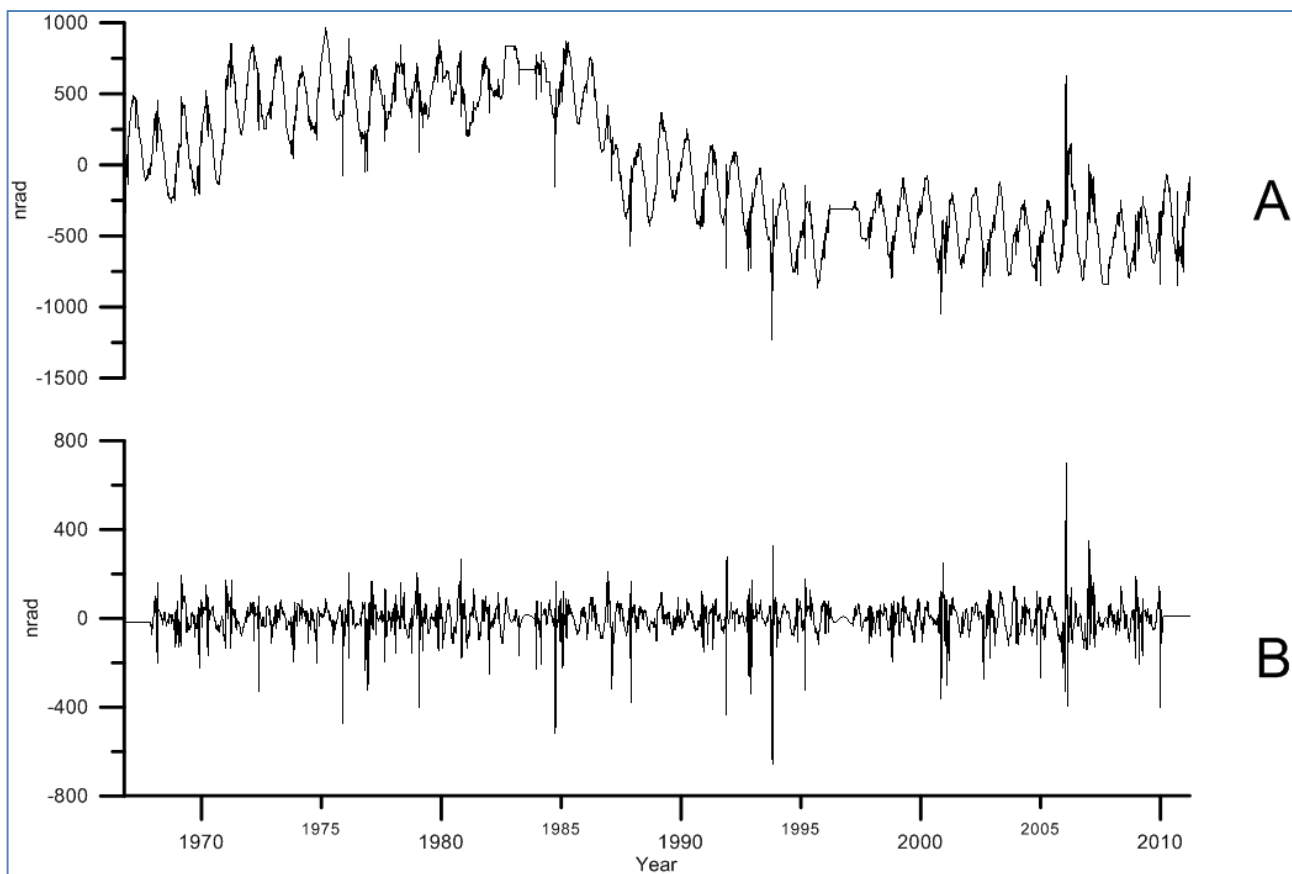
Fig. 6- The EW component before and after the signal processing for the time interval October 13, 1966 to March 22, 2011. a) original recording; b): the signal used for the study.

After these operations, we start to evaluate direction, speed and amplitude of the signal during the days of the floods. In total we have selected 11 floods, and we select a time window of 20 days which covers the flood. The peak flood is chosen to coincide with the 8th day of the time window. All the plots in **Figure 7** represent the flood event of October 2, 1984. At the top left (**Figure 7a**) the variation of water level flow rate of the river Reka is shown, in the same figure below, the plots in **Figure 7b** and **Figure 7c** represent respectively the azimuth and the speed of the tilt, at the top right, **Figure 7d** shows the movement of tilt, lastly **Figure 7e** shows the azimuth and the speed of tilt together in a rose diagram. **Figure 7d** shows the composite movement of tilt where the EW and NS components are used for the X and Y axes, respectively. The numbers on the curve on **Figure 7d** and **7e** indicate the sequential days of the flood. The first day of the sequence (day 1) matches the beginning of the time series we have extracted corresponding to the flood event. We define the direction of the tilt with the value of the azimuth, the angle counted clockwise from north, during
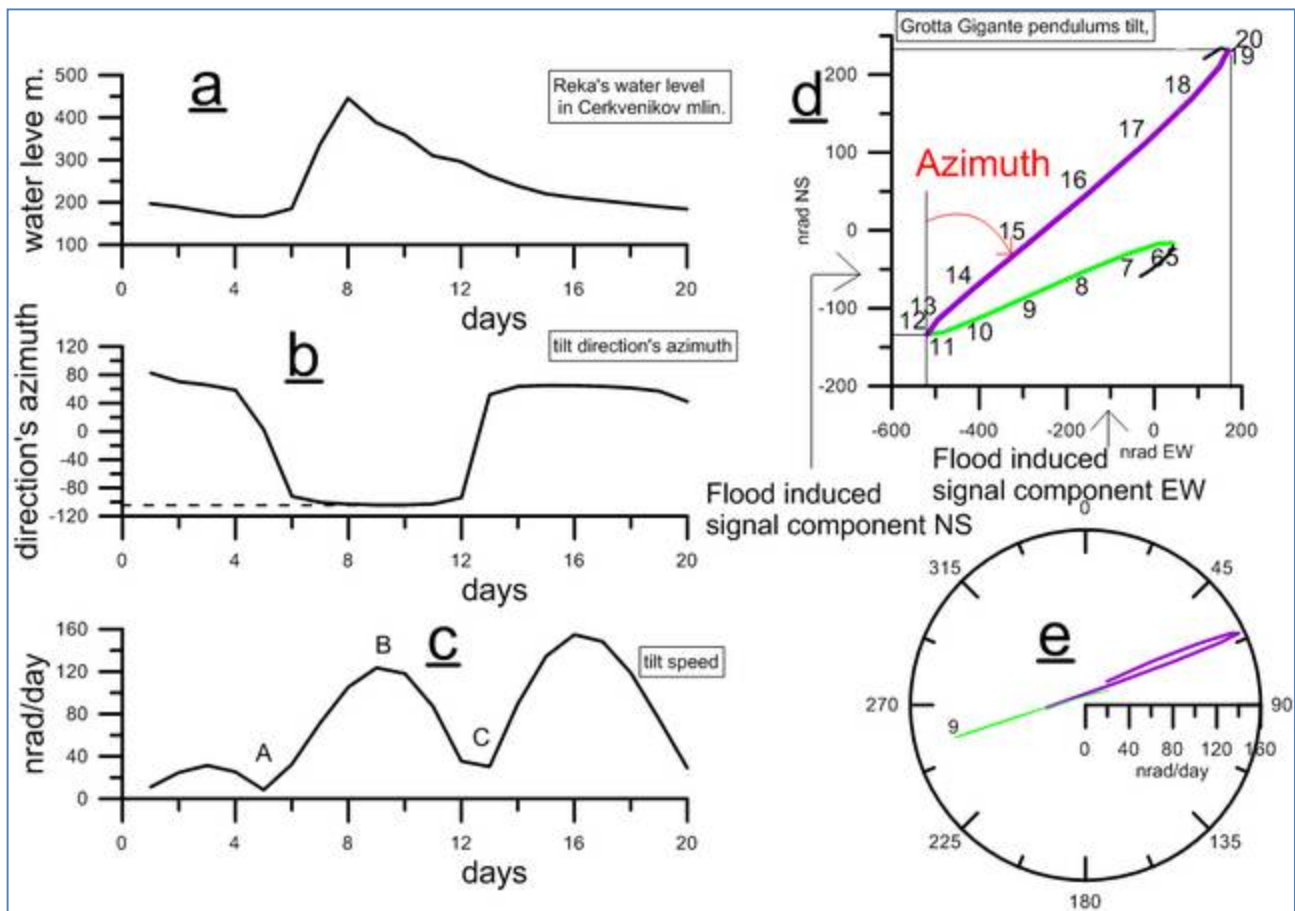
Fig. 7- The plots used to characterize the deformation during a flood event. All the plots concern the 20 days covering the flood of October 2, 1984: a) flow rate of the river Reka recorded in Cerkvenikov mlin; b) azimuth of the tilt directions; c) tilt speed; d) pendulum total tilt with the two components plotted together; definition of the azimuth of the signal induced by the floods; e) tilt represented in a rose diagram plotted with the azimuth and the speed. The "outgoing" and the "return" signal are highlighted in green and purple, respectively.

the different phases of the flood induced movement (**Figure7d**). The magnitude of the vector is equal to the tilt's speed counted in nrad per day.

As shown in **Figure 7,** the complete signal induced by the flood is characterized by specific phases in correlation to the river flow. The overall signal can be divided in two phases: the "outgoing signal" (green line in **Figure 7d** and **7e**) and the "return signal" (purple in **Figure 7d** and **7e**). During the first phase the signal moves towards SW (day 6). As confirmed by the plot, the speed is minimal in the turning points (day 5, point A in **Figure 7c**) and the direction changes drastically (sharp drop between the 4th and 6th day shown in the direction plot). After that (second phase and begin of the "outgoing signal") the direction does not change from the 6th to 9th day, but the speed increases. This phase ends with the maximum speed point (point B in the speed plot **Figure 7c**, also point 9 in **Figure 7e**). The third phase, from the 9th to the 13th day, is characterized by a constant direction, almost the same as in the previous phase, and by a decrease of speed. The direction remains approximately the same until a specific day (in this case the 13th) when the tilt's speed is minimum and the signal changes to the direction N65E (point C in the speed plot **Figure 7c**). The fourth and last phase begins from an abrupt change of direction, which defines the end of the "outgoing signal". In the clearest signals the tilting direction during the "return" phase is almost the same as during the "outgoing" phase, there is only a change of verse. In fact, we have called this

phase "return signal" because the signal returns to the previous tilt position.

As clearly demonstrated, the tilt-speed increases during the flood, and then gradually abandons the direction because the water has no longer effect on the tilt. In the tilt plot (at the top right in **Figure 7d**) we highlight how to define the value of amplitude of the flood signal. The signal often presents a clear difference between the amplitude of the "outgoing signal" and the "return signal", therefore we have measured both of them for each event.
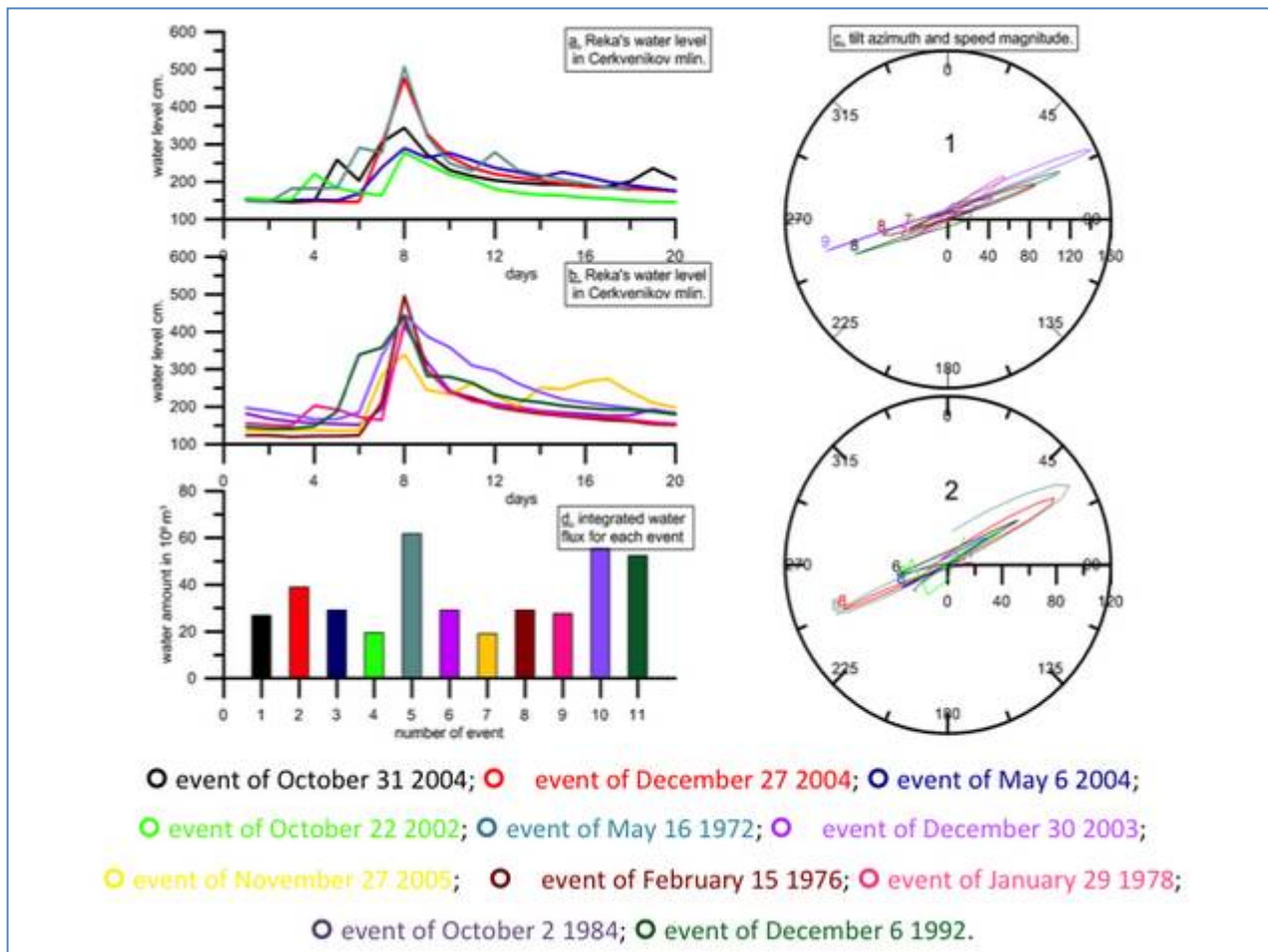
Fig. 8 Summary of the deformation during eleven selected floods: a) water level of river Reka in Cerkvenikov mlin for flood numbers 1-5; b) same as a) for floods 6-11; c) rose diagram representing the azimuth of the tilt and the magnitude of the speed plotted together. Upper graph (1) for flood numbers 1-5, lower graph (2) for floods 6-11; d) value of the integrated water flux for all considered events.

We have repeated the above analysis for all the floods marked green in the **Figure 4**, and have superposed the resulting tilting time sequences in **Figure 8**. The superposition of the different events highlights the consistency in the time evolution of the deformation induced by the flood.

The characteristic signal defined above is repeated in the same pattern, maintaining the SW tilting of the pendulums and successive recovery. The floods we have selected have been taken from a time interval of 40 years, therefore demonstrating that in these last four decades the water flow during floods has taken the same pathway, as it induces the same geodetic deformation.

Finally, we calculate the time integral of the flow rate over the time interval of the floods and compare this value with the maximum tilting induced by the flood. In **Figure 9a** the maximum value of water level and of flood rate are plotted against the maximum tilting. We find that for some

events (for instance events 4,3,11,10) the proportionality between water and tilting fails. The proportionality is greatly enhanced if we plot the maximum tilting against the integrated flood rate, this being the total amount of water that influences the instruments. As demonstrated in **Figure 9b** the tilting is proportional to the integrated water volume that entered the Karst system. We interpolate the values linearly, and obtain the following relation, where g_{tilt} is the maximum tilting induced by the flood, V the integrated volume of water entering the Karst during the flood, a the linear coefficient and c a second parameter:

$$g_{tilt} = a\,V + c \qquad\qquad (1)$$

We find the values $a = 10.7\ 10^{-6}$ nrad/m^3 and $c = -55.5$ nrad. The parameter c is the intercept in the linear relation (1) and tells us that the minimum amount of water volume necessary to deform the cave is $V_0 = 5.2\ 10^6$ m^3; the coefficient a tells us that the tilting amounts to $10.7\ 10^{-6}$ nrad for 1 m^3 of water flowing into the Karst.
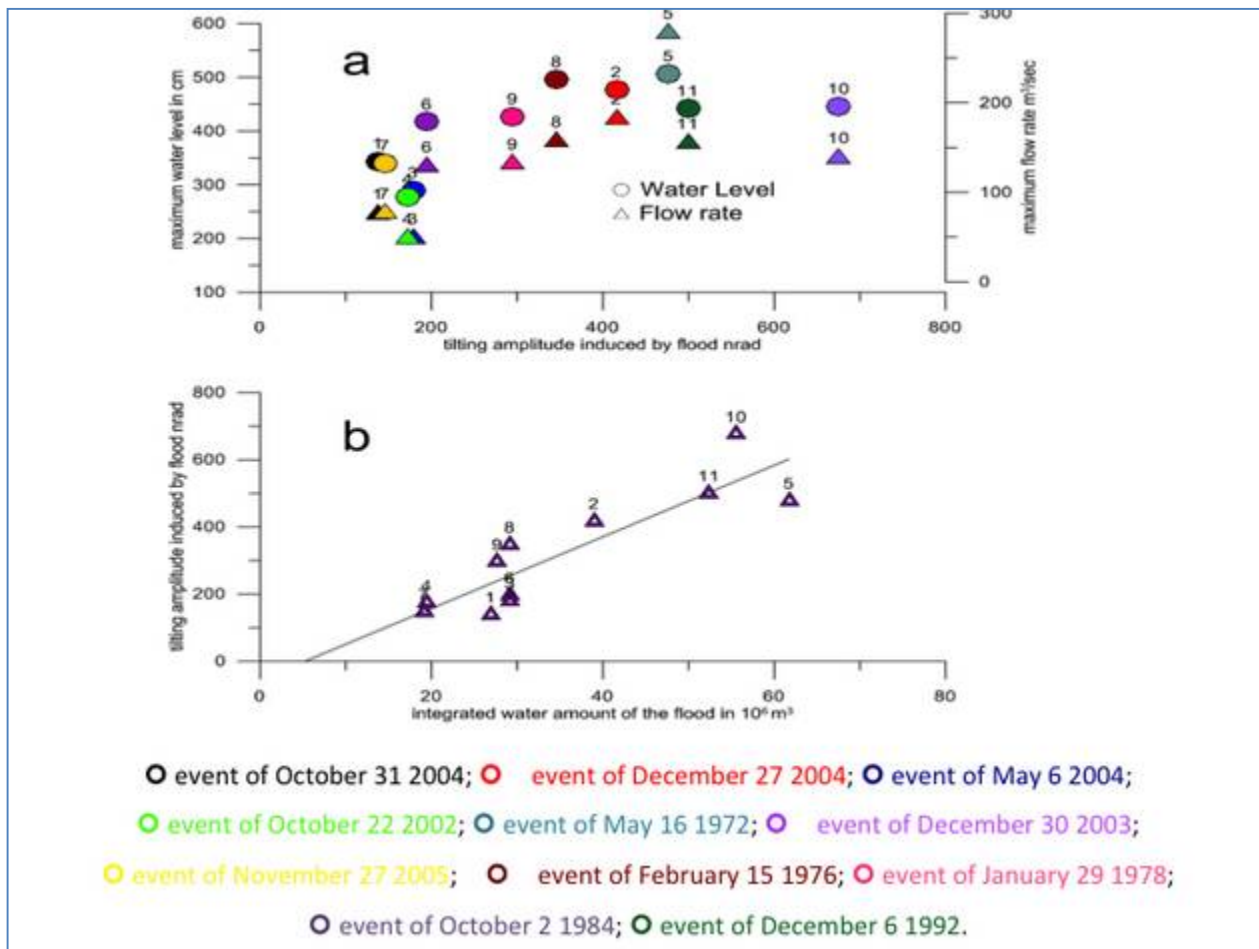
Fig. 9 -The relation between the tilting amplitude recorded in the Grotta Gigante and the floods in terms of a) water level and flow rate and b) integrated water flux recorded at Cerkvenikov mlin; in b) the linear regression is also shown.

Discussion and conclusions

The goal of the present work was to quantify the deformation of a natural cave induced by the environmental factors of temperature, rainfall and water flow. The atmospheric pressure was not considered here, as it was shown in previous works to have a much smaller effect compared to

temperature and the hydrologic agents (e.g. Braitenberg et al., 2006). The physical link between temperature and deformation is due to the thermal expansion of rocks and the consequent thermal stresses to which the rock fabric responds by a volume deformation. The yearly surface temperature variation penetrates into the earth by thermal conductivity, leading to yearly temperature variations with exponentially decreasing amplitude and increasing phase lag with depth. Adopting the equations of Turcotte and Schubert (2002) and assuming a value for thermal diffusivity of $K=5 \ 10^{-6}$ m^2/sec which could be representative of a limestone with crevasses and air-filled voids (Turcotte and Schubert, 2002), the yearly surface variation with amplitude of 9.2°C would lead to a variation of 1.2°C , time shifted by 64 days at a depth of 14 m. This is the time-shift we find for the annual variation of the tilting of the cave, which is the compound effect of an annual temperature variation that is maximal at the surface and decays at greater depths, and would indicate that the deformation is equivalent to that of the superior part of the cave, considering that the cave is 105 m high. Since the temperature variation inside the cave is affected by air currents, the above estimate is only indicative as it does not take into account the convective air currents inside the cave which alter the predictions from a purely conductive heat model. The convective contribution shifts the depth at which the surface temperature has an effect to greater depths and reduces the phase-shift. In any case with the purely conductive model we obtain an equivalent depth that corresponds to the expected temperature variations in the rocks casing the cave and corresponding to the observed phase shift of the deformation. The geodetic deformation and the temperature variation have in common that the yearly variation is a very strong signal, that emerges more than 10 times above the remainder of the spectral energies. This is not the case for the hydrologic parameters as rain, river level, and river flow rate, where the annual signal is smaller or not too much greater (factor two to three) than the semi-annual signal. The geodetic signal has in common with the hydrologic signal, that the semi-annual variation is split into more than one spectral peak, at the periods of 183, 172 and 168 days. The peaks at the periods of 172 and 168 days are absent in the temperature variation, and are thus distinctive of the hydrologic influence. Beyond the mere coincidence of spectral energies deduced from the spectral analysis, the one to one coincidence of a characteristic deformation in correspondence with the floods of the river Reka is a proof of the fact that the hydrology induces a deformation of the cave. We deduce from the results that the yearly deformation of the cave is dominated by the thermal deformation, whereas at the semi-annual variation and at periods of a few days to 20 days the deformation has a greater hydrologic origin with respect to the thermal influence. The hydrologic and thermal deformations are superimposed to the other deformations of tectonic origin like free oscillations, seismic waves, co-seismic deformations and long period tectonic deformations.

References
Bensi S., Fanucci F., and Podda F.; 2009: *Strutture a macro e mesoscala dalla Dinaridi triestine (carta GEO-CGT del FVG)*. Rendiconti online Società Geologica It., **5**, 32-35.

Boy J. P., Longuevergne L., Boudin F., Jacob T., Lyard F., Llubes M., Florsch N. and Esnoult M.-F.; 2009: *Modelling atmospheric and induced non-tidal oceanic loading contributions to surface gravity and tilt measurements*. Journal of Geodynamics, **48**, 182-188.

Braitenberg C.; 1999: *The Friuli (NE Italy) tilt/strain gauges and short term observation*. Annali di Geofisica, **42**, 1-28.

Braitenberg C.; 2011: *Ultra broad band horizontal geodetic pendulums*. In Encyclopedia of geophysics, Springer Editor, Heidelberg, 336-340.

Braitenberg C. and Zadro M.; 1999: *The Grotta Gigante horizontal pendulums- instrumentation and observation*. Boll Geof. Teor. Appl., **40**, 577-582.

Braitenberg C. and Zadro M.; 2007: *Comparative analysis of the free oscillations generated by the Sumatra-Andamans Islands 2004 and the Chile 1960 eatrhquakes*. Bulletin of the Seismological Society of America, **97**, No. 1A, pp. S6-S17, January 2007, doi: 10.1785/0120050624.

Braitenberg C., Nagy I., Negusini M., Romagnoli C., Zadro M. and Zerbini S.; 2001: *Geodetic measurement at the northern border of the adria plate*. J. Geodynamics, **32**, 267-286.

Braitenberg C., Romeo G., Tacetti Q. and Nagy I.; 2006: *The very broad-band long base tiltmaters of Grotta Gigante (Trieste, Italy) secular term tilting and the great Sumatra-Andaman Islands earthquake of December 26, 2004*. J. Geodynamics, **41**, 164-174.

Carulli G.B. and Cucchi F.; 1991: *Propostad interpretazione strutturale del Carso triestino*. Atti Ticinensi di Scienze della Terra, 161-166.

Cucchi F., Casagrande G., Manca P. and Zini L.; 2001: *Il Timavo ipogeo tra l'Abisso di Trebiciano e la Grotta Meravigliosa di Lazzaro Jerko*. Le Grotte d'Italia, **2**, 39-48.

Florsch N., Llubes M., Woeppelmann G., Longuevergne L. and Boy J. P.; 2009: *Oceanic loading monitored by ground-based tiltmeters at Cherbourg (France)*, Journal of Geodynamics, **48**, 211-218.

Gilli E., Boudin F., Audra Ph. and Florsch N.; 2009: *Geodesic variations induced by hydrology on the karstic plateau of Calern (Alpes-Maritimes, France)*. Geophysical Research Abstracts, **11**, EGU2009-13578, EGU General Assembly 2009.

Grillo B., Braitenberg C., Devoti R. and Nagy I.; 2011: *The study of Karstic acquifers by geodetic measurements in Bus de la Genziana station - Cansiglio Plateau (Northeastern Italy)*. Acta Carsologica, **40/1, 161-173.**

Jacob T., Bayer R.,Chery J. and Le Moigne N.; 2010: *Time‐lapse microgravity surveys reveal water storage heterogeneity of a karst aquifer*. J. of Geophys. Res., **115**, B06402, doi:10.1029/2009JB006616.

Jahr T., Jentzsch G., Gebauer A. and Lau T.; 2008: *Deformation, seismicity, and fluids: Results of the 2004/2005 water injection experiment at the KTB/Germany*, J. Geophys. Res., **113**, B11410, doi:10.1029/2008JB005610.

Jahr T., Jentzsch G. and Weise A.; 2009: *Natural and man-made induced hydrological signals, detected by high resolution tilt observations at the Geodynamic Observatory Moxa/Germany*. J. of Geodyn., **48**, 126-131, doi:10.1016/j.jog.2009.09.011.

Kümpel, H.J.; 1986: *Model calculations for rainfall induced tilt and strain anomalies*. In: Vieira R. (ed), Proceedings of the Tenth International Symposium on Earth Tides. Madrid, pp. 889–901.

Latynina, L.A., Abashizde, V.G., Alexandrov, Kapanadze, A.A. and Karmaleeva, P.M.; 1993: Deformation observations in epicentral areas. Fizika Zemli 3, 78–84, in Russian.

Longuevergne L., Florsch N., Boudin F., Oudin L. and Camerlynck C.; 2009: *Tilt and strain deformation induced by hydrologically active natural fractures: application to the tiltmeters installed in Sainte-Croix-aux-Mines observatory (France)*. Geophys. J. Int., **178**, 667–677.

Marussi A.; 1960: *The University of Trieste station for the study of the tides of the vertical in the Grotta Gigante*. Proceedings of the Third International Symposium on Earth Tides, Trieste: 45-52.

Rossi G. and Zadro M.; 1996: *Long-therm crustal deformation in NE Italy revealed by tilt-strain gauges.* Phys.Earth.Planet.Int., **97**, 55-70.

Tenze D., Braitenberg C., Nagy I. and Cucchi F.; 2010: *Deformazioni indotte da flussi idrici sotterranei nel Carso Triestino*. Atti e momorie della Commissione Grotte "Eugenio Boegan", **43**, 41-55.

Turcotte D.L. and Schubert G.; 2002: *Geodynamics*. 2nd ed., Cambridge University Press Cambridge, New York, Melbourne, ISBN 0521 66186 2, 456 pp.

Weise A., Jentzsch G., Kiviniemi A. and Kaariainen J.; 1991: *Comparison of long-period tilt measurements: results from the two clinometric stations Metsahovi and Lohja, Finland*. J. Geodyn. **27**, 237–257.

Wessel P. and Smith W.H.F.; 1998. *New, improved version of generic mapping tools released*. EOS Trans. AGU 79 (47), 579.

Zadro M. and Chiaruttini C.; 1975: *Loading effects of the Mediterranean tides*. Proceedings of the Seventh Symposium on Earth Tides, 495 501.

Zadro M. and Braitenberg C.; 1999: *Measurement and interpretation of tilt-strain gauges in seismically active areas.* Earth Sci. Rev., **47,** 151-187.

Zöllner K.F.; 1872: *Zur Geschichte des Horizontalpendels*, Kgl. sächs. Gesellsch. der Wissensch. zu Leipzig, math.-phys. Klasse, November 1872.

7 Ringraziamenti

8 Riferimenti bibliografici per i capitoli 1-4

Braitenberg, C. (1999a). The Friuli (NE Italy) tilt/strain gauges and short term observations. *Annali*

Braitenberg, C., (1999b). Estimating the hydrologic induced signal in geodetic measurements with predicitive filtering methods. Geophys. Res. Letters 26, 775-778.

Braitenberg, C., and M. Zadro (1999). The Grotta Gigante horizontal pendulums – instrumentation and observations, *Boll. Geof. Teor. Appl.,* **40**, 577-582.

Braitenberg C., Zadro M. (2007) Amplitude ratios of the free oscillations generated by the Sumatra-Andaman Islands 2004 and the Chile 1960 earthquakes, Bulletin of the Seismological Society of America, Vol. 97, No. 1A, pp. S6–S17, January 2007, doi: 10.1785/0120050624.

Braitenberg, C., G. Romeo, Q. Taccetti, and Nagy I. (2005). The very-broad-band long-base tiltmeters of Grotta Gigante (Trieste, Italy): secular term tilting and the great Sumatra-Andaman Islands earthquake of December 26, 2004, *J. of Geodynamics*, in press.

Braitenberg, C., I. Nagy, G. Romeo, and Q. Taccetti (2004). The very broad-band data acquisition of the long-base tiltmeters of Grotta Gigante (Trieste, Italy) in: *Progress in Geodesy and Geodynamics*, Zhu Yaozhong and Sun Heping (Eds.), 457-462, Hubei Science and Technology Press, Wuhan, ISBN 7-5352-3194-2/P.10.

Dahlen, F.A. and Sailor, R.V. (1979) Rotational and elliptical splitting of the free oscillations of the Earth, Geophysical Journal International, 58, 609-623.

Kanamori, H. (1977). The energy release in great earthquakes, J. Geophys. Res., 82, 2981-2987.

Neic (2010) National Earthquake Information Center – NEIC, http://earthquake.usgs.gov/regional/neic/

Pagot E.,(2002) Effetti mareali, atmosferici e tettonici rilevati nelle stazioni clinometriche al bordo NE della placca adriatica, Tesi di laurea in Scienze Geologiche, Università di Trieste, a.a. 2000-2001.

Park, J., T. A. Song, J. Tromp, E. Okal, S. Stein, G. Roult, E. Clevede, G. Laske, H. Kanamori, P. Davis, J. Berger, C. Braitenberg, M. Van Camp, X. Lei, H. Sun, H. Xu, and S. Rosat (2005). Earth's free oscillations excited by the 26 December 2004 Sumatra-Andaman earthquake, *Science*, **308**, 1139-1144.

Romeo G., (2000) Digitization of optical lever instruments – Annali di Geofisica, Vol 43 545-557

Stein, S., and E. Okal (2005). Speed and size of the Sumatra earthquake, *Nature*, **434**, 581-582.

Stravisi F., Purga N. (2009): Dati meteorologici di Trieste - anno 2008, Dipartimento di Scienze della Terra, Università di Trieste, internal report,114, (06/1), 49 pag.

Zadro, M., and C. Braitenberg (1999). Measurements and interpretations of tilt-strain gauges in seismically active areas. *Earth Science Reviews*, **47**, 151-187.

9 Pubblicazioni recenti del gruppo di lavoro (dal 2006)

Braitenberg, C., Wienecke, S., Wang, Y. 2006. Detection of buried structures along a ridge axis from satellite derived gravity field, Journ. Geophys. Res, VOL. 111, B05407, doi:10.1029/2005JB003938,

Pinato Gabrieli C., Braitenberg C., Nagy I., Zuliani D. 2006. Tilting and horizontal movement at and across the northern border of the Adria plate, Edts. Gil A.J. e Sansò F., Geodetic Deformation Monitoring: From Geophysical to Engineering Roles, 306 pp., Springer Verlag. 129-137. ISBN-10: 3-540-38595-9. (IAG Symposium Jaén, Spain, March 7-19,2005; Series: International Association of Geodesy Symposia , Vol. 131) http://www.springer.com/italy/home/generic/search/results?SGWID=6-40109-22-173674905-0

Braitenberg C., Zadro M. 2007. Amplitude ratios of the free oscillations generated by the Sumatra-Andaman Islands 2004 and the Chile 1960 earthquakes, Bulletin of the Seismological Society of America, Vol. 97, No. 1A, pp. S6–S17, January 2007, doi: 10.1785/0120050624.

Wienecke S., Braitenberg C., Goetze H.-J. 2007. A new analytical solution estimating the flexural rigidity in the Central Andes, Geophys. J. Int., 169, 789-794, doi:10.1111/j.1365-246X.2007.3396.x.

Shin, H. Xu, C.Braitenberg, J. Fang, Y. Wang 2007. Moho undulations beneath Tibet from GRACE-integrated gravity data, Young H. Geophys. J. Int., doi: 10.1111/j.1365-246X.2007.03457.x, 1-15.

Ebbing, J., Braitenberg C. & S. Wienecke 2007. Insights into the lithospheric structure and the tectonic setting of the Barents Sea region from isostatic considerations, Geophys. J. Int., Vol. 171, pp. 1390-1403, doi: 10.1111/j.1365-246X.2007.03602.x

Shin Y. H., Shum C.-K., Braitenberg C., Lee S. M., Xu H., Choi K. S., Baek J. H., Park J. U. 2009. Three – dimensional fold structure of the Tibetian Moho from GRACE gravity data. Geophysical Research Letters, Vol. 36, L01302, doi:10.1029/2008GL036068, 2009.

Braitenberg, C., Ebbing, J. 2009. The GRACE-satellite gravity and geoid fields in analysing large scale, cratonic or intracratonic basins, Geophysical Prospecting, vol. 57, no. 4, 559-571, DOI: 10.1111/j.1365-2478.2009.00793.x

Braitenberg, C., Ebbing, J 2009. New insights into the basement structure of the west-Siberian basin from forward and inverse modelling of Grace satellite gravity data,. J. Geophysical Res., 114, B06402, doi:10.1029/2008JB005799, 2009.

Antonioli F., Ferranti L., Fontana A., Amorosi A. M., Bondesan A., Braitenberg C., Dutton A.,. Fontolan G., Furlani S., Lambeck K., Mastronuzzi G., Monaco C., Spada G., Stocchi P. 2009. Holocene relative sea-level changes and vertical movements along the Italian and Istrian coastlines, Quaternary International, 206, 102-133, ISSN 1040-6182, DOI: 10.1016/j.quaint.2008.11.008.

Mariani P., Braitenberg C., Antonioli F. 2009. Sardinia coastal uplift and volcanism. Pure and Applied Geophysics, 166, 1369-1402. DOI :10.1007/s00024-009-0504-3

Gimenez M. E., Braitenberg C., Martinez M. P., Introcaso A. 2009. A comparative analysis of seismological and gravimetric crustal thicknesses below the Andean Region with flat subduction of the Nazca Plate. International Journal of Geophysics, Volume 2009, Article ID 607458, 8 pages, doi:10.1155/2009/607458

Pinto L. G. R., Pádua M. B., Ussami N., Vitorello I., Padilha A. L., Braitenberg C. 2010. Magnetotelluric deep soundings, gravity and geoid in the south São Francisco craton: Geophysical indicators of cratonic lithosphere rejuvenation and crustal underplating, Earth and Planetary Science Letters, 297, 423-434, doi:10.1016/j.epsl.2010.06.044

Barnaba C., Marello L., Vuan A., Palmieri F., Romanelli M., Priolo E., Braitenberg C. 2010. The buried shape of an alpine valley from gravity surveys, seismic and ambient noise analysis. Geophysical Journal International, 180, 715-733, doi:10.1111/j.1365-246X.2009.04428.x

Braitenberg C., Mariani P., Tunini L., Grillo B., Nagy I. 2010. Vertical crustal movements from differential tide gauge observations and satellite altimetry in southern Italy. Journal of Geodynamics, doi:10.1016/j.jog.2010.09.003

Braitenberg C. 2011. Ultra broad band horizontal geodetic pendulums. In: Harsh K. Gupta (ed.) Encyclopedia of Solid Earth Geophysics, DOI 10.1007/978-90-481-8702-7, Springer Science+Business Media B.V. 2011, Chapter No:231

Braitenberg C., Mariani P., Tunini L., Grillo B., Nagy I. 2011. Vertical crustal movements from differential tide gauge observations and satellite altimetry in southern Italy. Journal of Geodynamics, 51, 233-244, doi:10.1016/j.jog.2010.09.003

Grillo B., Braitenberg C., Devoti R., Nagy I. 2011. The study of karstic aquifers by geodetic measurements in Bus de la Genziana station – Cansiglio Plateau (Northeastern Italy), Acta Carsologica 40/1, 161-173.

Riviste nazionali

Braitenberg C., Grillo B., Nagy I. , Zidarich S., Piccin A., 2007. La stazione geodetico-geofisica ipogea del Bus de la Genziana (1000VTV) - Pian Cansiglio, Atti e Memorie della Commissione Grotte "E. Boegan", Società Alpina della Giulie CAI, Trieste, Italia, Vol. 41:105-120.

Grillo B.. 2007. Contributo alle conoscenze idrogeologiche dell'Altopiano del Cansiglio. Atti e memorie della Commissione "E. Boegan", Vol.41, 5-15.

Guidi P., Grillo B. 2008. Una grotta imperiale.Cent'anni di esplorazioni, turismo e ricerche nella Grotta Gigante. Speleologia, Anno XXIX – Giugno 2008, 58, 24-30.

Grillo B., Braitenberg C., Nagy I. 2010. I clinometri del Bus de La Genziana (1000VTV). Speleologia Veneta, 18, 109-117.

Grillo B. 2010. Manutenzione al Bus de la Genziana (1000vtv), Speleologia Veneta, 18, 93-98.

Tenze D., Braitenberg C., Nagy I., Cucchi F. 2011. Deformazioni indotte da flussi idrici sotterranei nel Carso Triestino. Atti e Memorie della Commissione Grotte "E. Boegan", Vol.43, 41-55.

Presentazioni a Convegni:

Braitenberg C., Wienecke S, Ebbing, J. , Born, W., Redfield, T. 2007 JOINT GRAVITY AND ISOSTATIC ANALYSIS FOR BASEMENT STUDIES - A NOVEL TOOL, Extendended Abstracts, EGM 2007 International Workshop, Innovation in EM, Grav and Mag Methods: a new Perspective for Exploration, Villa Orlandi, Capri - Italy , 15-18 April 2007 (http://www2.ogs.trieste.it/egm2007/),

Braitenberg, C., Ebbing, J. 2007 The gravity potential derivatives as a means to classify the Barents Sea Basin in the context of cratonic basins, Extendended Abstracts, EGM 2007 International Workshop, Innovation in EM, Grav and Mag Methods: a new Perspective for Exploration, Villa Orlandi, Capri - Italy , 15-18 April 2007 (http://www2.ogs.trieste.it/egm2007/)

Braitenberg C., Grillo B., Mariani P., Arena G. 2008. Tassi di innalzamento da osservazioni mareografiche e altimetriche satellitari. In: Di Bucci D., Neri G., Valensise L. (Edts.) 1908 –

2008 Scienza e Società a cento anni dal Grande Terremoto, Reggio Calabria, 10-12 Dicembre 2008, Miscellanea INGV, 2008_3, pp. 21-22.

Mariani P., Braitenberg C. 2008. Sea level change and relationship with the volcanic load: the Sardinian Volcanism. In: Oggiano, L. Carmignani, A. Funedda, P. Conti. (Edts.), Rendiconti On line Società Geologica Italiana, 84° Congresso Nazionale Sassari 15-17 settembre 2008. Sassari, Sassari 15-17 settembre 2008 G. vol. 3, p. 526-527.

Mariani P., Braitenberg C., Antonioli F. 2008. Variazione della linea di costa in relazione al carico vulcanico: il caso del vulcanismo sardo. In: Riassunti estesi, 27° Convegno Nazionale Gruppo Nazionale di Geofisica della Terra Solida. Trieste, 6-8 Ottobre 2008., pp. 71-74.

Braitenberg C., Ebbing J. 2008. New insights into the basement structure of the West Siberian basin from forward and inverse modelling of Grace Satellite gravity data, In: Riassunti estesi, 27° Convegno Nazionale Gruppo Nazionale di Geofisica della Terra Solida. Trieste, 6-8 Ottobre 2008., pp. 409-411.

Pinto L.G.R., Pádua M.B., Ussami N., Vitorello I., Padilha A.L., Braitenberg C. 2008. Integração de dados Gravimetricos, Geoide e Magnetotelluricos no SE do Craton S. Francisco: underplating magmatico, soerguimento e erosão no Cretaceo Inferior, III Simpósio Brasileiro de Geofísica, 26 a 28 de novembro de 2008, Hotel Crowne Plaza, Belém, Pará, Brasil, 1-5, Copyright 2008, SBGf, Sociedade Brasileira de Geofisica

Grillo B., Braitenberg C., Nagy I., Dilena C. 2009. The study of karstic aquifers by geodetic measurements in Friuli Venezia Giulia. Epitome Congresso Nazionale GeoItalia - Federazione Italiana di Scienze della Terra: 73, Rimini 07 - 11 settembre 2009.

Braitenberg C., Grillo B., Mariani P., Tunini L., Nagy I. 2009. Vertical crustal movement from tide gauges and satellite altimetry. Abstract. Convegno annuale dei progetti sismologici (S1), Roma, 19-21 ottobre 2009.

Braitenberg C., Mariani P., Grillo B., Nagy I. 2009. Vertical crustal movements from comperative analysis of spaceborn and local sea level change observations. 3rd Coastal Altimetry Workshop, 17-18 September 2009, Frascati (Rome), Italy, Abstract List, pp.8, www.coastalt.eu

Grillo B., Braitenberg C., Nagy I., Piccin A. 2009. Tilting tra il Friuli-Venezia Giulia ed il Veneto dal 2006 al 2008, Atti del 3° Congresso Nazionale AIGA - Centro di GeoTecnologie, Universita' di Siena, San Giovanni Valdaro (AR), 25-27 Febbraio 2009

Braitenberg C., A. Russian, P. Mariani, J. Ebbing, 2009. Gravity-gradient fields in mapping unknown structures of the African plate, Out of Africa, 140 years with Kevin Burke and Lee Ashwal, 15-18 november, 2009, Witwatersrand University, Johannesburg, South Africa. Abstract book, p. 14. , http://www.geodynamics.no/outofafrica/outofafrica-abstractbook-upd.pdf

Braitenberg C., Cucchi F., Devoti R., Grillo B., Nagy I., Tenze D., Zini L. 2010. The study of karstic aquifers by geodetic measurements in Friuli Venezia Giulia (North East Italy) for a water sustainable management, Abstract, Hydro Predict' 2010, International Interdisciplinary

Conference on Prediction for Hydrology, Ecology and Water Resources Manegement, Prague, 20-23 September, 2010.

Ferrante S., Braitenberg C., Ebbing J. 2010. The basalt geometry in the west siberian basin from satellite gravity, magnetics ans seismics. EGM 2010 International Workshop, Adding new value to Electromagnetic,, Gravity and Magnetic Methods for Exploration, Capri, Italy, April 11-14, 2010. 1-4.

Braitenberg C., Russian A., Mariani P., Nagy I. 2010. The new global gradient tensor in detecting basement units. Geophysical Research Abstract Vol.12. EGU2010-12894-3, EGU General Assembly Vienna, 02-07 May 2010.

Mariani P., Braitenberg C., Ussami N. 2010. The new satellite derived gradient fields for gaining a better understanding of the Parana' Basin. EOS Trans. AGU, 91(26), Meet. Am. Suppl. Abstarct G13A-02 (The Meeting of the Americas – AGU, Foz do Iguassu, Brazil, 8-12 August 2010)

Zadro M., Braitenberg C., Nagy I. 2010. The free oscillations models of Chile 2010 and 1960 events observed with the Grotta Gigante horizontal pendulums. Eos Trans. AGU, 91(26), Meet. Am. Suppl., Abstract U41A-01 (The Meeting of the Americas – AGU, Foz do Iguassu, Brazil, 8-12 August 2010)

Uieda L., Ussami N., Braitenberg C. 2010. Computation of the gravity gradient tensor due to topographic masses using tesseroids, Eos Trans. AGU, 91(26), Meet. Am. Suppl. Abstract G22A-04, (The Meeting of the Americas - AGU, Foz do Iguassu, Brazil, 8-12 August, 2010)

Braitenberg C., Reguzzoni M. 2010. Expected sensitivity of GOCE satellite to detect basement and Moho undulations, Eos Trans, AGU, 91(26), Meet. Am. Suppl., Abstract G22A-02, (The Meeting of the Americas - AGU, Foz di Iguassu, Brazil, 8-12 August, 2010)

Braitenberg C., Reguzzoni M. 2010. Sensitivity of satellite GOCE to detect basement and Moho undulations. In: Riassunti estesi, 29° Convegno Nazionale Gruppo Nazionale di Geofisica della Terra Solida. Prato, 26-28 Ottobre 2010, 511.

Sansò F., Gatti A., Reguzzoni M., Sampietro D., Sabadini R., Barletta V., Bordoni A., Braitenberg C., Mariani P., Poulain P. M., Mauri E., Casotto S., Panzetta F., Solitro F., Fontan E., Fermi M., Chersich M., Osmo M., Bianco G. 2010. GOCE-ITALY: un progetto dell'Agenzia Spaziale Italiana per applicazioni geofisiche nell'area del mediterraneo basate sui dati della missione spaziale GOCE, In: Riassunti estesi, 29° Convegno Nazionale Gruppo Nazionale di Geofisica della Terra Solida. Prato, 26-28 Ottobre 2010, 537-540.

Grillo B., Braitenbreg C., Devoti R., Zuliani D., Nagy I., Fabris P. 2010. The study of aquifers by geodetic mesurements in Cansiglio Plateau (North – Eastern Italy), In: Riassunti estesi, 29° Convegno Nazionale Gruppo Nazionale di Geofisica della Terra Solida. Prato, 26-28 Ottobre 2010, 411-414.

Tenze D., Braitenberg C., Nagy I. 2010. Deformazioni del Carso in risposta ai fattori ambientali, In: Riassunti estesi, 29° Convegno Nazionale Gruppo Nazionale di Geofisica della Terra Solida. Prato, 26-28 Ottobre 2010, 125-126.

Tunini L., Braitenberg C., Ricker R., Mariani P., Grillo B. 2010. Vertical land movement for the Italian coasts by altimetric and tide gauges measurements. ESA Living Planet Symposium, Bergen, 27/06/2010-02/07/2010.

Sansò F., Bianco G., Braitenberg C., Casotto S., Fermi M., Poulain P., Sabadini R., Solitro F. 2010. GOCE ITALY: Scientific tasks and first results. ESA Living Planet Symposium, Bergen, 27/06/2010-02/07/2010.

Braitenberg C., Mariani P., Reguzzoni M., Ussami N. 2010. GOCE observations for detecting unknown tectonic features. Proceedings 'ESA Living Planet Symposium', Bergen, Norway, 28 June – 2 July 2010 (ESA SP-686, December 2010).

Braitenberg C., Mariani P., Pivetta T., Uieda L. 2011 Relevance of GOCE gradients to detect unknown geologic structures in areas of natural resources. EGU General Assembly 2011, Vienna, 3-8 Aprile 2011.

Mariani P., Braitenberg C., Ussami N. 2011. Unvealing the border of a craton by the gravity gradient with example of the Parana' Basin. EGU General Assembly 2011, Vienna, 3-8 Aprile 2011.